



저작자표시-비영리-변경금지 2.0 대한민국

이용자는 아래의 조건을 따르는 경우에 한하여 자유롭게

- 이 저작물을 복제, 배포, 전송, 전시, 공연 및 방송할 수 있습니다.

다음과 같은 조건을 따라야 합니다:



저작자표시. 귀하는 원저작자를 표시하여야 합니다.



비영리. 귀하는 이 저작물을 영리 목적으로 이용할 수 없습니다.



변경금지. 귀하는 이 저작물을 개작, 변형 또는 가공할 수 없습니다.

- 귀하는, 이 저작물의 재이용이나 배포의 경우, 이 저작물에 적용된 이용허락조건을 명확하게 나타내어야 합니다.
- 저작권자로부터 별도의 허가를 받으면 이러한 조건들은 적용되지 않습니다.

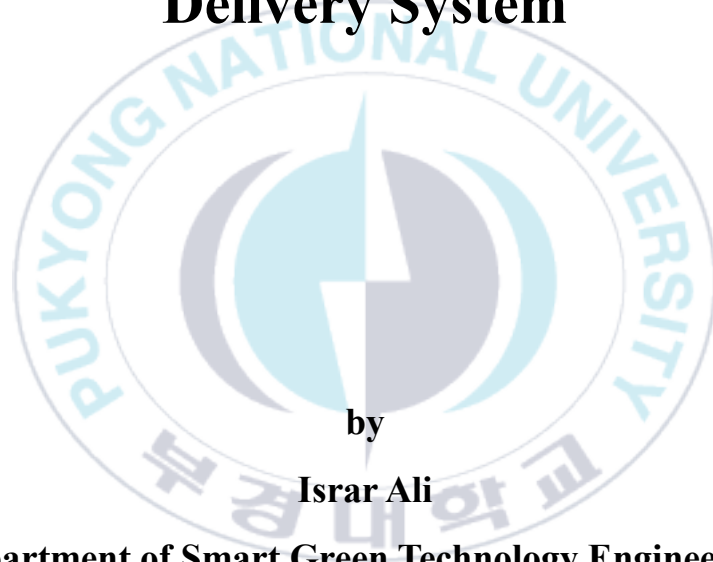
저작권법에 따른 이용자의 권리는 위의 내용에 의하여 영향을 받지 않습니다.

이것은 [이용허락규약\(Legal Code\)](#)을 이해하기 쉽게 요약한 것입니다.

[Disclaimer](#)

Thesis for the degree of Doctor of Philosophy

**Development of Stimuli-responsive Hydrogels
based on Carboxymethyl-Cellulose for Drug
Delivery System**



by

Israr Ali

Department of Smart Green Technology Engineering,

The Graduate School

Pukyong National University

February 2024

Development of Stimuli-responsive Hydrogels based on Carboxymethyl-Cellulose for Drug Delivery System

(약물 전달 시스템을 위한 카르복시메틸 셀룰로오스 기반 자극 반응성 하이드로겔의 개발)

Advisor: Prof. Kwon Taek Lim



by

Israr Ali

**A thesis of submitted in partial fulfillment of the requirements
for the degree of**

Doctor of Philosophy

**in Department of Smart Green Technology Engineering, The Graduate School,
Pukyong National University**

February 2024

**Development of Stimuli-responsive Hydrogels based on
Carboxymethyl-Cellulose for Drug Delivery System**

A dissertation

by

Israr Ali

Approved by:

(Chairman): Prof. Kwon Taek Lim

(Member): Prof. Bonggi Lee

(Member): Prof. Sang-Hyug Park

(Member): Prof. Yeong-Soon Gal

(Member): Prof. Yong-Hyun Kim

February 16th, 2024

Table of Contents

List of Figures	vii
List of Tables	xi
List of Schemes	xii
Glossary of abbreviations and symbols	xiii
Acknowledgements	xvi
Abstract	xviii
요약	xxii
Chapter 1 : Introduction	1
1.1 Smart hydrogels in drug delivery system	1
1.2 Natural polymers	6
1.2.1 Cellulose	9
1.2.1.1 Carboxymethyl-cellulose	10
1.3 Fabrication of hydrogel	12
1.3.1 Cross-linking of hydrogels	12

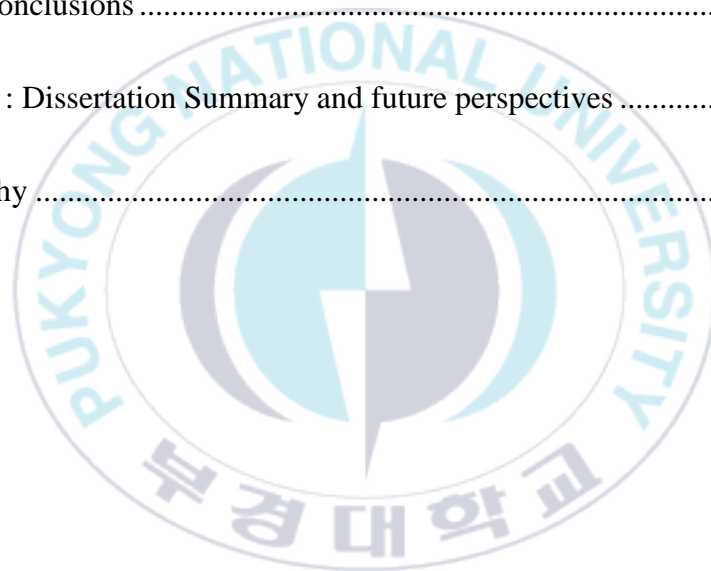
1.3.2	Bio-orthogonal Click chemistry reactions	13
1.3.3	On-demand cleavage of cross-linkers	16
Chapter 2 : Reduction-responsive and bio-orthogonal carboxymethyl cellulose based soft hydrogels cross-linked <i>via</i> IEDDA click chemistry for cancer therapy application 18		
2.1	Introduction	18
2.2	Experimental and Characterization	24
2.2.1	Materials	24
2.2.2	Synthesis of water-soluble DSe-DPEG-DTz cross-linker	28
2.2.3	Synthesis of CMC-Nb.....	29
2.3	Preparation of hydrogels	30
2.4	Characterization of materials	33
2.4.1	Rheological analysis	33
2.4.2	Swelling study.....	34
2.4.3	Drug loading	35
2.4.4	Drug release analysis	36
2.4.5	Hemolysis assay.....	36

2.4.6	<i>In vitro</i> degradation study of hydrogels	37
2.4.7	Cell culture and cytotoxicity evaluation	38
2.4.8	Live/ Dead assay	39
2.5	Results and discussion.....	40
2.5.1	Synthesis of CMC-Nb.....	40
2.5.2	Preparation and characterization of hydrogels.....	43
2.5.3	Drug loading and <i>in vitro</i> reduction-triggered release of DOX from hydrogels.....	49
2.5.4	Cytotoxicity studies	53
2.5.5	Live/dead analysis.....	56
2.5.6	Hemolytic activity of hydrogels.....	58
2.5.7	Biodegradation study	60
2.6	Conclusions	62
Chapter 3 : NIR-responsive carboxymethyl-cellulose hydrogels containing thioketal-linkages for on-demand drug delivery system.....		
3.1	Introduction	64
3.2	Materials and methods	72

3.2.1	Materials	72
3.2.2	Methods.....	73
3.2.2.1	Synthesis and characterization of precursors	73
3.2.2.1.1	Synthesis of ROS-cleavable small molecule thioketal-di-tetrazine cross-linker (TK-DTz).....	73
3.2.2.1.1.1	Synthesis of thioketal diacid (TKDA).....	73
3.2.2.1.2	Synthesis of Amino-Functionalized Tetrazine (Tz-NH ₂) .	73
3.2.2.1.2.1	Synthesis of Tert-butyl 4-cyanobenzylcarbamate (TBC)	73
3.2.2.1.2.2	Synthesis of Tert-butyl 4-(1,2,4,5-tetrazin-3-yl)benzylcarbamate (Tz-NH-Boc)	74
3.2.2.1.2.3	De-protection of BOC-group to obtain Tz-NH ₂	75
3.2.2.1.2.4	Synthesis of TK-DTz.....	76
3.2.3	Functionalization of CMC with Nb	77
3.3	Formulation of hydrogels	77
3.4	Characterization	80
3.4.1	Measurements and instruments.....	80

3.4.2	Drug loading and release assessment.....	80
3.4.3	<i>In vitro</i> cytotoxicity analysis of precursors and fabricated hydrogels.....	82
3.4.4	<i>In vitro</i> anti-tumor activity of DOX+ICG-encapsulated hydrogels	83
3.4.5	Hemolysis assay	84
3.4.6	<i>In vitro</i> evaluation of ROS production.....	85
3.4.7	Statistical analysis	85
3.5	Results and discussion.....	86
3.5.1	Synthesis of TK-DTz	86
3.5.2	Synthesis of CMC-Nb.....	90
3.5.3	Fabrication and characterization of the hydrogels	93
3.5.4	Gelation times and viscoelastic properties of CMC hydrogels..	93
3.5.5	Swelling and water retention properties.....	96
3.5.6	Morphological analysis	98
3.5.7	Drug loading and release studies	100

3.5.8	<i>In vitro</i> cytocompatibility of precursors, blank hydrogels and DOX/ICG-encapsulated hydrogels.....	105
3.5.9	Hemolytic activity of hydrogels.....	108
3.5.10	The anti-cancer activity of formulated hydrogels.....	110
3.5.11	<i>In vitro</i> ROS production.....	115
3.6	Conclusions.....	117
Chapter 4	: Dissertation Summary and future perspectives.....	119
Bibliography	123



List of Figures

Figure 1. Smart hydrogels and their emerging applications	3
Figure 2. Drug delivery strategies	5
Figure 3. Various kinds of click chemistry reactions matches with click chemistry.....	15
Figure 4. ¹ H NMR spectra (a) PEG-tosyl (b) DSe-DPEG (c) DSe-DPEG-DTz.	26
Figure 5. FTIR spectrum of (a) PEG-tosyl (b) DSe-DPEG (c) DSe-DPEG-DTz.	28
Figure 6. (a) ¹ H-NMR spectrum of CMC-Nb in D ₂ O, (b) FTIR spectrum of CMC-Nb, and (c) FTIR spectrum of the hydrogel.	42
Figure 7. (a) The storage modulus (G') and loss modulus (G'') of hydrogels as a function of time, (b) storage modulus (G') and loss modulus (G'') as a function of angular frequency under 1 % strain at 25 °C, (c) the strain amplitude sweep experiments, (d) swelling behavior of hydrogels, and (e) representative photograph of hydrogels formation.....	47

Figure 8. (a) SEM micrographs of cross-sectional area of hydrogels and (b) optical microscopic images of hydrogels.....	49
Figure 9. DOX release studies of hydrogels in 10 mmol GSH and simulated physiological buffer (PBS, pH, 7.4).....	52
Figure 10. Cell viabilities (%) of HEK-293 cells determined using WST assays after treatment with (a) CMC-Nb, (b) DPEG-DSe-DTz, (c) blank-hydrogels (IZ-3 and IZ-2), and (d) in vitro anti-tumor activity against BT-20 cells after treatment with free-DOX and DOX-loaded hydrogels.....	55
Figure 11. Confocal microscopy images of BT-20 cells treated with free DOX, blank-hydrogels (IZ-3 and IZ-2 and DOX-loaded hydrogels (IZ-3and IZ-2). Scale bars indicating 100 μ m.....	57
Figure 12. Hemocompatibility of hydrogels. (a) photographs of hemolysis test performed using saline (negative control), deionized water (positive control), and hydrogels (IZ-2 and IZ-3), and (b) hemolysis ratio of the hydrogels.	60
Figure 13. Biodegradation of formulated hydrogels (IZ-3). (a) in PBS (pH, 7.4) and (b) in GSH (10 mmol).....	61

Figure 14. ¹ H-NMR spectrum of TKDA (a), TBC (b) Tz-NH-BOC (c) Tz-NH2 (d), and TK-DTz cross-linker (e).	89
Figure 15. (a) ¹ H-NMR spectrum of CMC-Nb, (b-c) FTIR spectra of CMC-Nb and formulated hydrogel.	92
Figure 16. Mechanical properties of TKHG-C, TKHG-B, TKHG-A hydrogels. (a) Photograph pictures of hydrogels formation, (b-d) Storage and loss modulus as a function of respective step time, (e-g) Storage and loss modulus as a function of angular frequency.	95
Figure 17. Swelling behavior of hydrogels in physiological condition.	97
Figure 18. Morphology of hydrogels (a) optical microscopic images to find porosity by entrapment of N ₂ bubbles inside hydrogels generated by IEDDA click reaction (b) SEM images of cross-sections of hydrogels.	99
Figure 19. Cumulative DOX release profiles of the hydrogels TKHG-C. (a) Drug release profile of hydrogels in physiological condition, (b) drug release profile of DOX + ICG-encapsulated hydrogels when irradiated with NIR-light (808 nm, 4-W/cm ² , 20 min), (c) drug release profile of hydrogels in H ₂ O ₂ (0.5%).	103

Figure 20. Biodegradation of formulated hydrogels (TKHG-C). (a) in PBS (pH, 7.4) without NIR irradiation, (b) irradiated with NIR light (808 nm, 4-watt), and (c) in H₂O₂ (0.5% in PBS). 104

Figure 21. Cytotoxicity assessment of precursors and TKHG-C hydrogel (a) cytotoxicity of CMC-Nb (b) Cytotoxicity of TK-DTz (c) hydrogel (d) Cell viabilities were assessed by Live/dead assays to validate the cytocompatibility of CMC-Nb, TK-DTz, and TKHG-C hydrogel, respectively. 107

Figure 22. Anti-cancer efficacy against Hela cancer cells treated with free-DOX and DOX + TKHG-C, and DOX + ICG-encapsulated hydrogels under NIR irradiation; (b) Hela cancer cells viability of the ICG-encapsulated hydrogels with or without NIR-light; (c) Photothermal conversion of ICG and ICG-encapsulated/ICG + DOX hydrogels after NIR irradiation (d) Graph of change in the optical densities of DPBF as a function of ROS production under NIR irradiation to ICG/ICG-encapsulated TKHG-C hydrogel..... 116

List of Tables

Table 1. Composition, gelation time (t_{gel}), drug encapsulation efficiency (DEE %), and % drug contents (DC %) of IZ-1, IZ-2, and IZ-3 hydrogels. ... 31

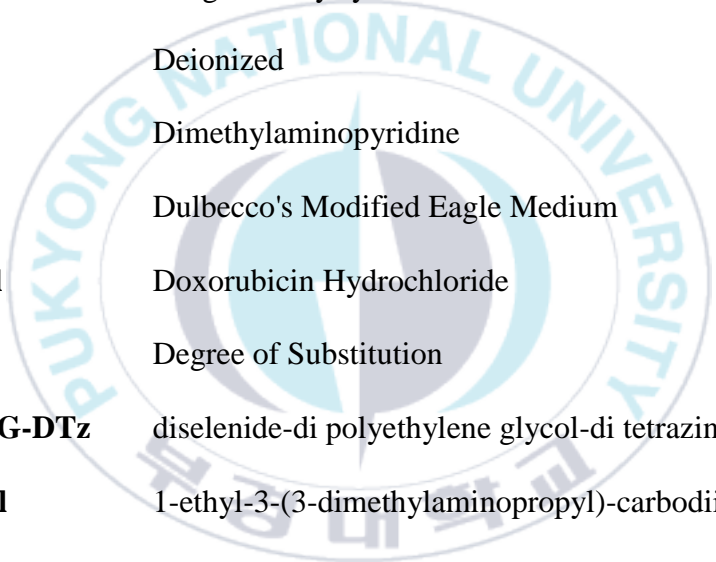
Table 2. Formulations and gelation times of CMC hydrogels. 78



List of Schemes

- Scheme 1.** Schematic illustration of the development and drug release mechanism of reduction responsive CMC-based hydrogels..... 23
- Scheme 2.** Schematic representation of synthesis of (a) Di-Selenide-Di-PEG (DSe-DPEG) (b) Tetrazine-carboxylic acid (Tz-COOH). 25
- Scheme 3.** Schematic representation of the synthesis of (a) reduction-responsive water soluble cross-linker (DPEG-DSe-DTz), (b) synthesis of CMC-Nb, and (c) formation of hydrogel via IEDDA click reaction. 32
- Scheme 4.** Graphical representation for development of ROS-responsive CMC hydrogels and their release mechanism by cleavage of thioketal bonds upon exposure of NIR irradiation. 71
- Scheme 5.** Schematic synthetic route path of precursors (a) TKDA, (b) tetrazine amine (c) ROS-responsive cross-linker (TK-DTz), and (d) development of CMC hydrogels. 80

Glossary of abbreviations and symbols



CMC	Carboxymethyl cellulose
CMC-Nb	Carboxymethyl cellulose norbornene
DC	Drug content
DDS	Drug delivery system
DI	Deionized
DMAP	Dimethylaminopyridine
DMEM	Dulbecco's Modified Eagle Medium
DOX.HCl	Doxorubicin Hydrochloride
DS	Degree of Substitution
DSe-DPEG-DTz	diselenide-di polyethylene glycol-di tetrazine
EDC. HCl	1-ethyl-3-(3-dimethylaminopropyl)-carbodiimide hydrochloride
FBS	Fetal bovine serum
G'	Shear Storage modulus
G''	Shear Loss modulus
GSH	Glutathione
ICG	Indocyanine green

IEDDA	Inverse electron demand Diels Alder
IEDDA	Inverse electron demand Diels-Alder
LVR	Linear viscoelastic region
NaBH₄	Sodium borohydride
Nb-NH₂	5-norbornene-2-methylamine
NHS	N-hydroxysuccinamide
NIR	Near Infrared
PEG	Polyethylene glycol
PTT	Photothermal therapy
ROS	Reactive Oxygen Species
TEA	Triethylamine
Tz	Tetrazine
γ_c	Critical strain
DEE	Drug encapsulation efficiency
TK	Thioketal
FDA	Food and Drug Administration
TKDA	Thioketal diacid
TBC	Tert-butyl 4-cyanobenzylcarbamate
DLE	Drug loading efficiency
MWCO	Molecular weight cut-off

DPBF

1,3-diphenylisobenzofuran



Acknowledgements

I would like to express my deepest gratitude to my supervisor and committee chair, Prof. Kwon Taek Lim for his continuous support of my PhD research, motivations, encouragements and immense knowledge. His guidance and expertise helped me during the research and writing the manuscript and this thesis. Without his valuable support, it would not be possible to conduct this project.

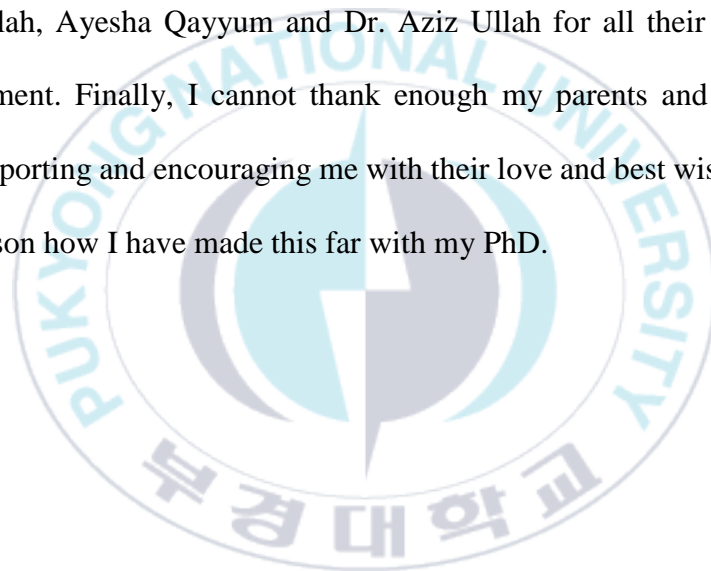
I would also like to thank Prof. Sang-Hyug Park for providing me the opportunity to join his team at *LATTE* Lab, and have access to the research facilities needed for the completion of my research. It was an amazing three years working as part of the professional group.

Besides my advisor, I would like to thank the rest of my dissertation committee: Prof. Bonggi Lee, Prof. Yeong-Soon Gal, and Prof. Yong-Hyun Kim for their insightful suggestions and participation.

I would like to thank all the Lim group members for always being helpful and supportive in all the ups and downs. In particular, I would specifically mention Dr. Muhammad Gulfam, Ali Rizwan, Trung Thang Vu, Sonyabapu Yadav, Huong Thi Hoang, Dr. Viswanathan Karthika, Dr. Parveen Kumar, Yi-jun Jo,

and Soo-Bin Joo among the past and present Lim group members. Thank you for always ready to lend a helping hand during lab work and ideas to the problems with the experiments. My sincere thank also goes to Sung-Han Jo for helping me out with the cell experiments and a lot of valuable discussions. Outside the Lim group members, I would like to thank Dr. Geun-Oak Lee, Mazahir Naqvi, Siraj ul Haq, Kashif Saleem, Muhammad Jahanzaib, Azhar Nawaz Lillah, Ayesha Qayyum and Dr. Aziz Ullah for all their support and encouragement. Finally, I cannot thank enough my parents and siblings for always supporting and encouraging me with their love and best wishes. You all are the reason how I have made this far with my PhD.

Israr Ali



Abstract

Development of Stimuli-responsive Hydrogels based on Carboxymethyl-Cellulose for Drug Delivery System

Israr Ali

Department of Smart Green Technology Engineering, The Graduate School,

Pukyong National University

Stimuli-responsive hydrogels have been widely studied in drug delivery system owing to the remotely controlled release of chemotherapeutic molecules at the targeted site. The premature drug release reduces the efficiency of therapeutic molecules and can induce unwanted adverse impacts. Whether to improve drug efficacy with minimal side effects, stimuli-responsive hydrogel could be a promising material enabled to control release of the drug under external or/and internal specific triggers (e.g. temperature, pH, redox, light, magnetic or electric field, enzyme, reactive oxygen species (ROS) etc.). The controlled dynamic behavior of the materials in transporting the therapeutic substance in physiological conditions could be regulated by carefully crafting the chemical structure of the crosslinkers.

The main objective of this dissertation is to develop and design stimuli-responsive hydrogels for on-demand drug delivery system by employing a novel crosslinkers which could be decomposed ideally under specific stimulus. Responsiveness is introduced by incorporating the cleavable moieties into the structure of crosslinkers. The hydrogels composed of carbohydrate based natural polymer i.e., carboxymethyl cellulose (CMC) crosslinked with degradable crosslinkers were synthesized and characterized. CMC was used in hydrogel system owing to the inherent properties of biocompatibility and biodegradability. The crosslinker and polymer backbone were covalently bonded through bio-orthogonal “click chemistry” reaction such as inverse electron demand Diels Alder (IEDDA) contributed to tailor the physiochemical properties of hydrogel system. This reaction was preferred since it occurred rapidly under physiological conditions by simple and facile procedure. The second part of this thesis is devoted to synthesize reduction-responsive hydrogels containing di-selenide bond. The responsive release behavior of the drug was investigated i.e., the cleavage of di-selenide bond and subsequently decomposed the hydrogel network under reducing environment. In the later part, NIR-responsive drug delivery system was developed by employing a reactive oxygen species (ROS)-cleavable thioketal crosslinker. A NIR-dye (FDA approved), indocyanine green (ICG) was encapsulated into the

hydrogel network to generate ROS-stimulus upon exposure of NIR-irradiation. The sustained and spatiotemporal release pattern of drug from its carrier was investigated by employing NIR-light known as an innocuous and non-invasive strategy.

Hydrogels were further studied in this dissertation using several characterization techniques such as, proton nuclear magnetic resonance (^1H NMR), field emission scanning electron microscopy (FE-SEM), ultraviolet-visible (UV-VIS) spectroscopy, and Fourier transform infrared spectroscopy (FTIR). The physiochemical properties were measured by using a rheometer. The gelation times, swelling behavior, porosity, and rheological properties were investigated by varying the concentration of cross-linker. The cytotoxicity of hydrogels was analyzed by using normal cells lines. Moreover, in vitro anti-tumor efficacy of the hydrogels against cancer cell lines were determined under NIR and reducing environment.

This study highlights the essential role of crosslinker involves in development and characterization of biopolymer-based stimuli-responsive drug delivery material. Reduction-responsive and biocompatible soft hydrogels derived from CMC were successfully prepared by employing diselenide (Se-Se) based crosslinker, DSe-DPEG-DTz. The hydrogels showed high swelling ratios (>35

times), tunable gelation times (1–5 min), and excellent doxorubicin (DOX) loading efficiencies (>85 %). The hydrogels demonstrated stimuli-responsive and fast release of DOX (99 %, after 12 h) in the presence of 10 mmol of glutathione as compared to the normal PBS solution (38 %). In developing of NIR-responsive hydrogels, the reactive oxygen species (ROS)-cleavable thioketal cross-linkers was used. Upon NIR-irradiation, the hydrogels showed spatiotemporal release of encapsulated DOX (>99%) owing to the cleavage of thioketal bonds by interacting with ROS generated from ICG. The in vitro cytotoxicity results revealed that the hydrogels were highly cytocompatible and did not induce any toxic effect on the HEK-293 cells. In contrast, the DOX+ICG-encapsulated hydrogels enhanced the chemotherapeutic effect and effectively inhibited the proliferation of Hela cancer cells when irradiated with NIR-light.

요약

스티뮬러스 반응성 하이드로겔은 특정 부위에서 화학요법 분자의 원격 조절된 방출 덕분에 의약품 전달 시스템에서 널리 연구되고 있다. 조기 약물 방출은 치료 분자의 효율성을 감소시키고 원하지 않는 부작용을 유발할 수 있다. 최소한의 부작용으로 약물의 효능을 향상시키기 위해, 스티뮬러스 반응성 하이드로겔은 외부 또는/그리고 내부 특정 트리거(예: 온도, pH, 산화환원, 빛, 자기장 또는 전기장, 효소, 반응산소종 (ROS) 등) 하에서 약물 방출을 조절할 수 있는 유망한 소재로 나타날 수 있다. 생체 적합성과 생분해성의 고유 속성으로 인해 탄수화물 기반 자연 고분자인 카르복시메틸 셀룰로오스(CMC)를 크로스링크된 디그레이더블 크로스링커로 사용하여 하이드로겔을 합성하고 특성화하였다. 크로스링커 및 폴리머 백본은 바이오-오소고널 "클릭 화합" 반응인 역전자 전자 수요 딜스-알더(IEDDA)와 같은 반응을 통해 공유결합되어 하이드로겔 시스템의 물리화학적 특성을 조절하는 데 기여했다. 이 반응은 생리학적 조건 하에서 간단하고 용이한 절차로 빠르게 진행되는 특성으로 인해 선호되었다.

논문의 후반부는 디셀레나이드 (Se-Se) 결합을 포함하는 환원 반응성 하이드로겔을 합성하는 데 전념되었다. 약물의 반응적 방출 행동, 즉 디셀레나이드 결합의 클리브리지 및 이후 환원 환경에서 하이드로겔 네트워크의 분해가 조사되었다. 나중에는 반응산소종 (ROS) 클리브러블 티오키탈 크로스링커를 사용하여 근적외선 (NIR) 반응성 약물 전달 시스템을 개발하였다. NIR-조사에 노출됨에 따라 ICG 에서 생성된 ROS 와 상호 작용하여 약물의 나노 지역적 방출 패턴이 조사되었다. NIR-조사는 무해하고 비침습적인 전략으로 알려져 있다.

이 논문에서 사용된 하이드로겔은 ^1H NMR, FE-SEM, UV-VIS 분광, FTIR 및 레오메트리와 같은 여러 특성화 기술을 사용하여 자세히 연구되었다. 크로스링커 농도를 변화시켜 젤레이션 시간, 팽만 행동, 기공도 및 레오로지적 특성을 조사했다. 하이드로겔의 세포 독성은 정상 세포 라인을 사용하여 분석되었으며, 무균 환경에서 암 세포 라인에 대한 하이드로겔의 체외 항암 효과가 NIR 및 환원 환경에서 결정되었다.

이 연구는 크로스링커의 중요한 역할을 강조하며 바이오 폴리머 기반 스텔러스 반응성 약물 전달 물질의 개발과 특성화에 관여함을 강조한다. 디셀레나이드 기반 크로스링커인 DSe-DPEG-DTz 를 사용하여 개발된

환원 반응성 및 생체 적합성 소프트 하이드로겔은 높은 팽만률(>35 배), 튜네이블 젤레이션 시간(1-5 분) 및 우수한 독소률(>85%)을 보여주었다. 이 하이드로겔은 글루타치온 10 mmol 의 존재하에서 PBS 솔루션 (38%)에 비해 글루타치온이 존재할 때 독소(DOX)의 유동 응답 및 빠른 방출(12 시간 후 99%)을 보여주었다. NIR 반응성 하이드로겔 개발에서는 ROS-클리블 티오키탈 크로스링커를 사용하였다. NIR-조사에 노출 됨에 따라 하이드로겔은 ICG 에서 생성된 ROS 와 상호 작용하여 NIR-조사에 노출되면 특이 및 지속적인 약물 방출 패턴을 보여주었다. 체외 세포 독성 결과는 하이드로겔이 높은.

Chapter 1 : Introduction

1.1 Smart hydrogels in drug delivery system

Hydrogels are cross-linked three-dimensional polymer network that are able to swell and retain high amount of water within their porous network. Hydrogels are three-dimensional, cross-linked networks of polymers with a porous structure that allows them to swell and store large amounts of water. These cross-linked hydrophilic networks make hydrogels soft, flexible, and elastic. Owing to their high-water content, porosity and soft structure, polymer-based hydrogels have been extensively used in diverse range of biomedical and technological applications such as tissue engineering, biosensors, cell culture, drug delivery systems, artificial implants, and tissue scaffolds [1, 2]. Because of their elevated water content, adaptable structure and porosity, hydrogels based on polymers are widely utilized in various medical and technological domains, such as artificial implants, tissue scaffolding, biosensors, cell cultivation, drug administration, and tissue engineering. The structural and mechanical properties, porosity, and stability of hydrogels depend on the type of cross-linking, composition of hydrogels and fabrication techniques [3]. The cross-linking method, hydrogel composition, and

manufacturing techniques are influential factors that determine hydrogel's mechanical and structural characteristics, stability and porosity. Further, a set of novel strategies have also been reported to prepare hydrogels which can respond smartly under internal or external stimuli such as pH, temperature, magnetic or electric field, light and redox potential. Furthermore, a variety of innovative approaches have been documented for the creation of hydrogels capable of exhibiting intelligent responses to external and internal stimuli, including pH, redox potential, temperature, light, magnetic as well as electric fields. By virtue of these stimuli, "smart" hydrogels have been widely employed in biomedical applications including drug delivery, gene delivery, and tissue regeneration [4, 5]. These stimuli have led to the widespread use of "smart" hydrogels in biomedical fields such as tissue regeneration, drug delivery, and gene delivery. Stimuli-responsive hydrogels and their emerging applications presented in Figure 1.

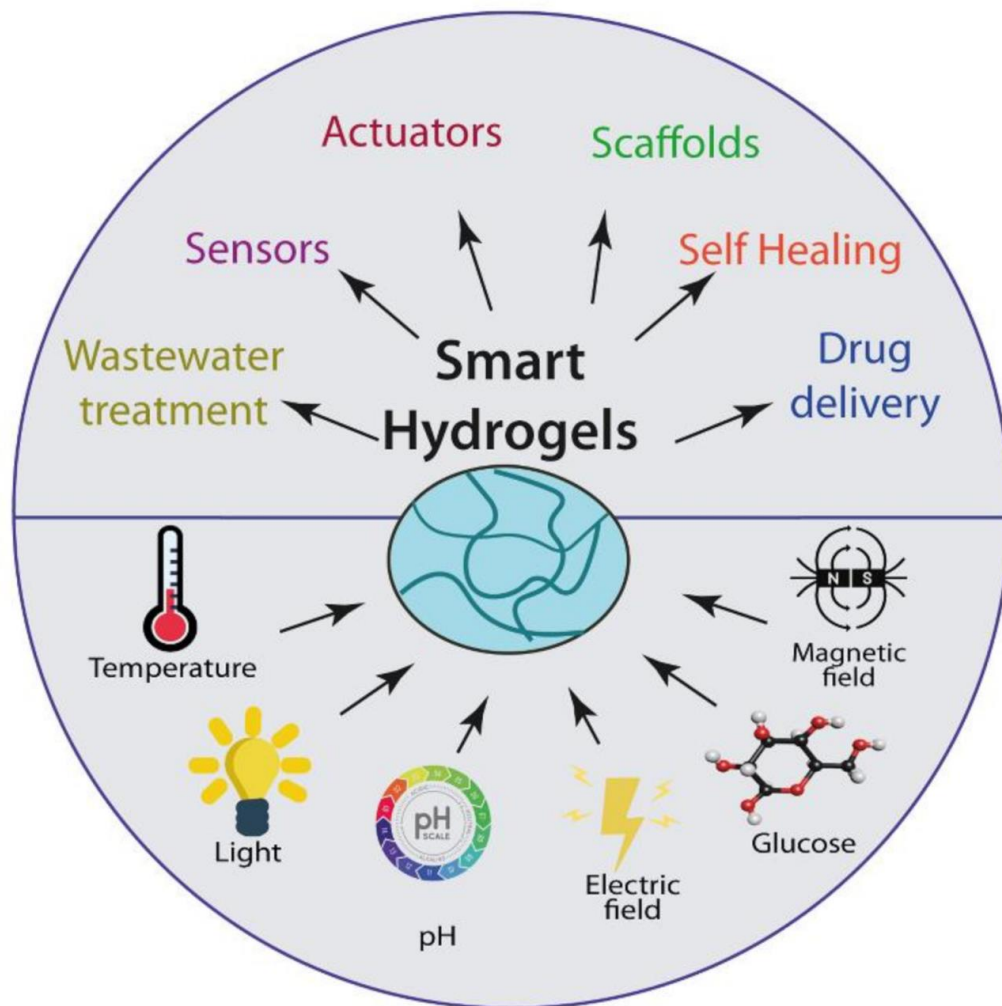


Figure 1. Smart hydrogels and their emerging applications

Natural as well as synthetic polymers have both pros and cons for applications in biomedicine, so can be used to develop hydrogels. Natural polymers are excellent in terms of their cell compatibility and biodegradability, however, they often have lower mechanical properties and are more challenging to change chemically. On the contrary, synthetic polymers offer favorable physicochemical characteristics but do not possess inherent degradability and compatibility to living tissues [6, 7].

Hydrogels based on natural polymers are mainly developed for the application in drug delivery systems (DDSs) [8]. The drug release profile is the most crucial factor to consider when creating DDSs, along with the ability to save drug molecules, loading capacity, stability, and biocompatibility. It has been demonstrated that DDSs based on hydrogels can administer medications orally, transdermally, or even by injection directly into particular tissues and organs. [9]. Various drug delivery strategies are presented in Figure 2.

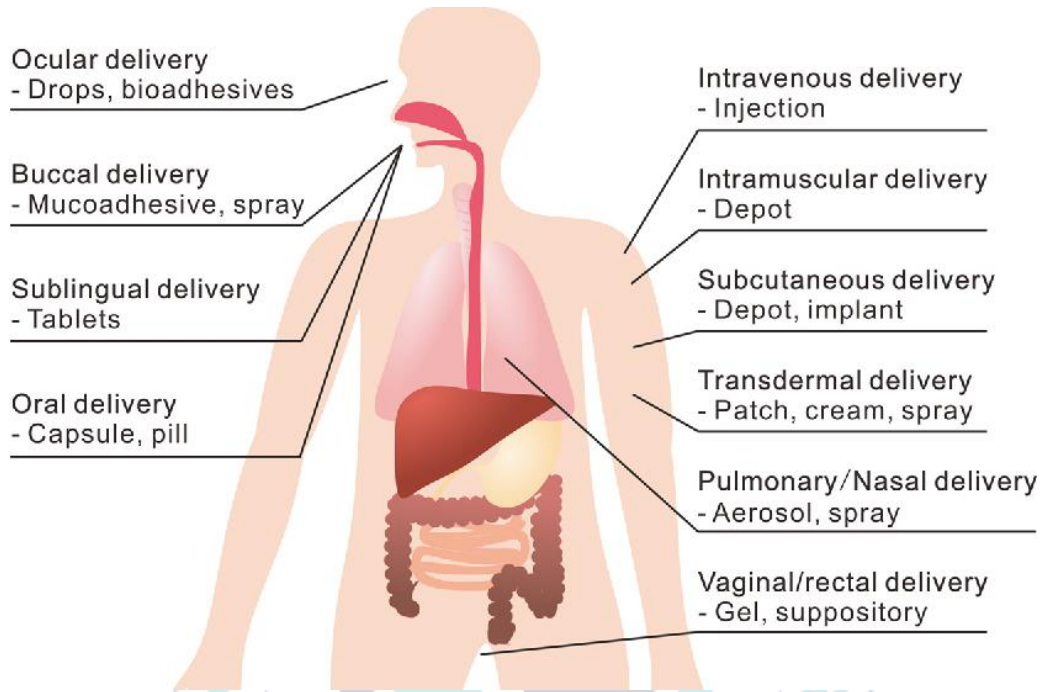


Figure 2. Drug delivery strategies

1.2 Natural polymers

Natural polymers are macromolecules which are derived from natural sources such as plant, animal, and micro-organisms. In comparison to synthetic polymers, natural polymers are attractive in biomedical applications due to their abundant availability, ubiquitousness, renewableness, biodegradability, and non-toxicity. Furthermore, the appealing biological features of natural polymers such as resemblance to the natural extracellular matrix (ECM) and excellent compatibility with living tissues offer to use in tissue engineering and drug delivery systems [10]. Based on their chemical makeup, natural polymers can be divided into two main groups: proteins and polysaccharides. Along with other macromolecules like protein and nucleotides, polysaccharides are most common carbohydrate polymers, and they are sourced from renewable materials like algae, plants, as well as microorganisms such as fungi and bacteria [11]. They are composed of several repeating units of monomeric sugars interconnected with glycosidic linkages. Polysaccharides are not only essential for providing structure and energy for organisms but also contribute in diverse biological activity and functions, including cell matrix-communication,

adhesion, and immune recognition. In addition, they are particularly important for humans because of their therapeutic properties, including their effects on the gut, antitumor, antibacterial, and antioxidant capacities [12]. Polysaccharides have gained substantial interest in design and synthesis of hydrogels owing to their exceptional qualities, which include increased hydrophilicity, biodegradability as well as excellent biocompatibility. Polysaccharide-based hydrogels are a promising class of biomaterials for biomedical applications due to their tunable biological and chemical attributes. Many polysaccharides, such as hyaluronic acid (HA), chitosan, alginate, and cellulose, can be used to synthesize the hydrogels, which offer a diverse range of advantages, including biocompatibility, biodegradability, and mucoadhesiveness [13]. Applications for cellulose, including methyl cellulose, hydroxypropyl cellulose, and carboxymethyl cellulose are currently investigated in the fields of tissue engineering and drug delivery. Water soluble carboxymethyl cellulose (CMC) has garnered increasing attention recently as a means of improving the biological and physiochemical characteristics of hydrogels based on carbohydrates [14]. The structural resemblance of hyaluronic acid (HA) to glucosaminoglycans (GAGs), which are crucial for controlling cells in the extracellular matrix (ECM), makes HA an especially appealing polymer for

biomedical applications. HA hydrogels have been used for a variety of biomedical applications, including drug delivery, tissue engineering, and wound healing [15]. A cationic polymer derived from the shells of crustaceans is called chitosan. It is biocompatible and biodegradable with good mucoadhesive qualities. Hydrogels based on chitosan are frequently employed in applications involving cell/tissue attachment and drug delivery. However, chitosan has limited solubility at neutral pH, which can be a challenge for some applications [16]. An anionic polymer derived from brown algae is called alginate which is both biocompatible and biodegradable. It can form hydrogels through ionic crosslinking with divalent cations such as calcium. Alginate hydrogels are widely used in food additives, drug delivery, tissue engineering, and wound dressings. However, alginate hydrogels have poor inherent cell adhesion and non-physiological degradation properties, which need to be considered for in vivo applications [17]. Overall, polysaccharide-based hydrogels offer a number of advantages for biomedical applications, including tunable properties, biocompatibility, biodegradability, and mucoadhesiveness. These hydrogels have the potential to be used for a wide range of biomedical applications, such as drug delivery, tissue engineering, wound healing, and regenerative medicine.

1.2.1 Cellulose

The term "cellulose" was first used in 1838 by the French chemist Anselme Payen, who combined the French terms "cellule" (which means a living cell) and "glucose" to emphasize the molecular structure and biological source of this essential material. Cellulose structure is composed of linear chains of β -D-glucopyranose units linked together by β -(1 \rightarrow 4) glycosidic bonds [18]. Hydrogen bonds can form between and within molecules of cellulose chains due to the existence of free hydroxyl groups, which also create a compact crystalline structure. As a bio-sourced, cellulose is inherently bioactive, biocompatible and biodegradable, possessing several advantages in health areas for its antibacterial activity, however, its main application is in the generation of materials and metrics [19].

Cellulose exhibits unique properties, including a nanometer-scale fibrous structure with high surface area, adjustable porosity, and outstanding mechanochemical characteristics, similar to those of nanofibrous polymers. Although, cellulose is typically not soluble in water and has few functional groups which make it limited in biomedical applications [20]. However, cellulose possesses several functional groups (e.g. hydroxyl groups) on the backbone structure, which provide active sites

for further functionalization. The cellulose derivatives, particularly soluble in water such as (methyl cellulose (MC), hydroxypropyl cellulose (HPC), and sodium carboxymethyl cellulose (Na-CMC)) have been received significant attention as biomaterials for 3D bioprinting, tissue engineering, drug delivery and biosensors, [21] owing to their inexpensive, high hydrophilicity, cell compatibility, and biodegradability.

1.2.1.1 Carboxymethyl-cellulose

Cellulose is a naturally occurring polymer with a large number of hydroxyl groups on its backbone, it is bioactive, biodegradable, and biocompatible by nature. These hydroxyl groups also serve as active sites for additional functionalization [22]. Carboxymethyl cellulose (CMC) is a readily available cellulose derivative that is produced by partially substituting carboxymethyl groups for hydroxyl groups on cellulose's pyranose group. CMC is a negatively charged polymer with a molecular weight ranging from thousands to millions of Daltons. It appears as a white fibrous and possesses qualities of being odorless, tasteless, and hygroscopic. CMC has the tendency to disperse in water and form a transparent colloidal solution, i.e., clear gel like solution [23]. Since carboxyl groups are available, these qualities provide

additional benefits like low viscosity, high hydrophilicity, and film-forming abilities, which makes it a desirable hydrogel matrix component [24]. Thanks to its low toxicity, minimal immunogenicity, and good biodegradability and biocompatibility, CMC-gels have been shown to be an extremely promising substance for clinical drug delivery applications. The key feature of a hydrogel is its ability to absorb large amounts of liquid while maintain its structural integrity with optimal mechanical strength [25]. However, CMC hydrogels are found superabsorbent with high degree of swelling ratio. This is because the carboxylate groups (COO⁻) of CMC are hydrophilic and polar, which enables the polymer chains to grow and interact with molecules of water. Since they can hold the most therapeutic agent in their porous and hydrophilic network, CMC hydrogels are appealing because of this feature. Meanwhile, the loaded drug retains into the crosslinked network of hydrogels and subsequently delivers to the targeted area with inhibition of premature release [26]. Different cross-linking agents can be used to create CMC hydrogels for cancer therapy through chemical or physical cross-linking techniques. Non-covalent interactions like ionic bonding, hydrogen bonding, or associative polymer-polymer interactions result in the formation of physical cross-linked hydrogels. Conversely, covalent bonds made with a cross-

linking agent form the basis of chemically cross-linked hydrogels [27]. In this dissertation, the CMC hydrogels prepared from novel biocompatible cross-linkers have been studied to investigate the physiochemical properties and drug loading efficiency.

1.3 Fabrication of hydrogel

Synthesis of hydrogels is typically a complex mechanism that requires a good understanding of how polymers interact with each other and how crosslinks between polymer chains influence the hydrogels composition and characteristics. Typically, the attributes of a hydrogel are contingent upon the cross-linking method, the cross-linking agent employed, and the chemical nature of the cross-linking reaction.

1.3.1 Cross-linking of hydrogels

Hydrogels are formed by the incorporation of Crosslinkers which interconnected the polymeric chains through cross-linked bridges and give strength to the hydrogel network. Various kind of crosslinkers have been established to fabricate hydrogels such as ionic crosslinkers and covalent crosslinkers [28]. The hydrogels developed

from ionic crosslinkers are useful due to reversible and dynamic bond but their structure is weak and unstable. However, the hydrogels with covalently linkages are generally appealed for drug delivery application. These hydrogels are not only stable but also offer some additional advantages. For covalent linkages, “bio-orthogonal click reactions” have been accepted as a promising approach. Further, crosslinkers with specific structures, covalent bonding chemistry, and on-demand dissociation links could be designed and fabricated. This could later be used to develop a trigger-release or localized on-demand drug delivery system.

1.3.2 Bio-orthogonal Click chemistry reactions

Carolyn R. Bertozzi, and Morten Meldal, and K.B Sharpless received the 2022 Nobel Prize in Chemistry for introducing the concept of Bio-orthogonal reactions and Click chemistry. K.B Sharpless proposed the term “Click Chemistry” associated with such type of chemical reactions that can occur in biological systems with high yield, high chemo-selectivity at their targets, wide in scope, and proceed under mild conditions, and generate only byproducts which could be separated without chromatography [29]. Click chemistry is a new approach permits to molecular assembly of biomolecules by simple and fast reaction and allows to the

attachment of other particles. The design of click chemistry was inspired by the principal of nature. Various kinds of click chemistry reactions are presented in Figure 3. Inverse electron demand Diels Alder (IEDDA) reaction and norbornene tetrazine ligation are the set of “bio-orthogonal click” pathways which are facile and common reactions applied in click chemistry technique.



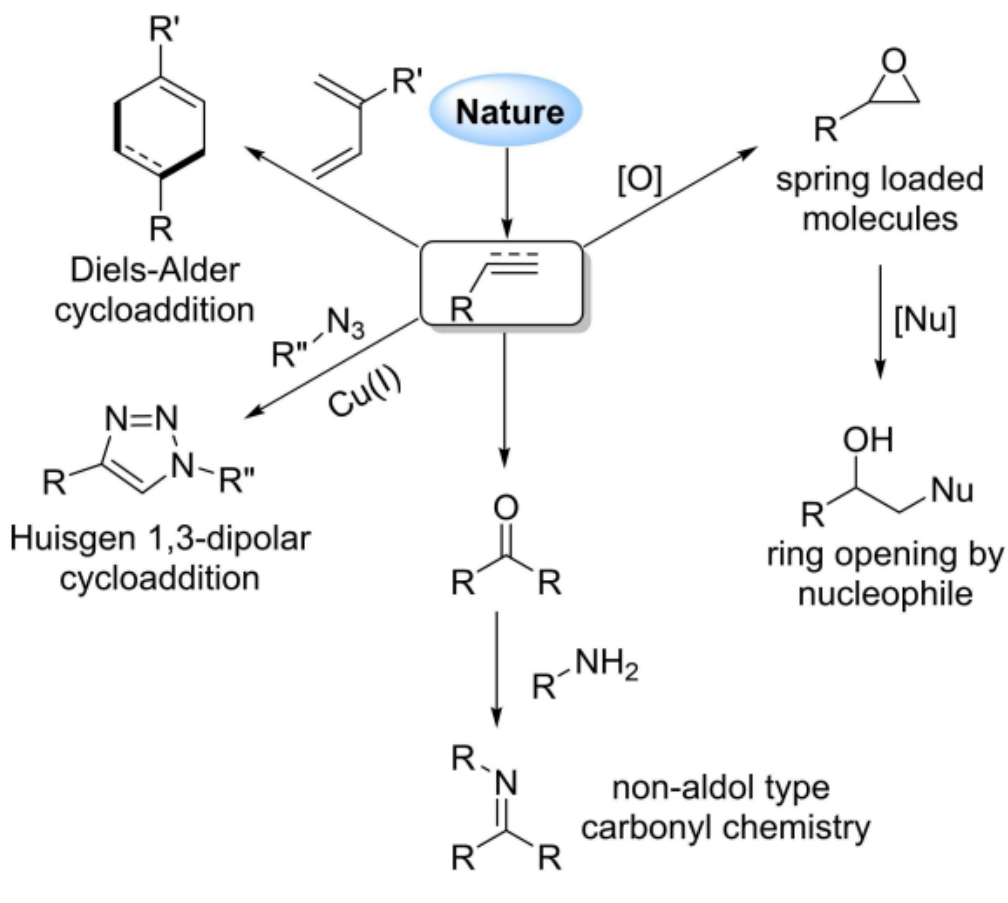


Figure 3. Various kinds of click chemistry reactions matches with click chemistry

In this dissertation, the clickable crosslinkers and biopolymer backbones with strained alkenes are set to design for click chemistry which can undergo a fast and facile reaction under physiological conditions. The precise control and on-demand

drug release system depends on primarily two major factors: 1) type of click chemistry 2) design of crosslinker.

1.3.3 On-demand cleavage of cross-linkers

During the drug transportation, the premature drug release is not only increasing the loss of therapeutic substance but also reduce the therapeutic efficiency. To address this limitation, the localized on-demand drug delivery systems have gained utmost importance owing to the precise control and effective delivery of therapeutic substances to the targeted site. However, the promising on-demand drug delivery carriers have been designed which could smartly exploited in response of physical and chemical (internal or external) stimuli. The external triggers could be temperature, pH, redox, enzyme, reactive oxygen species (ROS) etc. and the external triggers include light (NIR or UV), electric or magnetic fields, and sound etc.

In constructing of stimuli responsive hydrogels for cancer therapy, the cleavable moieties are generally incorporated which could be triggered by applying the combination of internal and/or external stimuli. Redox potential gradient is well known naturally occurring trigger in tumorous environment. The other gradients

such as pH and ROS also exist in tumors cells owing to the high value of pH and ROS level as compared to normal cells. In this dissertation, NIR and reduction-responsive drug transportation system was developed by introducing the cleavable moieties in the hydrogel structure. This system was precisely controlled to deliver the therapeutic substances to the tumor sites by employing the smart hydrogels.



Chapter 2 : Reduction-responsive and bio-orthogonal carboxymethyl cellulose based soft hydrogels cross-linked via IEDDA click chemistry for cancer therapy application

2.1 Introduction

Hydrogels constructed from biopolymers possess inherent advantages i.e., high water absorbent, biocompatibility, biodegradability, and capability to mimic the microenvironment of native tissues [30]. These properties make them attractive for numerous biomedical applications including tissue engineering and drug delivery [31]. Among various drug carriers, injectable hydrogels have evolved into an efficient method for the treatment of solid tumors [32, 33]. This method is convenient, safe, and can reduce the discomfort of patients owing to its minimal invasiveness [34]. For injectable hydrogels, it is required to use a soft biopolymer which possesses inherent elastic properties mimicking the natural extracellular matrix of tissues/organs, has high biocompatibility, good swelling properties, fast degradation profile, and rapid clearance from the human body [35, 36]. In this framework, naturally existing carbohydrate-based polymers such as cellulose, alginate, chitosan, and hyaluronic acid containing long chains of mono/disaccharide

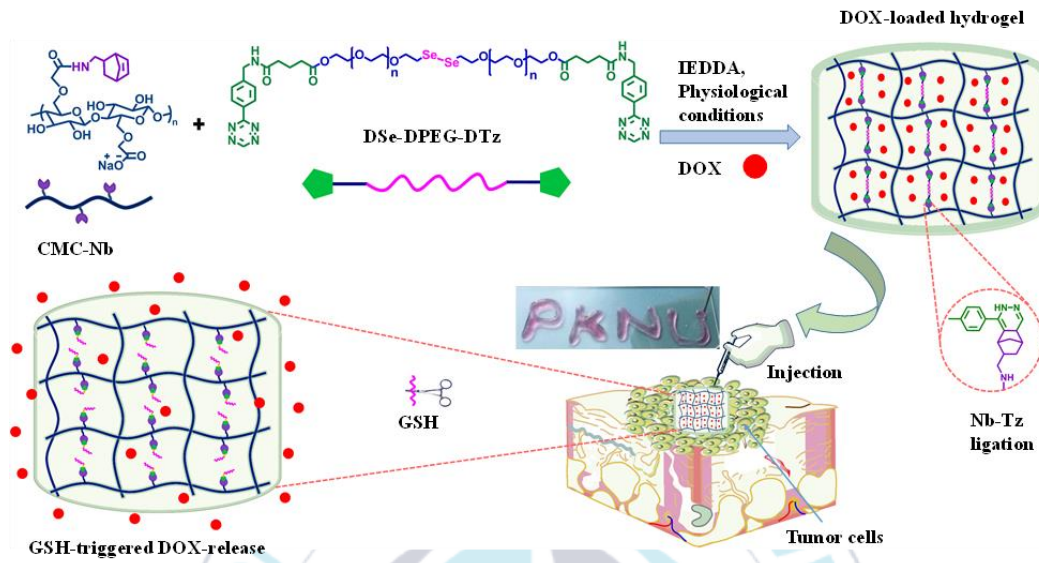
units connected with glycosidic linkages, are regarded as suitable biopolymers [37]. Particularly, cellulose is one of the most abundant, inexpensive, and renewable carbohydrate polymers. As a bio-sourced polymer, cellulose is inherently bioactive, biocompatible and biodegradable, possessing several functional groups (e.g. hydroxyl groups) on the backbone structure, which provide active sites for further functionalization. Compared to cellulose, carboxymethyl cellulose (CMC) obtained from the partial substitution of hydroxyl groups on a pyranose group of cellulose by carboxymethyl groups offers some additional advantages, such as high hydrophilicity, low viscosity, and film-forming properties owing to the availability of carboxyl groups, making it an attractive constituent of a soft hydrogel matrix [38]. A wide range of various cross-linking methods (e.g. physical and chemical cross-linking) have been carried out to synthesize CMC-based hydrogels, previously. Among them, chemical cross-linking has been accepted as a more powerful tool to stabilize the hydrogel networks. Chemical cross-linking strategies such as Schiff-base reaction, Michael addition, and azide-alkyne cycloaddition reactions have been used to engineer CMC-based hydrogels [39]. Although these reactions are simple and suitable for controlling the physical properties of the resulting hydrogels, a majority of the reactions needs toxic reagents and catalysts,

which often reduce the biocompatibility of the corresponding materials. To overcome these issues, “biorthogonal click” pathways have been developed as a substitute method to fabricate biocompatible hydrogels [40]. Our research group has recently utilized one of the bio-orthogonal click reactions (i.e. inverse electron demand Diels–Alder (IEDDA) reaction) between tetrazine (Tz) and norbornene (Nb) functional groups to design hydrogels [41, 42]. This facile reaction has shown considerable advantages in developing injectable hydrogels such as mild conditions, ultrafast reaction rate, and high chemo-selectivity. Additionally, the IEDDA reaction liberated N₂ gas as a by-product which generated additional porosity in the hydrogel networks. However, the low aqueous-solubility of the click-able cross-linker, necessitated the incorporation of an organic solvent (DMSO) during the preparation of hydrogels.

Over the last few years, ongoing research has been focused on the design of stimuli-responsive drug delivery system (DDS) to improve the tumor treatment efficacy and to decrease the significant adverse effects of chemotherapeutic drugs. Particularly, stimuli-responsive hydrogels found to be promising in DDS, which could be exploited elegantly in response to specific physical and chemical (internal or external) stimuli [43, 44]. These physiochemical triggers could be pH, enzymes,

temperature, redox potential, light, and electric or magnetic fields, etc. [45-50]. The stimuli-responsive hydrogels have shown numerous applications in biomedicine, tissue engineering, soft electronics, sensors, and actuators [48, 51-53]. Among them, redox responsive hydrogels have become a research hotspot in cancer therapy because of the naturally occurring redox potential gradient in a tumorous environment [54]. It has been investigated that the concentration of glutathione (GSH) in the intracellular fluids is substantially higher (~10 mmol) than found in the extracellular fluids (2-20 μmol) [55]. Furthermore, the intracellular quantity of GSH in tumor cells is at least 4-fold higher than found in healthy cells [56]. Therefore, reduction-labile groups (such as di-selenide or di-sulfide) could be incorporated in DDS because these are cleavable at an overexpressed concentration of GSH existing in tumor microenvironment, while remain relatively stable in healthy tissues, extracellular fluids, and plasma. [56, 57]. Di-selenide bonds which have weak bond energy (172 kJmol^{-1}) could be ruptured easily in the reducing environment [58]. On this account, cross-linked hydrogels containing di-selenide bonds could be utilized in a controlled DDS or other biomedical applications [41, 58, 59].

Recently, we have reported a di-selenide-based cross-linker designed to contain two PEG spacers, which increased the aqueous solubility of the cross-linker. Motivated by these findings, we paid attention to develop novel CMC-Nb based soft hydrogels chemically cross-linked by a highly aqueous-soluble and reduction responsive cross-linker through ultrafast IEDDA click reaction. It is hypothesized that this strategy will produce soft hydrogels with low storage moduli (G') and fast gelation time, which are required for injectable applications. In addition, the release kinetics of a loaded drug or a therapeutic molecule could be controlled by the reduction responsive cross-linkages in a tumor microenvironment. Scheme 1 illustrates the formation of injectable hydrogels and the drug release mechanism. The prepared hydrogels exhibited low storage moduli in the range of 74 ~ 160 Pa and high swelling ratios (>35 times). The drug release assessment showed that the formulated hydrogels released the encapsulated doxorubicin (DOX) rapidly in a reducing environment (10 mmol GSH), whereas no significant release of DOX was observed in PBS. The cytotoxicity results demonstrated that the synthesized cross-linker and the hydrogels were biocompatible with normal HEK-293 cells. Moreover, DOX-encapsulated hydrogels induced antitumor activity in a model cancer cell line (BT-20 cancer cells).

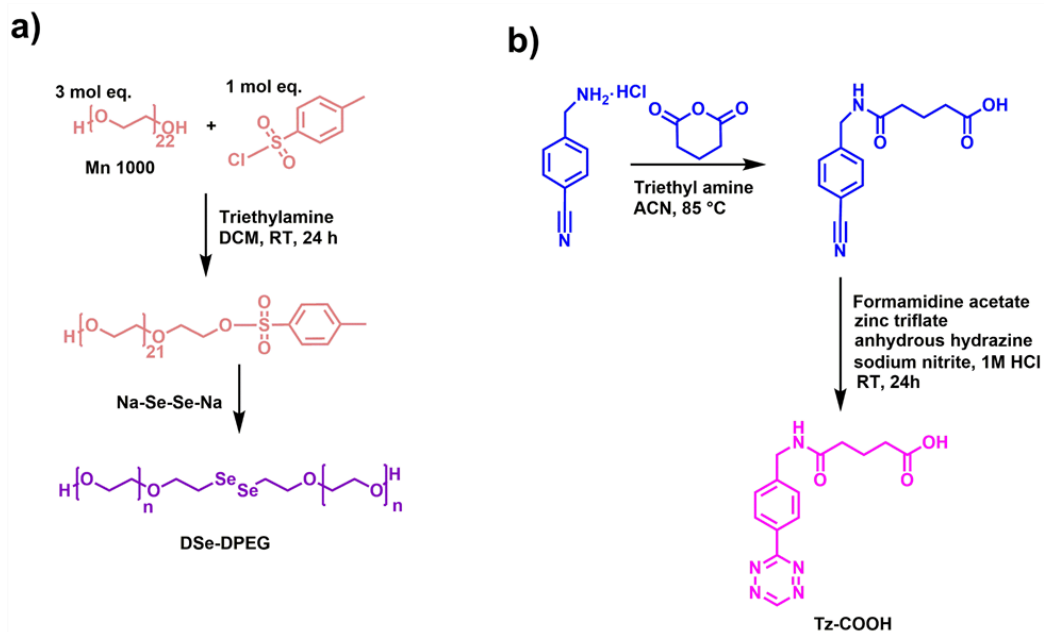


Scheme 1. Schematic illustration of the development and drug release mechanism of reduction responsive CMC-based hydrogels.

2.2 Experimental and Characterization

2.2.1 Materials

CMC (D.S=approx. 1050), 5-norbornene-2-methylamine (Nb-NH₂, 98 %), 1-ethyl-3-(3-dimethylaminopropyl)-carbodiimide hydrochloride (EDC. HCl, 99 %), N-hydroxysuccinamide (NHS, 98%), and selenium powder (99.99%) were purchased from Tokyo Chemical Industry (TCI, Japan) and used without further purification. Polyethylene glycol 2000 (PEG), sodium borohydride (NaBH₄, 99%), sodium chloride (NaCl, 99%), trimethylamine (TEA, 99%), 4-dimethylaminopyridine (DMAP), and L-Glutathione reduced (GSH) were procured from Sigma Aldrich (Korea). 4-(Aminomethyl)benzotrile hydrochloride (98%, Matrix Scientific), and zinc(II) trifluoromethanesulfonate (98%, TCI), and *p*-toluenesulfonyl chloride (98%) was obtained from Junsei Chemical Co., Ltd (Tokyo, Japan). DOX was supplied by Boryung Pharm. Co. (Korea). All other chemicals and solvents were of analytical grade and used as received. 2, 2'-((diselanediy)bis(ethane-2, 1-diy))bis(poly(oxyethylene) (DSe-DPEG) and 5-((4-(1,2,4,5-tetrazine-3-yl)benzyl)amino)-5-oxopentanoic acid (Tz-COOH) were synthesized according to our previous reports [60] with slight modifications (Scheme 2a-b), and fully characterized by proton NMR and FTIR (Figure 4a-b and Figure 5a-b, respectively).



Scheme 2. Schematic representation of synthesis of (a) Di-Selenide-Di-PEG (DSe-DPEG) (b) Tetrazine-carboxylic acid (Tz-COOH).

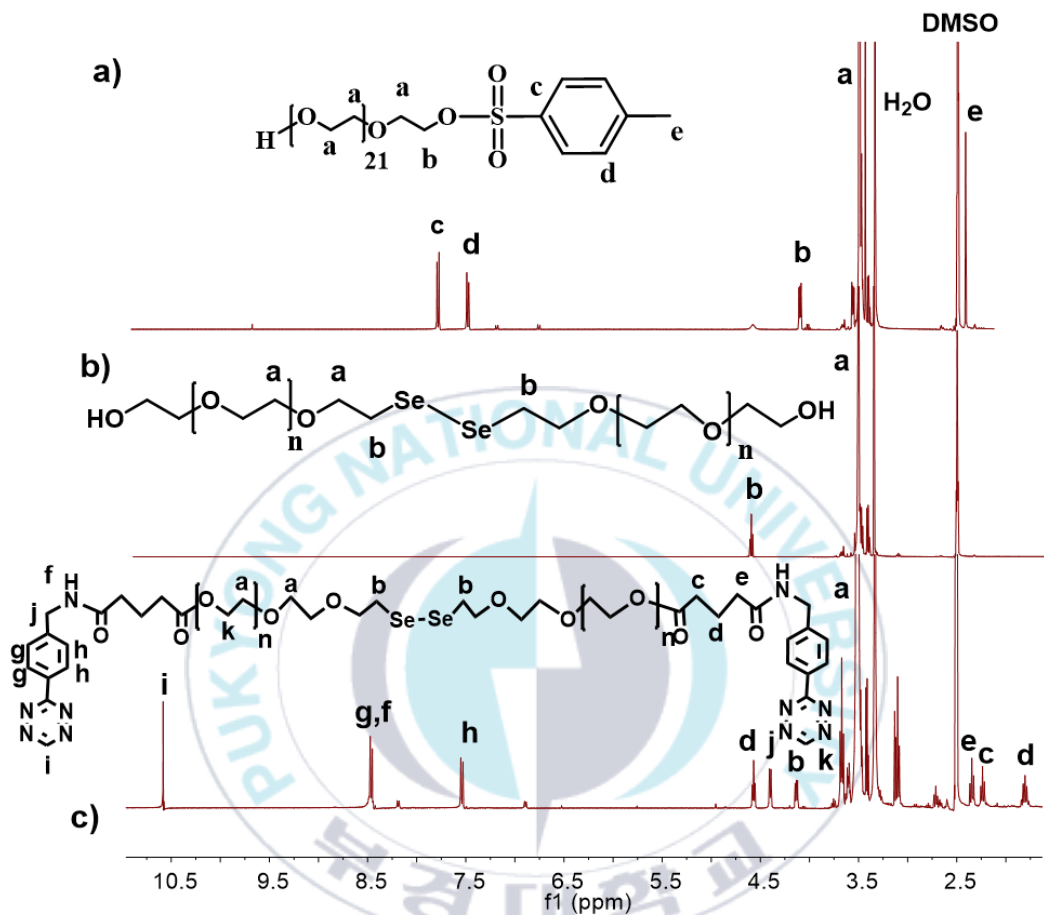


Figure 4. ^1H NMR spectra (a) PEG-tosyl (b) DSe-DPEG (c) DSe-DPEG-DTz.

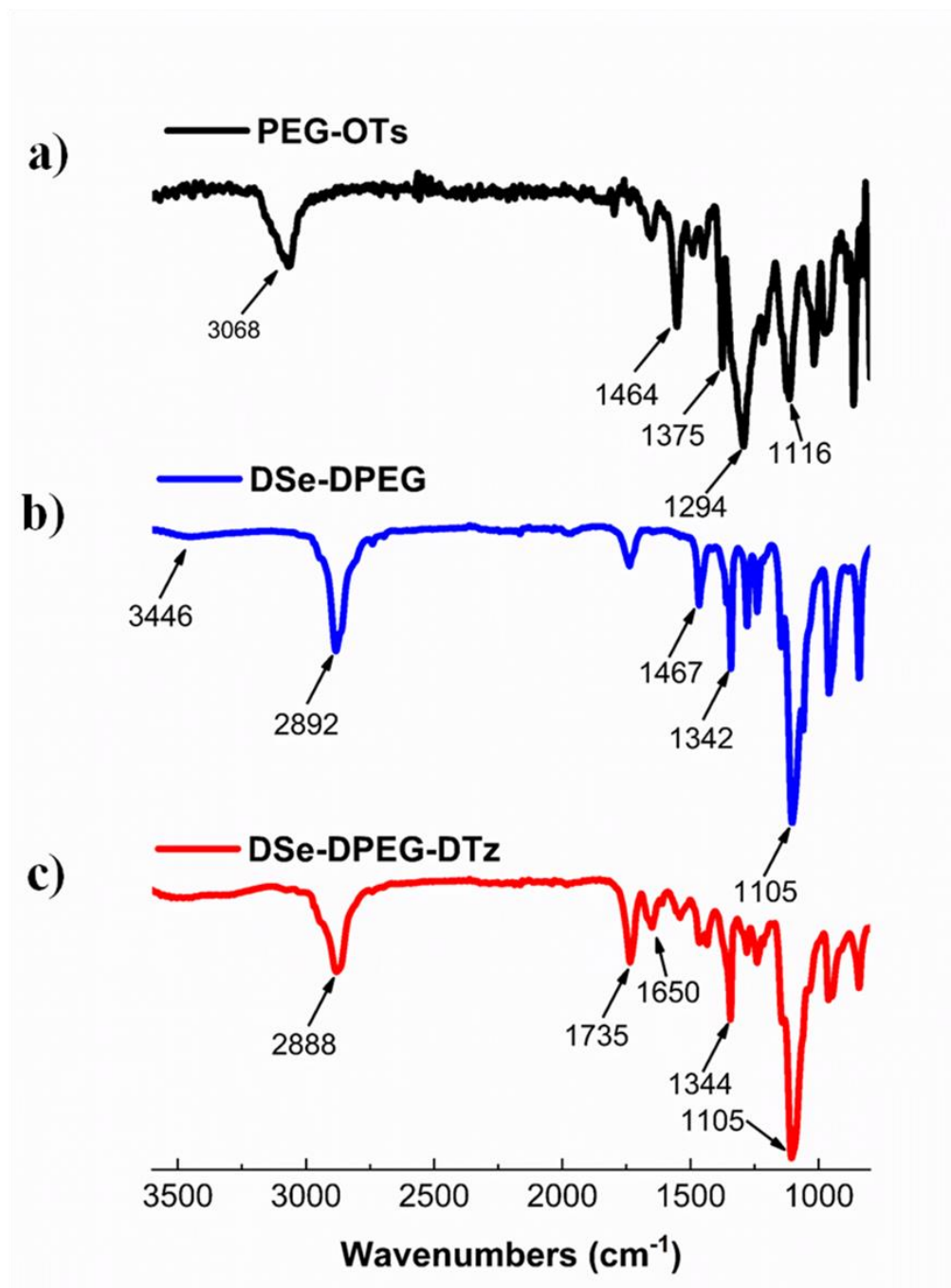


Figure 5. FTIR spectrum of (a) PEG-tosyl (b) DSe-DPEG (c) DSe-DPEG-DTz.

2.2.2 Synthesis of water-soluble DSe-DPEG-DTz cross-linker

The DSe-DPEG-DTz cross-linker was synthesized by an esterification reaction between Tz-COOH and DSe-DPEG according to an established protocol [60] with slight modifications, as illustrated in Scheme 2a. Briefly, Tz-COOH (200 mg, 0.633 mmol) was stirred in a mixed solvent system comprising DCM (9 mL) and DMSO (1 mL) in a round bottom flask at 0 °C under N₂. Afterwards, EDC (127.2 mg, 0.633 mmol) solution in DCM (5 mL) and DMAP (81.06 mg, 0.663 mmol, dissolved in 5 mL of DCM) were introduced into the reaction mixture. The reaction was stirred for 1 h under N₂. To this reaction mixture, DSe-DPEG (572.266 mg, 0.2654 mmol) solution in DCM (1 mL) was added. The reaction was first stirred at 0 °C for 1 h and then at room temperature (RT) for 48 h under N₂. The crude product was then mixed with 100 mL of DCM, washed with 100 mL of sodium bicarbonate and 2 × 100 mL of deionized (DI) water, and then with 50 mL of brine. A small amount of anhydrous magnesium sulfate was introduced to dry the organic layer. Subsequently, the organic phase was filtered and dried by using a rotavap. Finally, the product was recrystallized in a 4-fold ice-cold diethyl ether, filtered, and dried

under vacuum to obtain a pink solid. The final product was confirmed by ^1H NMR and FTIR spectroscopy, as shown in Fig. S2c and S3c, respectively.

2.2.3 Synthesis of CMC-Nb

CMC was functionalized with Nb groups *via* an EDC coupling reaction based on a previous work with slight modifications [61], as shown in Scheme 2b. Briefly, 1 g (0.0036 mmol) of sodium-CMC was dispersed in 100 mL of DI water to prepare a uniform solution (1 wt. %). Next, 0.58 g (3.04 mmol) of EDC. HCl and 0.34 g (3.04 mmol) of NHS were incorporated into the CMC solution, and then the reaction was stirred at RT for 1 h to activate the carboxylic acid functionalities of CMC. Afterwards, 0.37 mL (3.04 mmol) of 5-norbornene-2-methylamine was introduced, and the mixture was stirred continuously at RT for 24 h. A small quantity of NaCl was added and the contents were stirred again for 1 h. The product was precipitated by adding 5-fold ice-cold acetone. Subsequently, white precipitates were collected after vacuum filtration using a Buchner funnel. The precipitates were re-dissolved in DI water at 1 % (w/v) and dialyzed against DI water by using a dialysis membrane (MWCO ~ 12-14 kDa) for 3 d. The pure CMC-Nb product was obtained after lyophilization.

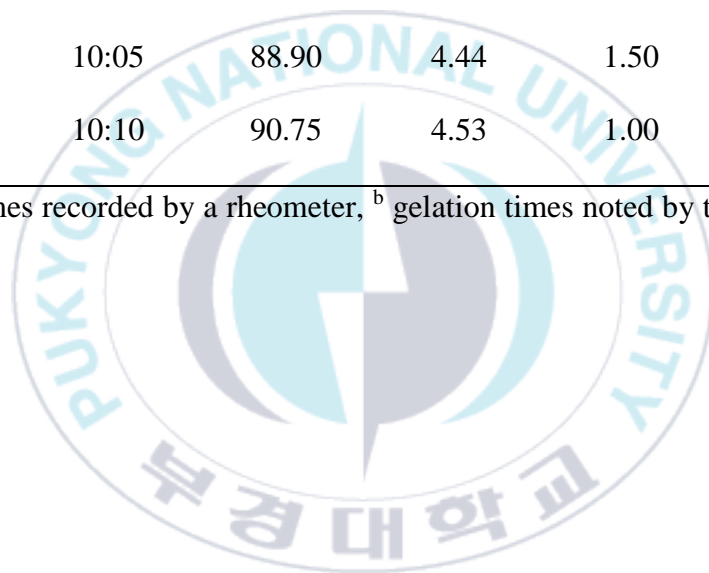
2.3 Preparation of hydrogels

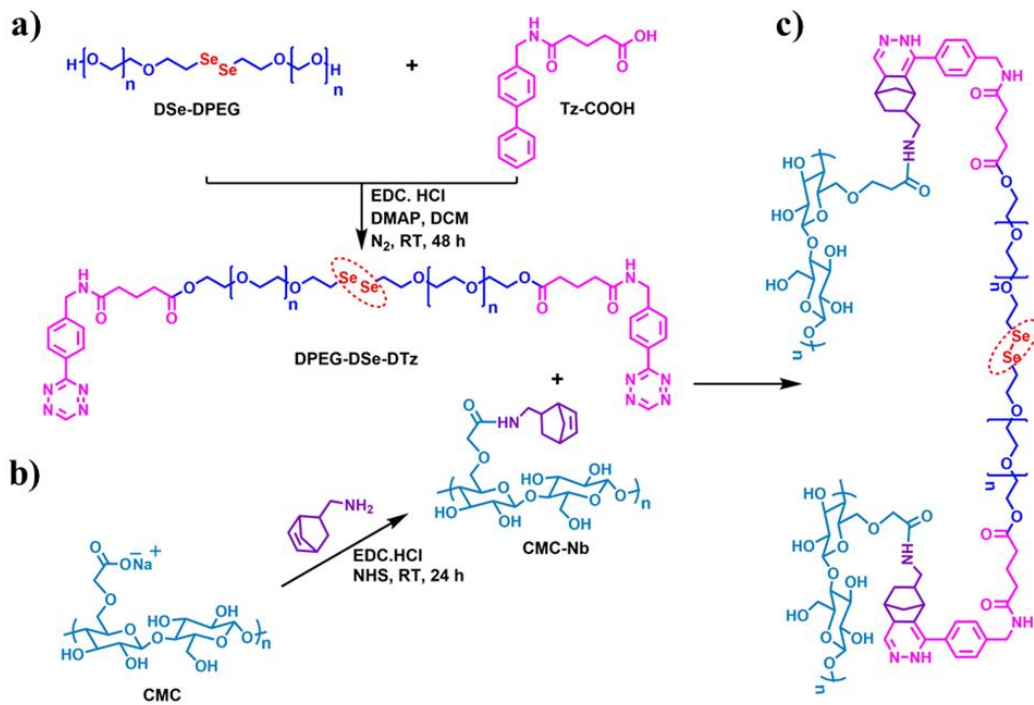
In a typical procedure, CMC-Nb solutions were mixed with DSe-DPEG-DTz at ambient temperature to form chemically cross-linked hydrogels with fast gelation time (Scheme 3c). The hydrogels were formulated with three different ratios of the cross-linker (coded as IZ-1, IZ-2, and IZ-3) to investigate the physicochemical properties of the hydrogels. Briefly, 200 μL of 2% solution (w/v) of CMC-Nb was prepared in DI water, and various molar concentrations of the cross-linker (10/10, 10/05, 10/2.5 Nb/Tz molar ratio, as shown in Table 1) were mixed with the solutions by using a vortex to form hydrogels. The gelation times of the hydrogels were recorded by an inverted-tube test using a digital time meter.

Table 1. Composition, gelation time (t_{gel}), drug encapsulation efficiency (DEE %), and % drug contents (DC %) of IZ-1, IZ-2, and IZ-3 hydrogels.

Samples	Feed ratio (Nb:Tz)	DEE (%)	DC (%)	Gelation time (t_{gel})	
				(t_{gel}) ^a	(t_{gel}) ^b
IZ-1	10:2.5	85.60	4.28	4.83	6.00
IZ-2	10:05	88.90	4.44	1.50	4.41
IZ-3	10:10	90.75	4.53	1.00	2.50

^a gelation times recorded by a rheometer, ^b gelation times noted by the invert-tube method.





Scheme 3. Schematic representation of the synthesis of (a) reduction-responsive water soluble cross-linker (DPEG-DSe-DTz), (b) synthesis of CMC-Nb, and (c) formation of hydrogel via IEDDA click reaction.

2.4 Characterization of materials

¹H NMR spectra were obtained using a JEOL nuclear magnetic resonance (NMR) spectrophotometer. Scanning electron microscopy (SEM) was performed using a MIRA3 TESCAN SEM to investigate the surface morphology of hydrogels. An Agilent Cary640 Fourier transform infrared (FTIR) spectrometer was used to confirm the functional groups of the synthesized materials. Samples were placed in liquid nitrogen for 2 min and cut carefully with a scalpel blade to examine cross-sectional morphology. An ultra-thin layer of gold metal was coated on the sample before SEM analysis. UV-vis spectroscopy was conducted to record the wavelength range between 400 and 600 nm using a UV-vis spectrophotometer (Optizen POP). Rheological properties were measured from a strain-controlled rheometer (ARES-G2M TA Instruments) using an 8mm diameter parallel plate fixture at 25 °C.

2.4.1 Rheological analysis

To investigate the viscoelastic behavior of the hydrogels, CMC-Nb and DSe-DPEG-DTz cross-linker were mixed uniformly for 15 s using a vortex before the mixture was placed on the measuring disk of a rheometer. All rheological assessments were carried out at 25 ± 0.1 °C on a 20 mm geometry and a 250 μ m

gap. In the time sweep test, a continuous strain of 1% and an angular frequency of 10 rad/s were used, whereas, the frequency sweep test was carried out at ascending angular frequencies (0 to 100 rad/s) at a constant strain of 1%. Whereas, the dynamic oscillatory strain amplitude sweep experiments were recorded at ascending strains ranging from 0.1 to 10000% at a constant frequency of 10 rad/s.

2.4.2 Swelling study

A simple gravimetric method was used to determine the swelling behavior of the hydrogels. Briefly, dried hydrogels were immersed in PBS (pH 7.4) at RT. Then, the swollen hydrogels were weighed at specific time intervals after removing excess PBS from the surface of the hydrogels using a filter paper. This procedure was repeated until an equilibrium swelling was achieved. The equilibrium swelling ratio (ESR) was calculated by using the following Eq. (1).

$$\text{ESR (\%)} = \frac{W_s - W_d}{W_d} \times 100 \quad (1)$$

Where W_d and W_s are the weights (mg) of dried and swollen hydrogels, respectively.

2.4.3 Drug loading

An anticancer drug (DOX) was used as a model therapeutic molecule to estimate the drug encapsulation efficiency (DEE %) and % drug contents (DC %) of the formulated hydrogels. A DOX solution was prepared at a 1 mg/mL concentration in PBS. Then, it was incorporated with the CMC-Nb solution by using a vortex for 5 min at RT. Subsequently, the cross-linker (DSe-DPEG-DTz) solution in PBS was added into the mixture (conforming to various mol. ratios as described in Table 1), and the solution was gently mixed by using a vortex. Finally, the hydrogels were frozen and lyophilized. To determine DEE % and DC %, dried DOX- loaded hydrogels were submerged in PBS for 15 min to remove the unloaded drug from the surface of the hydrogels. After rinsing, the concentration of DOX in the rinsing solution was analyzed by a UV-Visible spectrophotometer at 485 nm. DEE (%) and DC (%) were calculated by following equations 2, and 3, respectively:

$$\text{DEE (\%)} = \frac{\text{Amount of DOX in feed} - \text{Amount of DOX in supernatant}}{\text{Amount of DOX in feed}} \times 100 \quad (2)$$

$$\text{DC (\%)} = \frac{\text{Weight of loaded DOX}}{\text{Weight of hydrogels}} \times 100 \quad (3)$$

2.4.4 Drug release analysis

To investigate the drug release profile, the rinsed hydrogels IZ-2/DOX and IZ-3/DOX were immersed in 35 mL of either PBS (pH~7.4) or 10 mmol GSH solution and were gently agitated (100 RPM) at 37 °C. Aliquots of 3 mL were collected from vials periodically at a predetermined time interval. Additionally, a fresh solution of 3 mL of PBS or GSH was added back into each vial to compensate the withdrawn volume. The quantity of released DOX was assessed by using a UV-Visible spectrophotometer (485 nm) based on a calibration curve of DOX. The dilution factor was considered to calculate the cumulative release of DOX.

2.4.5 Hemolysis assay

Hemolysis assays were performed to evaluate the hemocompatibility of the prepared hydrogels (IZ-2 and IZ-3) with mouse red blood cells (RBCs). First, the hydrogels were immersed in saline, and extracts of the hydrogels (500 µL) were collected after 2 h. Then, freshly collected mouse blood was added into the extracts of the hydrogels and samples were incubated for 2 h at 37 °C. The positive and negative controls were distilled water and saline solution (without extracts of hydrogels), respectively. The incubated samples were centrifuged at 3000 rpm for

10 min, and the supernatants were collected and absorbance of hemoglobin was measured by a microplate reader (SpectraMax ABS Plus, Molecular Devices, San Jose, CA, USA) at a wavelength of 540 nm. The percentage of hemolysis ratio was calculated by the following equation:

$$\text{Hemolysis ratio (\%)} = \frac{A_{\text{sample}} - A_{\text{negative}}}{A_{\text{positive}} - A_{\text{negative}}} \times 100 \quad (4)$$

Where A_{sample} , $A_{\text{negative control}}$, and $A_{\text{positive control}}$ are the absorbance values of the supernatant fraction of the samples, negative and positive controls, respectively. All experiments were carried out in triplicates ($n=3$) and data are expressed as mean \pm SD.

2.4.6 *In vitro* degradation study of hydrogels

The sample IZ-3 was selected to conduct the *in vitro* degradation of the hydrogels in simplified (serum-free) physiological conditions (PBS, pH=7.4). The hydrogels were fabricated and transferred into pre-weighed vials. Subsequently, the hydrogels were frozen overnight and lyophilized for 24 h. The dried hydrogels were put into 15 mL of PBS (pH, 7.4) and incubated for 30 d at 37 °C. Similarly, dried hydrogels were immersed in GSH solution (10 mmol in PBS, pH~5.5) and incubated at 37 °C

for 2.5 d to analyze their GSH-triggered degradation. The percent weight remained of a hydrogel was measured by using the following equation:

$$\text{Weight remained (\%)} = \frac{W_t}{W_0} \times 100 \quad (5)$$

Where W_0 is the initial weight of the dried hydrogel and W_t is the dried weight of the hydrogels after degradation at each time point.

2.4.7 Cell culture and cytotoxicity evaluation

The cytotoxicity of the CMC-Nb, DSe-DPEG-DTz, empty hydrogels, and the DOX-encapsulated hydrogels were determined by using WST assays. To evaluate the biocompatibility of the CMC-Nb and the cross-linker, HEK-293 cells were cultured in a cell culture medium containing 10% fetal bovine serum (FBS) and Dulbecco's Modified Eagle Medium (DMEM) at a cell-density of 10^4 cells/well in 48 well-plates and incubated for 24 h to completely attach the cells on the surface of well-plates. Next, various concentrations of UV-sterilized CMC-Nb and DSe-DPEG-DTz were dissolved in the cell culture medium and incubated with the HEK-293 cells for 24 h. To investigate the cytocompatibility of the hydrogels, UV-sterilized hydrogels were incubated with the HEK-293 cells. After 24 h, the cell

culture medium was aspirated and cells were rinsed with PBS and then treated with the WST-assays (200 μ L) for 30 min. Next, optical densities were recorded at a 450 nm wavelength by using a microplate reader. Similarly, the above procedure was performed with free-DOX (10-40 μ g/mL) and the DOX-loaded hydrogels (40 μ g/mL equivalent of free-DOX) against BT-20 cancer cells.

2.4.8 Live/ Dead assay

The fluorescence-based live/dead assays were performed to elucidate the effect of blank hydrogels, DOX-encapsulated hydrogels and free-DOX against BT-20 cells. Briefly, blank hydrogels, DOX-encapsulated hydrogels and free-DOX were immersed in cell culture medium in an incubator for 24 h at 37 °C. Then, BT-20 cells were incubated with extracts of the hydrogels and the free-DOX solution for 24 h. Subsequently, the cells were immuno-stained with calcein-AM and ethidium bromide assays to identify the live and the dead cells by using a fluorescence microscope.

2.5 Results and discussion

2.5.1 Synthesis of CMC-Nb

CMC-Nb was prepared by a simple, one step reaction between CMC and 5-norbornene-2-methyl amine using a carbodiimide coupling reagent (EDC). The functionalized CMC was purified by first recrystallizing in acetone and then by dialyzing in DI water. Finally, lyophilization of the product produced CMC-Nb in high yield (85%). The Nb functional groups on the backbone of CMC provide reactive sites which could undergo the IEDDA click reaction with the Tz groups in the DSe-DPEG-DTz cross-linker to form hydrogels. The ^1H NMR spectrum confirmed the functionalization of CMC with Nb as shown in Figure 6a. The peaks at 5.9-6.1 ppm could be attributed to the alkene protons of the Nb groups, while the peak at approximately 4.81 ppm corresponded to the proton linked with the glycosidic bond of anhydro-glucose repeating units of the CMC backbone [62]. The integration ratio of the protons of the Nb groups and those of the glycosidic bonds of the hydro-glucose was considered to calculate the degree of substitution (DS %), which was found to be about 32%. The conjugation of the Nb groups with the carboxyl group of the CMC backbone was also confirmed by the FTIR spectroscopy of the CMC-Nb (Figure 6b). The broad peak at 3300 cm^{-1} is ascribed

to the stretching vibration of —OH groups of the CMC. The additional adsorption peaks observed at 1533 cm^{-1} and 1600 cm^{-1} could be attributed to the N—H bending and C=O stretching, respectively. The small peak appeared at 673 cm^{-1} could be ascribed to cis di-substituted alkene bends, indicating the successful conjugation of Nb to the backbone of CMC.



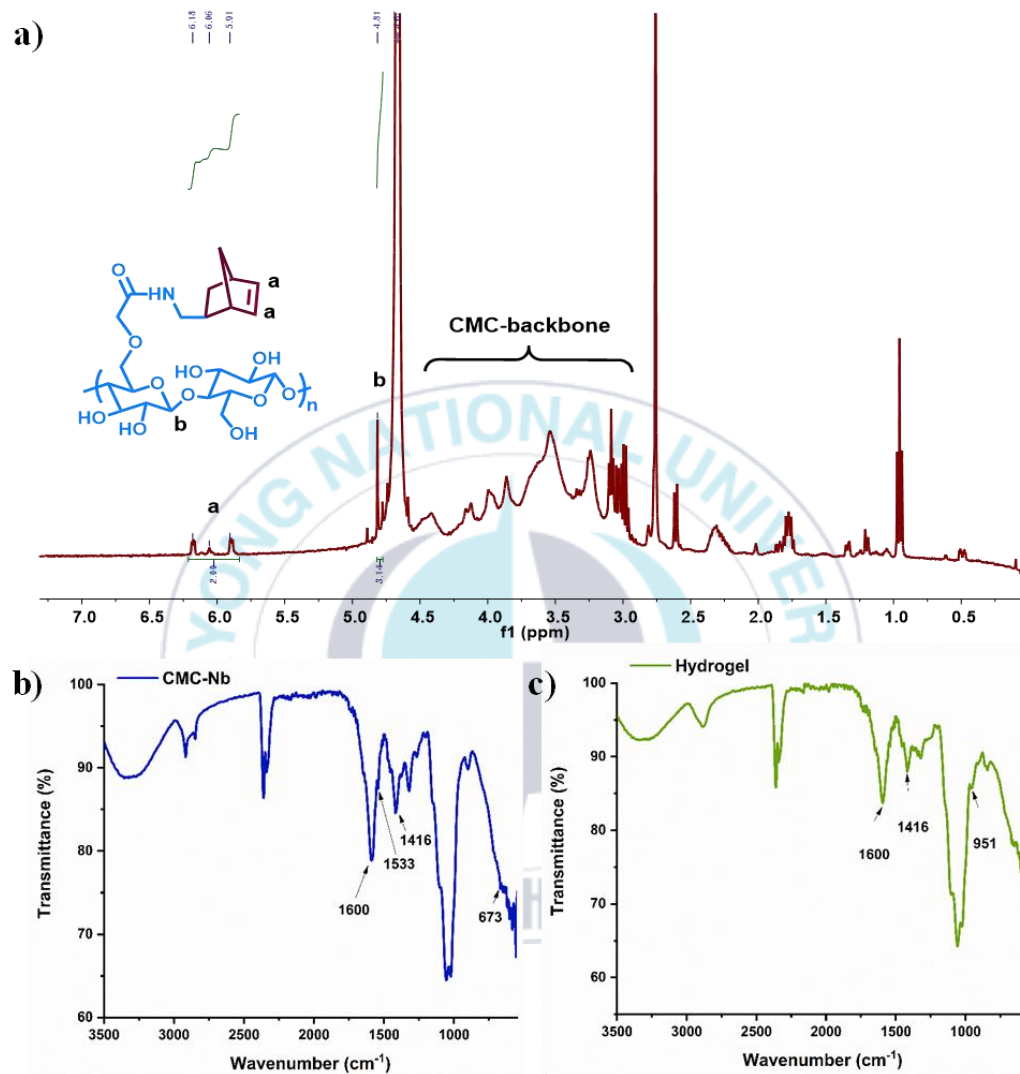


Figure 6. (a) $^1\text{H-NMR}$ spectrum of CMC-Nb in D_2O , (b) FTIR spectrum of CMC-Nb, and (c) FTIR spectrum of the hydrogel.

2.5.2 Preparation and characterization of hydrogels

Key advantages of using Nb-Tz click chemistry for the preparation of hydrogels are rapid gelation time, stoichiometric control, tunability of hydrogel properties and potential for scale up. Due to the robustness of Nb-Tz click reaction, the di-tetrazine molecule can cross-link the CMC-Nb to form a gel. In this study, three formulations of hydrogels with different feed ratios of Nb/Tz (10:2.5, 10:05, and 10:10) were prepared to determine the effect of cross-linking density on the physical properties of the hydrogels, as listed in Table 1. The FTIR spectrum of the CMC hydrogel (Figure 6c) demonstrated a distinct absorption band of C—Se at 951 cm^{-1} , indicating the successful insertions of cross-linking bridges *via* IEDDA click reaction between the CMC-Nb and the DSe-DPEG-DTz.

For injectable hydrogels, the gelation time is an important factor for their delivery strategies. [63]. The time required to form a stable gel could be determined roughly using a tube inversion technique. Dynamic rheological analysis could be employed to assess the accurate time when polymers started to form a gel [64]. Our findings suggested that the gelation time, swelling behavior, and mechanical strength of the formulated hydrogel could be tuned easily by changing the complementary click

functional group's stoichiometric ratios (in this case, the ratio of Nb to Tz groups). The formation of a gel observed using the rheological analysis and tube inversion method is represented in Table 1 and Figure 7a. The hydrogel IZ-3 (Nb to Tz ratio of 10:10) showed the shortest gelation time (~ 1 min and 2.5 min as determined by the rheometer and tube inversion method, respectively). With decrease of the Tz ratio, the gelation time was gradually increased from 1.5 min to 4.83 min (determined by the rheometer) and 4.41 min to 6 min (determined by the tube inversion method) of hydrogels IZ-2 and IZ-1, respectively. These findings suggested that the gelation times of the hydrogels could be shortened by increasing the Nb/Tz ratios. The fast gelation time is an important feature of injectable hydrogels to maintain *in situ* structural integrity at a specific site and to prevent the free-flow of the polymer solution into neighboring tissues [65]. Storage modulus (G') and loss modulus (G'') exhibit the elastic and viscous properties of hydrogels, respectively [66, 67]. After addition of the cross-linker, IZ-1, IZ-2, and IZ-3 exhibited higher values of G' and G'' than the CMC-Nb precursor solution as shown in Figure 7b, which confirmed the formation of gels owing to the IEDDA click reaction between Nb and Tz functional groups. The hydrogel IZ-3 demonstrated the highest value of G' (160 Pa) while IZ-2 and IZ-1 imparted lower G' (approx. 126 to

74 Pa, respectively). According to the measured modulus value, these gels can be categorized as soft hydrogels. The difference in G' among the hydrogels could be ascribed to the difference in their cross-linking densities. Generally, it is reported that storage and loss moduli decrease as the degree of cross-linking of hydrogel decreases [68].

The dynamic oscillatory strain amplitude-sweep tests of hydrogels were carried out in the strain range of 0.1 to 10000% to investigate the viscoelastic nature of hydrogels at a fixed angular frequency of 10 rad/s. In this study, the exact strain percent was evaluated to confirm the linear viscoelastic region (LVR) of hydrogels, as shown in Figure 7c. It was revealed that the G' and G'' values of hydrogels under LVR were largely independent of the applied strain, indicating a typical viscoelastic behavior of hydrogels. The IZ-1, IZ-2, and IZ-3 hydrogels showed the LVR within a range of 0.1–7%, 0.1–4%, and 0.1–2.5%, respectively, indicating that higher cross-linking densities decreased the LVR of hydrogels. Generally, the LVR gradually decreases when hydrogel turns into more solid (gel) form as reported in literature [69]. The deviation of G' values by more than 5% from the plateau values could be designated as the critical strain ($\gamma_c\%$) of hydrogels [70], which was observed at different strain amplitudes of 10.5%, 8%, and 6.5% for IZ-1, IZ-2, and

IZ-3, respectively. Above $\gamma_c\%$, G' values gradually decreased, representing the transition of hydrogels from quasi-solid state to quasi-liquid state. Furthermore, the loss factors ($\tan(\delta) = G''/G'$) of hydrogels were measured in the range 0.08 – 0.4 - at frequency of 0.1-100 rad/s, suggesting that the hydrogels were elastic and energy-storing solids (gels) [71].

Figure 7d depicts the swelling behavior of the formulated hydrogels, indicating that hydrogels swelled rapidly during the initial 1 h of immersion in PBS (pH, 7.4) and reached to a swelling equilibrium after 48 h. The swelling ratios of hydrogels IZ-1, IZ-2, and IZ-3 increased up to 39, 28, and 23 times, respectively, as compared to the initial mass of dry hydrogels. All hydrogels showed high swelling ratios and maintained their form after water uptake. Multiple factors could affect the swelling ratios of hydrogels, such as cross-linking density, hydrophilicity of polymers etc. [72]. The higher swelling behavior of the formulated hydrogels could be attributed to the hydrophilic property of CMC due to hydrogen bonding between carboxylate groups (COO^-) and water molecules [73]. In addition, the PEG molecules in the cross-linker facilitated water uptake, which rapidly increased the swelling of hydrogels during the initial phase. Moreover, it was observed that the hydrogel IZ-1 can absorb more water than the IZ-2 and IZ-3 hydrogels. The relatively lower

swelling of IZ-3 could be ascribed to the higher cross-linking density, which resulted in reduced flexibility and mesh size of hydrogels [74]. The pictorial view of the hydrogel formation is represented in Figure 7e.

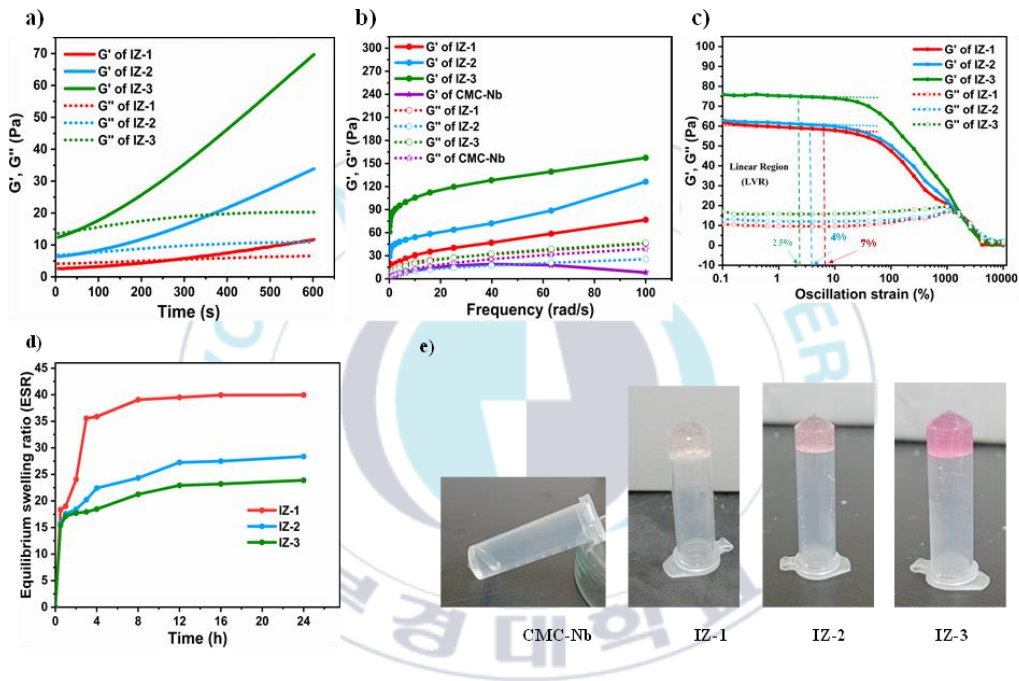


Figure 7. (a) The storage modulus (G') and loss modulus (G'') of hydrogels as a function of time, (b) storage modulus (G') and loss modulus (G'') as a function of angular frequency under 1 % strain at 25 °C, (c) the strain amplitude sweep experiments, (d) swelling behavior of hydrogels, and (e) representative photograph of hydrogels formation.

SEM was performed to investigate the surface and internal structures of the prepared hydrogels. Figure 8a shows the SEM images of the internal network obtained from the cross-section of the hydrogels. The micrographs show that all the formulated hydrogels have porous structures. The highly porous structures of hydrogels could be due to the microbubbles created by the N₂ gas released during the IEDDA reaction [75]. Interestingly, the hydrogel IZ-3 shows relatively smaller pores, whereas IZ-2 and IZ-1 show larger pores. This difference in the pore sizes can be attributed to the variations in their cross-linking densities [76]. The N₂ gas bubbles produced in the formulated hydrogels were confirmed by an optical microscopy (Figure 8b). It is observed that the sample IZ-3 produces more bubbles in network structure as compared to those of the hydrogels IZ-2 and IZ-1, which is attributed to the variations in the concentration of the cross-linker. The porosity and swelling behavior are crucial parameters which greatly influence the drug loading and release behavior of the hydrogels.

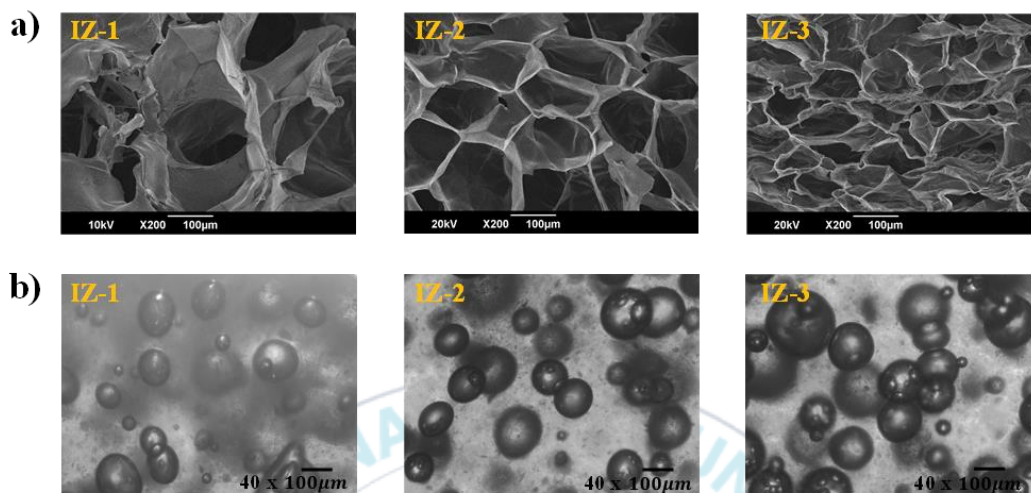


Figure 8. (a) SEM micrographs of cross-sectional area of hydrogels and (b) optical microscopic images of hydrogels.

2.5.3 Drug loading and *in vitro* reduction-triggered release of DOX from hydrogels

We used DOX as a model molecule to study the drug loading and release behavior of the CMC-based hydrogels. After drug loading, DC % and DEE % were measured and summarized in Table 1. The hydrogels IZ-3, IZ-2, and IZ-1 showed DC % of 4.53, 4.44, and 4.28%, and DEE% of 90.75, 88.90, and 85.60%, respectively. The higher DC % and DEE % of IZ-3 hydrogel can be due to the denser network

structures, which minimized the egress of the drug from the formulation during the loading process. The higher porosity may also contribute to the higher drug loading [75].

The *in vitro* drug release from hydrogels were assessed under a simulated physiological environment (PBS, pH 7.4) and in a reducing environment (GSH 10 mmol) at 37 °C, as shown in Figure 9. The hydrogels IZ-2 and IZ-3 were selected for drug release experiments because these hydrogels showed higher mechanical strength than IZ-1. The drug release investigations showed that the hydrogels released comparatively small amount of DOX in PBS, as compared to the reducing environment. Specifically, IZ-2 and IZ-3 released DOX in a controlled manner, showing about 99 % and 78 % DOX release after 12 h, respectively, in the presence of 10 mmol GSH. On the other hand, a small amount of the DOX release (42 and 36 %) was observed in PBS from the hydrogels IZ-2 and IZ-3, after 12 h, respectively. The drug release tendency of IZ-3 is relatively low as compared to IZ-2 in GSH and PBS, which corresponds to the difference in the crosslinking density and swelling ratios of these hydrogels, as discussed above. It could be observed (Fig. 4) that GSH robustly accelerated the release of DOX from the hydrogels owing to the scission of di-selenide bonds [77]. Whereas, DOX was not

significantly released from the hydrogels in PBS, which implies that the responsive DOX release was mainly associated with the reducing environment (GSH, pH ~ 5.5). The hydrogel network collapsed in GSH by de-cross-linking phenomenon, which led to the fast release of DOX. These findings could be interesting for tumor-specific drug delivery systems, as tumor tissues usually have a reducing and acidic environment while normal cells are at physiological conditions (pH ~ 7.4) [78, 79]. Moreover, electrostatic interactions between un-modified carboxymethyl groups of CMC-Nb and amine group of DOX might have played a significant role in controlling the drug release, as reported previously [80]. Specifically, at relatively lower pH (~ 5.5) of the 10 mmol GSH, the COO^- of CMC-Nb and amine group of DOX are protonated (COOH , and NH_3^+ , respectively). Consequently, electrostatic interactions between CMC-Nb and DOX are weakened, thereby increasing the dissociation and release of DOX in the medium [37]. On the contrary, a slow release of DOX in PBS can be explained by the fact that the carboxyl groups of CMC-Nb remained un-protonated in this pH range, which predominantly increased the polymer-drug interactions.

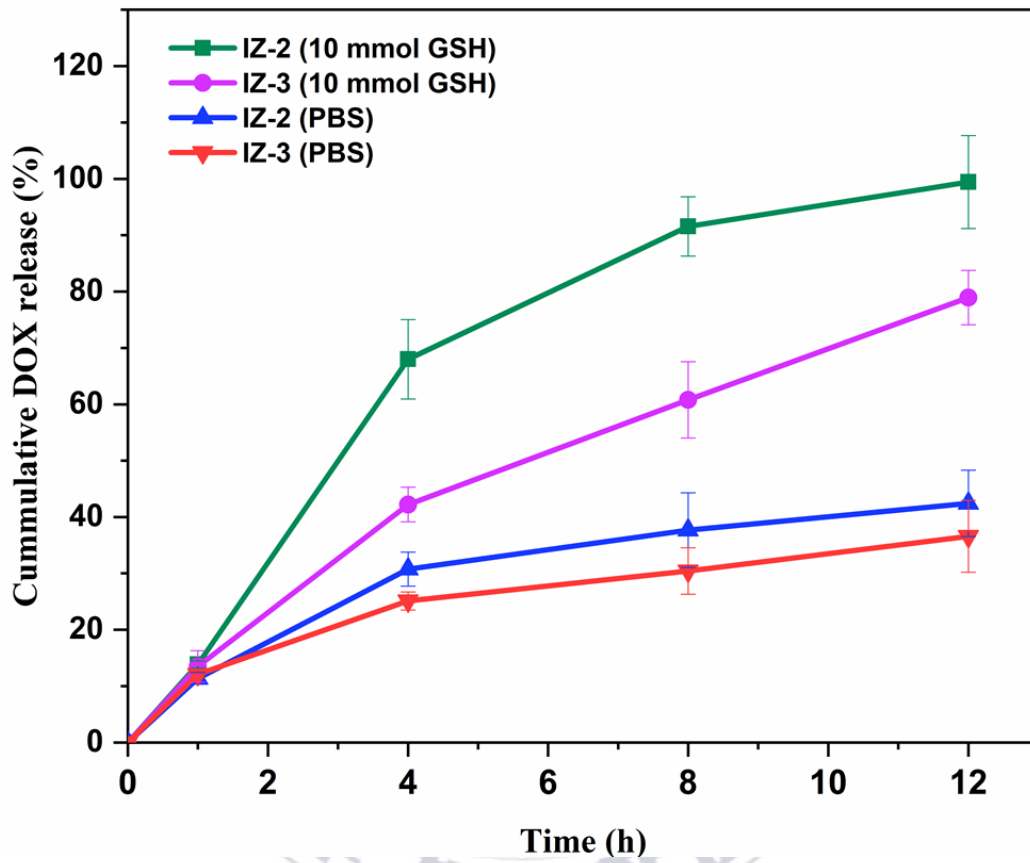


Figure 9. DOX release studies of hydrogels in 10 mmol GSH and simulated physiological buffer (PBS, pH, 7.4).

2.5.4 Cytotoxicity studies

In this study, different concentrations of CMC-Nb (100, 500, and 1000 $\mu\text{g/mL}$) and DSe-DPEG-DTz (25, 50, 75, 100, and 200 $\mu\text{g/mL}$) were treated with HEK-293 cells to analyze their cytocompatibilities (Figure 10a-b, respectively). Furthermore, *in vitro* cell viability (%) of the blank hydrogels were conducted (Figure 10c). It is apparent that neither the CMC-Nb, DSe-DPEG-DTz, nor the blank hydrogels significantly affected the growth of HEK-293 cells. Specifically, CMC-Nb showed more than 95% cell viabilities at the maximum tested quantities (1000 $\mu\text{g/mL}$). Similarly, HEK-293 cells treated with 100 $\mu\text{g/mL}$ of DSe-DPEG-DTz showed more than 88% cell viabilities. Similarly, the hydrogels, IZ-3 and IZ-2 were also highly cytocompatible ($\geq 95\%$ cell viabilities).

The *in vitro* anti-tumor efficacy of the DOX-encapsulated hydrogels was determined against breast cancer cells (BT-20), as shown in Figure 10d. The anti-tumor effects induced by the DOX-encapsulated hydrogels against cancer cells were compared with those of free-DOX (10, 20, and 40 $\mu\text{g/mL}$). It was observed that the DOX-encapsulated hydrogels induced slightly less cytotoxicity than free-DOX at a concentration of 40 $\mu\text{g/mL}$ against cancer cells. This relatively small

difference in cytotoxic effect of the DOX-loaded hydrogels as compared to those of the free-DOX treatments, could be ascribed to the slow release of the DOX from the hydrogels when treated *in vitro*. Specifically, cancer cells have lower concentration of GSH (2.99 fmol/cells, ~14.96 μ mol) when cultured *in vitro*, as compared to the concentration of GSH (10 mmol) tested for in vitro drug release experiments [81, 82].



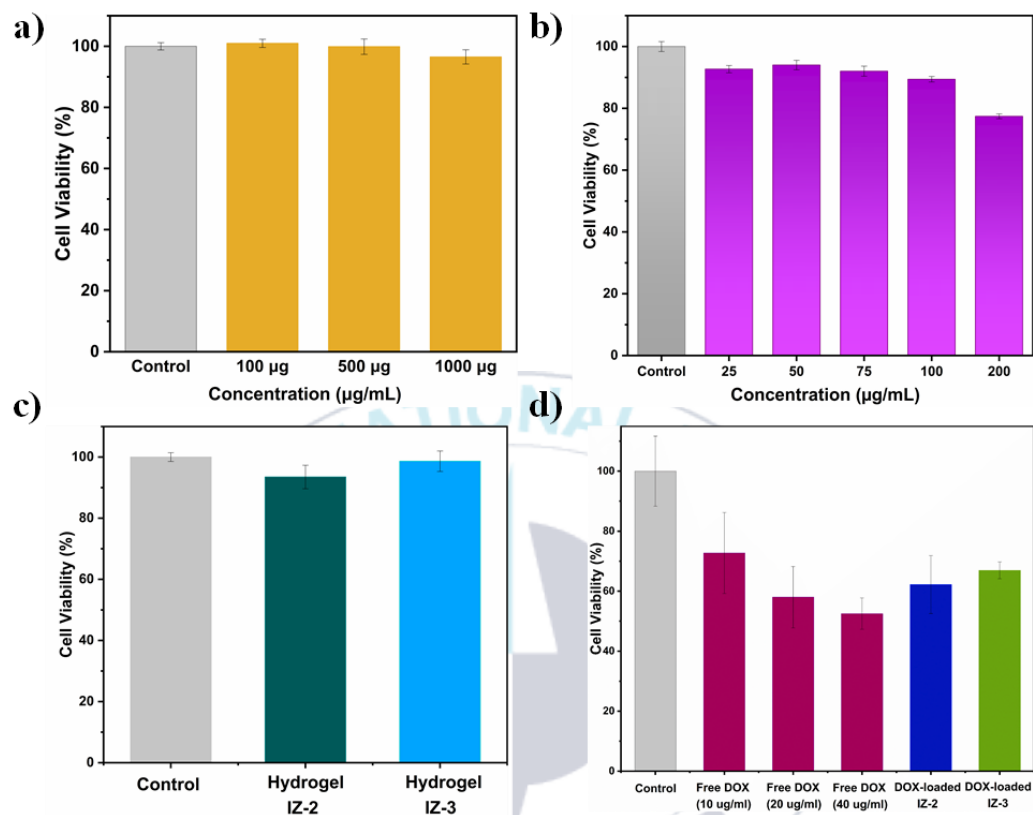


Figure 10. Cell viabilities (%) of HEK-293 cells determined using WST assays after treatment with (a) CMC-Nb, (b) DPEG-DSe-DTz, (c) blank-hydrogels (IZ-3 and IZ-2), and (d) in vitro anti-tumor activity against BT-20 cells after treatment with free-DOX and DOX-loaded hydrogels.

2.5.5 Live/dead analysis

The live/dead fluorescent immunostaining (calcein-AM and ethidium bromide) was used to assess the cell viability of BT-20 cancer cells, after treatment with the extract of the blank hydrogels, DOX-loaded hydrogels and free-DOX. In Figure 11, the live cells exhibit green fluorescence and the dead cells show red fluorescent. These results showed no considerable difference in the number of live and dead cells after incubation with the extracts of the controls and the blank hydrogels (IZ-2 and IZ-3). On the other hand, the higher number of dead cells (as shown by red dots in microscopic images) exhibited that DOX-encapsulated hydrogels induced cell death in BT-20 cells.

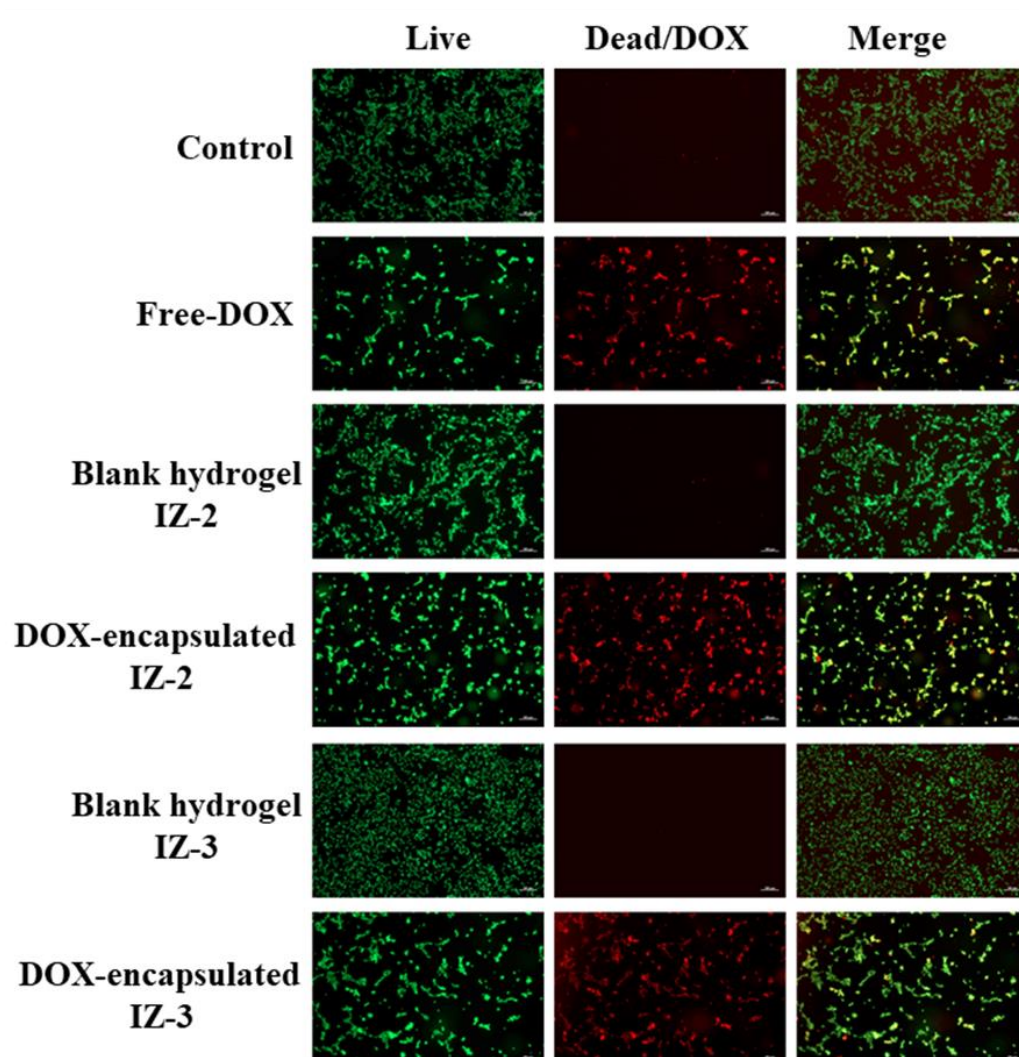


Figure 11. Confocal microscopy images of BT-20 cells treated with free DOX, blank-hydrogels (IZ-3 and IZ-2 and DOX-loaded hydrogels (IZ-3 and IZ-2). Scale bars indicating 100 μ m.

2.5.6 Hemolytic activity of hydrogels

Hemolytic activity analysis was conducted to determine the safety and hemocompatibility of the hydrogels in red blood cells. As presented in Figure 12a, the results of the hemolysis test showed no considerable hemolysis ratio in the negative control (saline solution) and the hydrogel samples, while the apparent hemolysis was observed in the positive control (distilled water). Specifically, the hemolysis value for the positive control was set as 100 %, while the extract of the hydrogels IZ-2, IZ-3, and negative control (saline solution) exhibited 1.24, 1.48, and 1.25% hemolytic ratios, respectively (Figure 12b). The results of hemolysis assays of the hydrogels are less than 5.0% as recommended by International Standard (ISO 10993—51,992) for biomaterials, indicating that the hydrogels were safe and possessed good hemocompatibility.

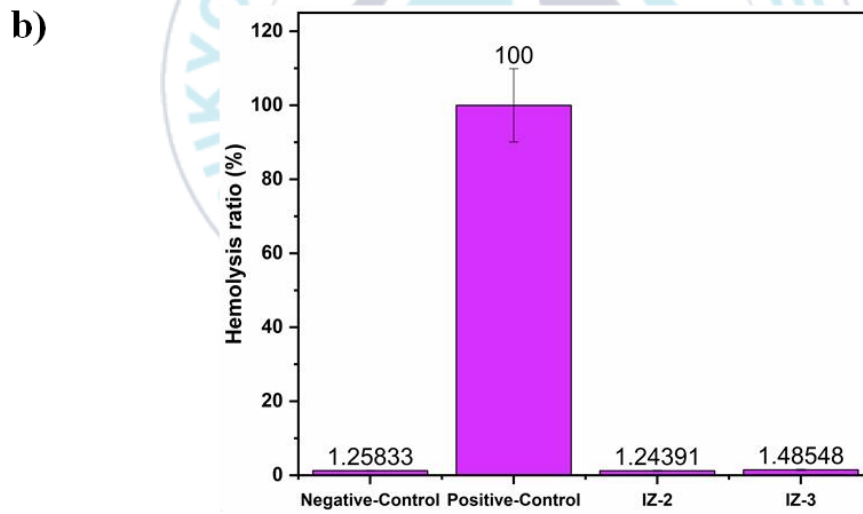
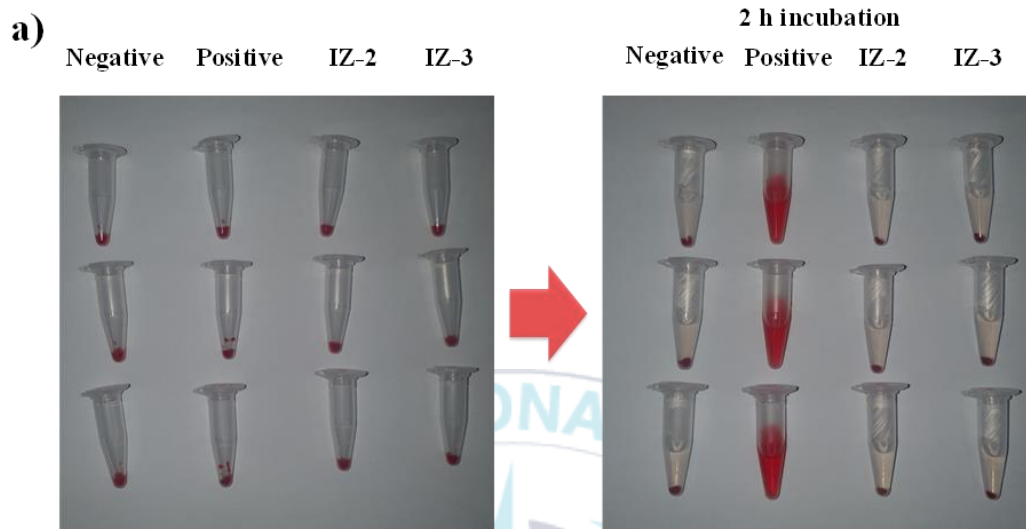


Figure 12. Hemocompatibility of hydrogels. (a) photographs of hemolysis test performed using saline (negative control), deionized water (positive control), and hydrogels (IZ-2 and IZ-3), and (b) hemolysis ratio of the hydrogels.

2.5.7 Biodegradation study

Typically, controlled biodegradation is considered as an important property of hydrogel used for drug delivery applications. The biodegradation study determines the structural integrity of hydrogels which could maintain their stability over predetermined time, and subsequently allows the pay-loaded hydrogels to disintegrate after the complete release of the drug at malignant site. [72]. The hydrogel IZ-3 was selected to monitor the *in vitro* biodegradation in PBS (pH, 7.4) and in GSH (10 mmol) at 37 °C. As shown in Figure 13a, the hydrogel immersed in PBS apparently showed no significant mass loss (< 5%) after 5d, followed by a temporal degradation phase, and approximately 81% mass loss was observed after 30d. On the other hand, the hydrogel incubated in GSH was disintegrated robustly with a substantial mass loss (~ 90%) just after 2.5d, as shown in Figure 13b. This result apparently showed a fast biodegradation in GSH, which could be ascribed to the scission of Se—Se bonds, ultimately cleaving the hydrogel networks. In contrast,

the slow degradation of the hydrogels was observed in PBS, which revealed that the hydrogels had relatively stable hydrogel network in the absence of a stimulus. Overall, these results together suggest that these stimuli-responsive highly biocompatible, and biodegradable hydrogels could be potential candidates for stimuli responsive drug delivery systems.

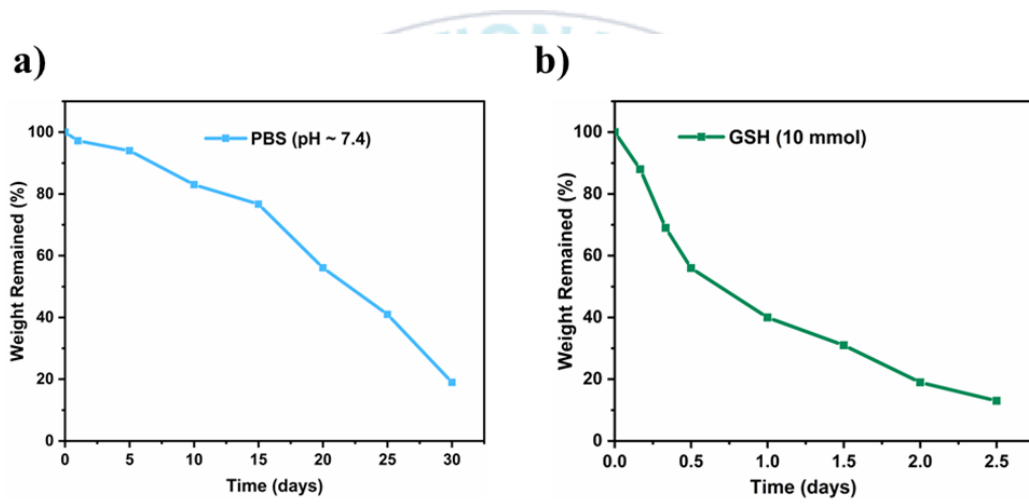


Figure 13. Biodegradation of formulated hydrogels (IZ-3). (a) in PBS (pH, 7.4) and (b) in GSH (10 mmol).

2.6 Conclusions

We developed novel injectable and reduction responsive soft hydrogels derived from CMC-Nb by using the water soluble cross-linker, DSe-DPEG-DTz. First, CMC was conjugated with Nb molecules and then chemically cross-linked *via* the IEDDA click reaction between Nb and Tz groups in an aqueous medium at physiological conditions. The resulting hydrogels of various crosslinking densities showed tunable gelation times and rheological properties, and high swelling ratios along with excellent drug encapsulation efficiency. The hydrogels showed significantly short gelation times and soft mechanical properties, indicating that the hydrogels were soft and could be suitable for injectable drug delivery applications. The drug release assessment demonstrated that ca. 99% of DOX was rapidly released from hydrogel (IZ-2) at tumor intracellular mimicking environment (GSH, 10 mmol), while showed low release rate (ca. 42%) of DOX at simulated physiological conditions (PBS, pH=7.4) after 12 h. The hydrogel (IZ-3) showed fast degradation rate (~ 90%) in GSH (10 mmol), whereas, slow degradation (< 5%) was observed in PBS (pH=7.4) after 2.5d. The cytotoxicity results exhibited that the precursors and the hydrogels are compatible with normal HEK-239 cells. In

contrast, the DOX-encapsulated hydrogels showed anti-tumor activity against BT-20 cancer cells.



Chapter 3 : NIR-responsive carboxymethyl-cellulose hydrogels containing thioketal-linkages for on-demand drug delivery system

3.1 Introduction

In the recent decades, localized on-demand drug delivery systems have gained utmost importance in biological, biomedical and tissue engineering applications owing to the precise control and effective delivery of therapeutic substances to the targeted sites [83]. However, as a promising candidate for on-demand drug delivery carriers, smart hydrogels that can respond in tumor specific triggers (e.g. temperature, pH, redox, enzyme, reactive oxygen species (ROS) etc.) exhibited a great potential to improve drug efficacy with minimal side effects [84]. Among them, ROS-responsive hydrogels have attracted special attention to deliver and release the drugs in cancer cells due to overproduction of ROS originated in tumor tissues, lesions, and pathogenic infections [85, 86]. Although quite well-known chemistries for constructing of ROS-responsive materials generally comprised of cleavable moieties such as sulfur [87], tellurium [88], di-selenide [89], phenylboronic acid/ester [90], thioether [91], and thioketal bridges [92]. Our

research group has reported the di-selenide based hydrogels for near infrared (NIR)-responsive drug delivery system. The di-selenide bond is more sensitive either by oxidation and reduction and could be cleaved by singlet oxygen under mild condition. However, Se-containing compounds are often difficult to synthesize and have susceptible concerns over physiological metabolism, and could generate possible toxicity in biological system in vivo applications [93]. The thioketal (TK) linkers have been selectively recognized as a ROS-sensitive material, which are simple and easy to synthesize in a one-step reaction, and could be interact with typical ROS oxidants, such as singlet oxygen ($^1\text{O}_2$), hydroxyl radical ($\cdot\text{OH}$), and H_2O_2 at a minimal concentration as low as $100\ \mu\text{M}$, and then undergo degradation into non-toxic thiols and acetone by-products [94].

NIR-light is innocuous and possesses the ability to deeply penetrate in biological tissues, without causing harm to healthy tissues. Upon NIR irradiation, an exciting photosensitive agents such as protoporphyrin IX (PpIX) [95], verteporfin [96], and indocyanine green (ICG) can undergo electron transfer reactions to generate massive ROS that can stimulate the apoptosis/necrosis of cancer cells and on-demand release of chemotherapeutic drugs from ROS-responsive materials in a spatiotemporal control [97]. Currently, the substantial attention has been focused to

integrate ROS-active compounds with photothermal therapy (PTT) to establish on demand drug delivery system for carrying out controlled drug release by ROS-stimulus triggered by NIR-light and combined chemo-photothermal therapy. Considering that, ICG (FDA approved) is a quintessential NIR-absorbing photothermal agent that can efficiently convert light energy to heat energy, which could be co-encapsulated in ROS-responsive nanomaterials [98]. Upon NIR light exposure, the incorporated ICG could produce ROS to stimulate on-demand drug release in a preferred mode through the ROS-mediated disruption of the thioketal linker which led to achieve combine chemo-photothermal cancer therapy [99].

ROS-responsive hydrogels can be prepared from natural or synthetic polymers. As a biodegradable biopolymer, carboxymethyl cellulose (CMC) is a most promising anionic and water-soluble linear polysaccharide derived from natural cellulose. The backbone of CMC contains repeating units of anhydro-glucose connected with β -1,4-glycosidic linkages [100]. The remarkable physiochemical characteristics of CMC, such as water wicking property in biological fluids, film forming ability, low immunogenicity, excellent biocompatibility, and biodegradability, render this biopolymer highly attractive in pharmaceutical applications [101]. Based on these favorable properties, CMC is appealing for potential application in biomedical field

including, wound healing, controlled-drug delivery and tissue engineering. However, the low mechanical strength and quick degradation of CMC limited its application in various biomedical applications. Although, many efforts have been reported to improve the mechanical properties of CMC, the strategies involving physical/ionically cross-linking to develop CMC-hydrogels typically exhibited weak mechanical properties.

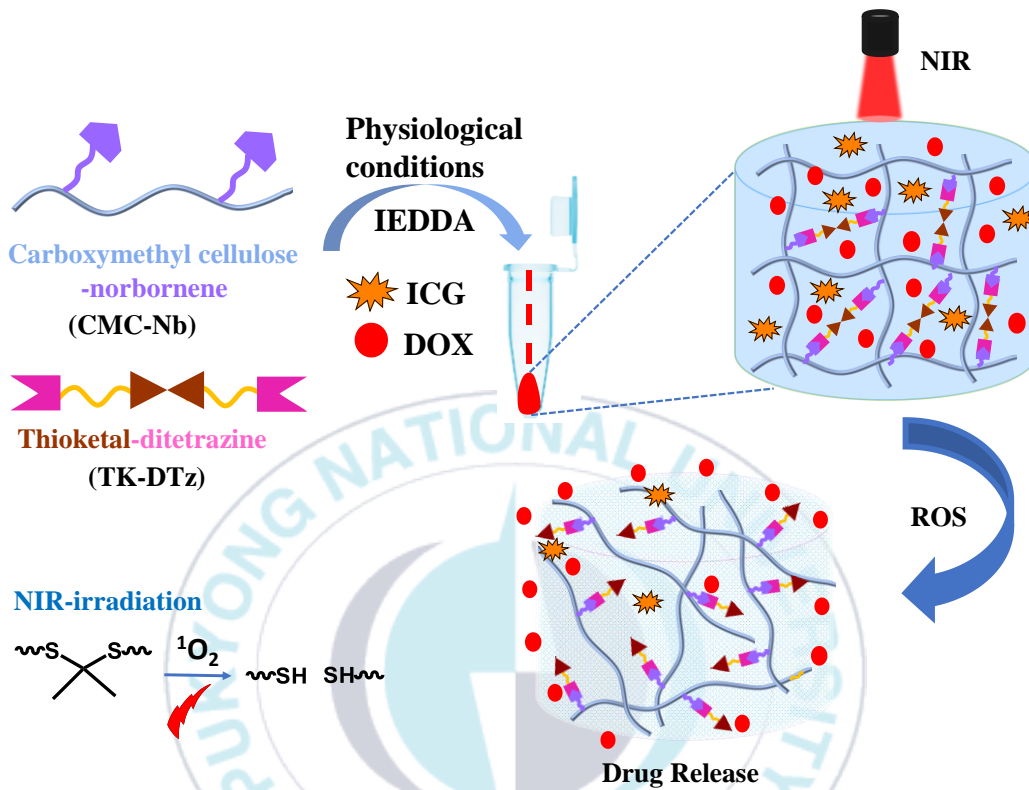
To address the limitations of intrinsic weak mechanical properties associated with physical cross-linked CMC-hydrogels, various covalent cross-linking strategies have been established to improve material attributes. The hydrogels developed from covalent cross-linking methods have been reported as stable and elastic by improving the mechanical properties of CMC. However, they employed the hazardous chemical cross-linking agents like glutaraldehyde (GA), diglycidyl ether (DGE), thiol, EDC/NHS [102-104]. In the past few years, click chemistry has appeared as an alternative approach to prepare covalent cross-linked hydrogels. In particular, these click reactions have become a promising approach due to their simplicity, ultra-fast reaction rate, high specificity and proceeded in physiological environment even in the presence of multiple functional groups without interfering or reacting with complex biological media [105]. Traditional click chemistry

reactions such as Cu(I)-catalyzed azide-alkyne cycloaddition reactions or thiol-yne photoclick reactions have some cytotoxicity concerns, and necessitate toxic reagents or catalysts that can compromise the biocompatibility [106, 107]. Recently, a set of "biorthogonal click" pathways have been established through advanced alternative methods, such as the inverse electron demand Diels-Alder (IEDDA) click reaction between tetrazine (Tz) and norbornene (Nb), which focused to construct the biomedical oriented mechanical stable hydrogels [108]. Furthermore, this facile reaction can occur spontaneously without requiring any additional additives, initiator, or catalyst, and liberates nitrogen gas as a by-product. The liberated nitrogen could generate porosity in the hydrogel networks, making it a promising approach for potential application in drug delivery system. Hence, it is hypothesized that CMC hydrogels of improved mechanical properties, excellent drug loading efficiency and on-demand drug delivery characteristic could be achieved by means of facile synthesis of TK cross-linkers and the subsequent bio-orthogonal IEDDA click cross-linking strategy. It is also assumed that ICG itself could provide additional photothermal effect on the anticancer therapy. To the best of our knowledge, this is the first report about the synthesis of Tz-conjugated TK cross-linkers to formulate NIR-responsive CMC hydrogels.

In this work, we constructed in situ IEDDA cross-linked ROS-responsive hydrogels by employing a novel TK-based cross-linker for on-demand release of a chemotherapeutic drug, doxorubicin (DOX) along with integrated chemophotothermal therapy tuned by NIR-light irradiation (Scheme 4). The ROS-cleavable TK cross-linker (TKDA) was conjugated with Tz end groups to undergo the IEDDA click reaction with Nb substituted CMC (CMC-Nb). Under physiological conditions, CMC hydrogels formed quickly upon the mixing of two precursors, CMC-Nb and TK-DTz, generating porous structures in the networks. The gelation times, swelling behavior, porosity, and rheological properties of hydrogels were investigated by varying the concentrations of cross-linker. The ROS-responsive drug delivery properties of the DOX + ICG-loaded hydrogels were studied in detail upon exposure to NIR irradiation or treatment with 0.5% H₂O₂. Moreover, the efficient anti-tumor activity of the hydrogels against Hela cancer cells was demonstrated under NIR irradiation. Our study presents a novel contribution to the development of a carboxymethyl-cellulose (CMC) based near-infrared (NIR)-responsive hydrogel using a bio-orthogonal click chemistry approach. The innovative aspect lies in the ability of hydrogel to achieve controlled on-demand drug release triggered by NIR irradiation. With its potential application

in cancer therapy owing to its responsiveness by NIR light, our hydrogel emerges as a promising candidate in the field of drug delivery systems and biomaterials.





Scheme 4. Graphical representation for development of ROS-responsive CMC hydrogels and their release mechanism by cleavage of thioketal bonds upon exposure of NIR irradiation.

3.2 Materials and methods

3.2.1 Materials

Sodium carboxymethyl cellulose (Na-CMC) ($n = \text{approx. } 1050$) ($M_w \sim 276 \text{ kDa}$), 1-ethyl-3-(3-dimethylaminopropyl)-carbodiimide hydrochloride (EDC. HCl, 99 %), formamidine acetate salt (99%), hydrazine monohydrate indocyanine green (ICG), and zinc (II) tri-fluoromethanesulfonate (98%) were procured from Tokyo Chemical Industry (TCI) Japan. Mercaptoacetic acid (98%), N-hydroxysuccinimide (NHS, 98%), triethyl amine (99.5%), 5-norbornene-2-methylamine (Nb-NH₂, 98 %) and di-tert-butyl dicarbonate (99%) were purchased from Sigma Aldrich. 4-(Aminomethyl) benzonitrile hydrochloride (4-AM, 97%) was purchased from Matrix Scientific, USA). DOX was supplied by LC Laboratories CO. (Woburn, MA, USA). Anhydrous hydrazine was obtained from the distillation of hydrazine monohydrate (98%, TCI). All the chemicals were of analytical grade and were used without purification.

3.2.2 Methods

3.2.2.1 Synthesis and characterization of precursors

3.2.2.1.1 Synthesis of ROS-cleavable small molecule thioketal-di-tetrazine cross-linker (TK-DTz)

3.2.2.1.1.1 Synthesis of thioketal diacid (TKDA)

TKDA was synthesized in a one-step reaction by following a previous protocol with some modifications [109]. Briefly, acetone (1 mL, 0.013 mol, 1 mol equi.) was added to thioglycolic acid (2.5 mL, 0.03 mol, 2.5 mol equi. dissolved in 30% of water) and magnetically stirred at 45 °C for 48 h. The precipitates of TK linkers were obtained by adding 100 g of crushed ice. After that, the precipitates were filtered and then washed with 3 × 50 mL of cold DI H₂O and then 100 mL of n-hexane. To obtain purified TKDA, the resultant white solid was subsequently dried under reduced pressure.

3.2.2.1.2 Synthesis of Amino-Functionalized Tetrazine (Tz-NH₂)

3.2.2.1.2.1 Synthesis of Tert-butyl 4-cyanobenzylcarbamate (TBC)

Tert-butyl 4-cyanobenzylcarbamate was synthesized using a previously established procedure with slight modification [110]. Briefly, 60 mL of acetonitrile was used

to dissolve 4-(aminomethyl) benzonitrile hydrochloride (1.5 g, 8.89 mmol) and triethyl amine (2.2 g, 22.23 mmol). The solution was magnetically stirred for 30 min under N₂ gas. Di-tert-butyl di-carbonate (1.9 g, 8.89 mmol) was gradually introduced into the solution and agitated at room temperature (RT) for 24 h. After completion of reaction, the solvent was evaporated and the residues were dissolved in deionized water. The pH of the mixture was reduced to 3 by the addition of 1 M HCl. Then product was extracted by adding EtOAc. The combined organic layer underwent three water washes (each requiring 100 mL), collected, and dried by the addition of anhydrous MgSO₄, and concentrated to give a white solid (yield 94%).
¹H NMR (400 MHz, DMSO-d₆, δ): 1.35 (s, 9H, C-(CH₃)₃), 4.15 (d, 2H, Ar-CH₂-NH-), 7.51 (s, H, -CH₂-NH-), 7.38 (d, 2H, Ar-H), 7.7 (d, 2H, Ar-H)

3.2.2.1.2.2 Synthesis of Tert-butyl 4-(1,2,4,5-tetrazin-3-yl)benzylcarbamate (Tz-NH-Boc)

In a 250 mL of glass flask, tert-butyl 4-cyanobenzylcarbamate (1g, 4.30 mmol) was mixed in 5 mL of DMF. Next, zinc (II) trifluoromethanesulfonate (0.078g, 0.215 mmol, 5 mol%) and formamidine acetate salt (4.48g, 43.05 mmol) were introduced to the reacting vessel. The anhydrous hydrazine (3.45g, 108 mmol) was then gently

incorporated into the solution until gas evolution stopped. The solution was agitated overnight at 30 °C. Sodium nitrite (5.94g, 86.10 mmol) was charged to the solution, then slowly added 1 M HCl until a pink color and a pH value of 3 were achieved. The product was extracted with EtOAc (100× 3 mL), and the mixed organic layer was dried over anhydrous MgSO₄. After filtration, the EtOAc was evaporated *via* a rotary evaporator. The residues were then dried in reduced pressure to obtain Tz-NH-BOC (yield 51%). ¹H-NMR (400 MHz, DMSO-d₆, δ): 1.41 (s, 9H, -C-(CH₃)₃), 4.25 (s, 2H, Ar-CH₂-NH-), 10.58 (s, 1H, -N-CH-N-), 7.54 (s, 1H, -NH-CO-), 8.47 (d, 2H, Ar-H), 7.54 (d, 2H, Ar-H)

3.2.2.1.2.3 De-protection of BOC-group to obtain Tz-NH₂

The dissolution of Tz-NH-BOC (0.87g, 3.02 mmol) was carried out in 20 mL of methanol in a glass flask and magnetically stirred for 15 min at RT. The oxalyl chloride (1.9g, 15.1 mmol) was carefully added to the solution by using a micropipette. After stirring at RT for 24 h, the solution was cooled down to 0 °C and then recrystallized in 3 × 100 mL of acetonitrile. The product (pink solid) was filtered off dried under reduced pressure (yield 70%). ¹H-NMR (400 MHz, DMSO-

d_6, δ): 4.17 (s, 2H, Ar-CH₂-NH₂), 7.82 (d, 2H, Ar-H), 10.63 (s, 1H, -N-CH-N-), 8.51 (d, 2H, Ar-H).

3.2.2.1.2.4 Synthesis of TK-DTz

The TK-DTz cross-linker was synthesized *via* amide coupling reaction. TKDA (200 mg, 0.89 mmol) was added in THF (10 mL) in a glass flask and the reaction was agitated for 30 min under N₂ atmosphere. Then EDC (345 mg, 1.8 mmol) and NHS (207.16 mg, 1.8 mmol) were added separately into the flask. After agitating for 2 h at 0 °C, the flask was filled with Tz-NH₂ (336 mg, 1.8 mmol). The reaction was agitated for 1 h at 0 °C and further 72 h at RT. The residues were collected by removing the solvent *via* rotary evaporator and again diluted with DCM. The mixture was washed with DI H₂O (3 × 100 mL) and brine (100 mL). The organic layer was collected, dried by addition of anhydrous magnesium sulfate and filtered through Whatman filter paper. The organic solvent (DCM) was removed *via* rotary evaporator to obtain the TK-DTz product (55% yield). ¹H-NMR (400 MHz, DMSO-*d*₆, δ): 4.09 (s, 2H, Ar-CH₂), 7.24 (d, 2H, Ar-H), 10.27 (s, 1H, -N-CH-N-), 8.14 (d, 2H, Ar-H), 1.21 (t, 6H), 3.05 (t, 2H).

3.2.3 Functionalization of CMC with Nb

CMC was modified with Nb moieties by using an established protocol of previous work [111] with slight modification. Typically, 1.5 g (0.0054 mmol) of Na-CMC was suspended in 150 mL of DI H₂O (1 % w/v) and agitated to make a homogeneous solution. EDC. HCl (0.55 g, 2.85 mmol) and NHS (0.328 g, 2.85 mmol) were separately introduced into the Na-CMC solution, while agitating the mixture for 1 h. Nb-NH₂ (0.35 g, 351 μL, 2.85 mmol) which was pre-dissolved in 3 mL of DMSO was then incorporated into the solution. After agitating for 24 h at RT, the mixture was dropwise added in excess cold acetone to yield a white precipitate. After filtration, the filtrate was dried under high vacuum. The impure solid was dissolved in water (1 % w/v) and carried out dialysis against DI H₂O in dialysis tube of 14 kDa (MWCO) for 5 d. After freezing the solution, dried CMC-Nb was recovered after freeze-drying (DS = 15 %, experimentally determined by NMR spectrum).

3.3 Formulation of hydrogels

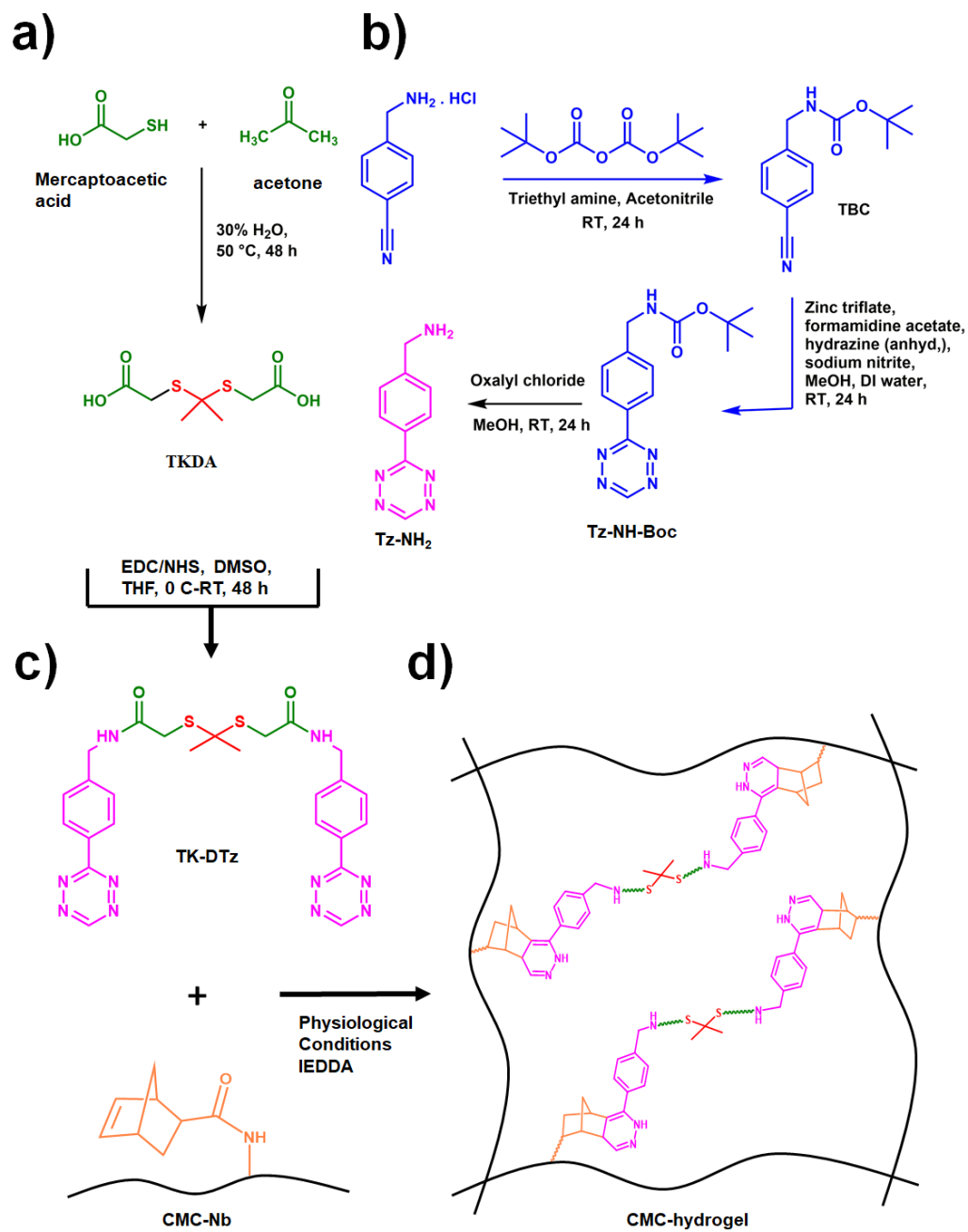
The one step mixing approach was employed to fabricate cross-linked hydrogels *via* the IEDDA click reaction between CMC-Nb and Tk-DTz. To investigate the physiochemical characteristics of hydrogels, three different cross-linker

compositions were used to fabricate the hydrogels (as shown in table 2). Typically, the hydrogels were formulated by gently mixing of 200 μ L of CMC-Nb (2 % w/v) in DI water and various mol. ratios of TK-DTz (10/2.5, 10/5, 10/10 Nb/Tz) in DMSO (DMSO: PBS = 1:10 v/v in final formulation) in an Eppendorf for 15 s. Inverted vial test was performed to note the gelation times of cross-linked hydrogels by using digital time meter and these measurements were further validated by using a rheometer

Table 2. Formulations and gelation times of CMC hydrogels.

Hydrogel code	Nb:Tz (% mol. ratio)	Gelation time (s) ^a
TKHG-A	100:25	495
TKHG-B	100:50	365
TKHG-C	100:100	170

^a Gelation time was evaluated by tube inversion test.



Scheme 5. Schematic synthetic route path of precursors (a) TKDA, (b) tetrazine amine (c) ROS-responsive cross-linker (TK-DTz), and (d) development of CMC hydrogels.

3.4 Characterization

3.4.1 Measurements and instruments

¹H NMR analyses were conducted employing a JEOL NMR spectrometer (JNM ECZ-400, JEOL, Akishima-Shi, Japan). An Agilent CARY 640 spectrometer was used to acquire FTIR spectra. UV-VIS analysis was conducted with an Optizen POP spectrometer. A field emission scanning electron microscope (FE-SEM) (MIRA 3 system TESCAN) was used to examine the cross-section micrographs of the hydrogels. A Discovery HR-2 hybrid rheometer (ARES-G2M TA Instruments) equipped with parallel horizontal plate-geometry (8 mm diameter) was used to assess the viscoelastic behavior of hydrogels at temperature of 25 ± 0.1 °C.

3.4.2 Drug loading and release assessment

The drug-encapsulated hydrogels were formulated by mixing DOX (1 mg/mL) or DOX (1 mg/mL) + ICG (1 mg/mL) in PBS with CMC-Nb to prepare a 2% solution of the polymer and the mixture was agitated until it was homogeneous. Next, the

cross-linker (TK-DTz) (dissolve in DMSO: PBS = 1:10 v/v) was added into the CMC-Nb solution (confirming to different mol. ratios as presented in Table 1). The mixture was agitated for 15 s using vortex. The resulting hydrogels were freeze dried under vacuum. The lyophilized DOX-encapsulated hydrogels were soaked in PBS for 15 min to eliminate unloaded or surface-adhering DOX/ICG. To measure the drug loading efficiency (DLE%), the optical absorbances of rinsed solutions were recorded by using a UV-Vis spectrophotometer (485 nm wavelength). DLE% was calculated by using the following equation:

$$\text{DLE (\%)} = \frac{\text{quantity of DOX in feed} - \text{quantity of DOX in supernatant}}{\text{quantity of DOX in feed}} \times 100 \quad (6)$$

The *in vitro* DOX-release experiments were conducted in a physiological medium (PBS, pH 7.4), and in 0.5% H₂O₂. Moreover, NIR-responsive drug release tests were conducted after exposing DOX + ICG-encapsulated hydrogels to NIR irradiation (4-watt power) for 20 min. For all release experiments, the washed hydrogels were transferred in dialysis bags (3.5 K MWCO) containing 5 mL of respective media and subsequently followed the dialysis against 30 mL of respective media. After specified time period, aliquots (3 mL) were drawn periodically and the optical absorbances of the released DOX were measured in

respective media using a UV-Vis spectrophotometer. After analyzing the absorbance (λ max = 485 nm) by using on a DOX calibration curve, 3 mL of respective new media were substituted back into the particular respective tubes to compensate the withdrawn volume.

3.4.3 *In vitro* cytotoxicity analysis of precursors and fabricated hydrogels

To evaluate the cytocompatibility of CMC-Nb, TK-DTz, and fabricated hydrogels, the water-soluble tetrazolium salt (WST) assays was performed using human embryonic (HEK 293) cells. In this experiment, HEK-293 cells were cultured in a 48-well plates at 1×10^4 cells/well in a growth medium (DMEM supplemented with FBS (10%) and 1% antibiotic-antimycotic solution), and incubated at 37 °C with 5% CO₂ for 24 h. After the incubation period, the culture media were removed, and fresh media containing various concentration of UV-sterilized CMC-Nb (0, 100, 250, 500, 1000, 1500, 2000 µg/mL), or TK-DTz (0, 10, 20, 30, 40, 50, 100 µg/mL) and TKHG-C hydrogels were added. After 48 h of incubation, each group of cells were washed twice with 100 L of PBS. Then, WST substrate (10 µL) was introduced into each well, and measured the optical absorbances at a wavelength of 450 nm. Additionally, a calcein AM/ethidium bromide kit was employed to validate

the cytocompatibility of the hydrogels. On confocal microscopy plates, HEK-293 cells were cultivated and then exposed to the precursor of CMC-Nb (2000 $\mu\text{g}/\text{mL}$), cross-linker (100 $\mu\text{g}/\text{mL}$), and TKHG-C hydrogels. The cells were then stained with ethidium bromide to detect non-viable cells and calcein-AM to visualize viable cells.

3.4.4 *In vitro* anti-tumor activity of DOX+ICG-encapsulated hydrogels

To study the release profile of encapsulated DOX in response to NIR light and subsequent effectiveness in combating tumors, we conducted experiments using HeLa cancer cells. These cancer cells were cultured in the lower chamber of trans-wells. In the upper chamber of the trans-wells, we placed different concentrations of free-DOX ranging from 5 to 20 $\mu\text{g mL}^{-1}$ and TKHG-C hydrogels containing equivalent amount of ICG and DOX and then exposed to NIR irradiation for 5 min at a power of 4 watts. Similarly, control tests were conducted without applying NIR light. Afterwards, the cells were allowed to grow in incubation chamber for 48 h, and anti-tumor effects were evaluated using WST-1 assays, as outlined previously. Further, the fluorescence-based live/dead assay was conducted to assess the cytotoxicity.

3.4.5 Hemolysis assay

In vitro hemocompatibility of TKHG-C hydrogels was evaluated by conducting hemolysis assay using a mouse red blood cell (RBCs). The hydrogels were first immersed in saline, and extracts of the hydrogels (500 μ L) were collected after 2 h. Subsequently, the hydrogel extracts were supplemented with freshly collected mouse RBCs and samples were incubated for 2 h at 37 $^{\circ}$ C. Distilled water and saline solution (without hydrogel extracts) served as the positive and negative controls, respectively. After centrifugation at 3000 rpm for 10 min, supernatants were collected, and the absorbance of hemoglobin was quantified using a microplate reader (SpectraMax ABS Plus, Molecular Devices, San Jose, CA, USA) at a wavelength of 540 nm. The percentage of hemolysis ratio was calculated by the following equation:

$$\text{Hemolysis ratio (\%)} = \frac{A_{\text{sample}} - A_{\text{negative}}}{A_{\text{positive}} - A_{\text{negative}}} \times 100 \quad (7)$$

where A_{sample} , A_{negative} control, and A_{positive} control are the absorbance values of the supernatant fraction of the samples, negative and positive controls, respectively.

3.4.6 *In vitro* evaluation of ROS production

The ROS production ability of hydrogels was monitored by the degradation rate of a fluorescent molecule, 1,3-diphenylisobenzofuran (DPBF). The experimental setup contained 20 μg of either ICG or TKHG-C hydrogels (containing equal amount of ICG) mixed in a solution of DPBF (DPBF: water = 1:10 v/v). After exposure to NIR irradiation ($4\text{-W}/\text{cm}^2$), the samples were placed in a quartz cuvette and their fluorescent intensities were recorded within the wavelength range of 420-700 nm while being excited at 410 nm.

3.4.7 Statistical analysis

At least three replicates were performed for all physiochemical experiments and cell culture trials were conducted using 4-replicas. All data are shown as mean \pm standard deviation (SD). All data are presented as mean \pm standard deviation (SD). GraphPad Prism version 9.3 (GraphPad, San Diego, CA, USA) was used to perform statistical analysis. from independent experiments. (ns: no significant, * $p < 0.05$, ** $p < 0.01$, and *** $p < 0.001$, calculated by using Student's t-test and one-way analysis of variance (ANOVA), followed by a Tukey-Kramer post hoc test).

3.5 Results and discussion

3.5.1 Synthesis of TK-DTz

The synthetic approaches to prepare the ROS-cleavable and bio-orthogonal IEDDA click-able TK-DTz cross-linker was schematically summarized in Scheme 2. TKDA was first synthesized by the reaction of mercaptoacetic acid with acetone, and the synthesis of TKDA was confirmed by ^1H NMR as depicted in Figure 14a. The chemical shifts corresponding to the protons of CH_3 and CH_2 appeared at 1.49 and 3.32 ppm, respectively, whereas the characteristic peak corresponding to the carboxylic group of TKDA appeared at 12.5 ppm. Next, amino functional tetrazine with a tert-butyloxycarbonyl (BOC-) protecting group was synthesized from tert-butyl 4-cyanobenzylcarbamate (TBC) following our previous report [110]. It has been reported that hydrazine could undergo a reaction with the amine group of TBC, therefore amine groups were protected with BOC groups [112]. The chemical structure of TBC was assessed by ^1H NMR (Figure 14b), showing a distinct peak at 1.39 ppm which attributed to the protons of $-\text{CH}_3$ groups of BOC. The proton peak associated with $-\text{NH}-$ of amide groups was observed at 7.54 ppm and the proton peaks appeared at 7.42-7.78 ppm were assigned to the aromatic ring of TBC. In a next step, the cyanide group of TBC was chemically modified to tetrazine rings

by adding catalyst (zinc(II)-trifluoromethanesulfonate) and anhydrous hydrazine in acidic media. The colorless solution changed to pink color during the reaction, confirming the creation of tetrazine rings. Tz-NH-BOC was assessed by the ^1H NMR spectrum (Figure 14c). The ^1H NMR signal of $-\text{CH}_3$ protons appeared at the same position at 1.39 ppm verifying the presence of the BOC group. In addition, a new signal was observed at 10.57 ppm, which can be attributed to the $-\text{CH}$ proton of the tetrazine ring, indicating the conversion of cyanide groups into tetrazine rings.

Afterwards, the BOC group was cleaved off by treating with oxalyl chloride, and the amine group was unprotected to produce pure tetrazine-amine (60%). All characteristic peaks of tetrazine-amine were confirmed by ^1H NMR analysis (Figure 14d). The chemical shift related to BOC groups completely vanished and a new ^1H NMR signal attributed to the $-\text{NH}_2$ group of the tetrazine-amine appeared at 8.5 ppm. Specifically, the signal of the $-\text{CH}$ proton of tetrazine ring slightly shifted from 10.57 ppm to 10.63 ppm, which confirmed the formation of Tz- NH_2 .

To synthesize the cross-linker (TK-DTz), the activation of COOH groups of TKDA were carried out by using DCC/NHS chemistry. Subsequently, these activated groups were utilized in the reaction with tetrazine-amine to synthesize TK-DTz (52%

yield). The successful synthesis of TK-DTz was verified by ^1H NMR (Figure 14e). Two peaks at 1.26 and 3.05 ppm could correspond to $-\text{S}-\text{C}-\text{CH}_3-$ and $-\text{S}-\text{CH}_2-$, respectively. Notably, the signal of $-\text{CH}$ proton of the tetrazine-ring was observed at 10.26 ppm while the proton signal of the $-\text{NH}-$ bond appeared at 8.4 ppm, which confirmed the formation of TK-DTz.



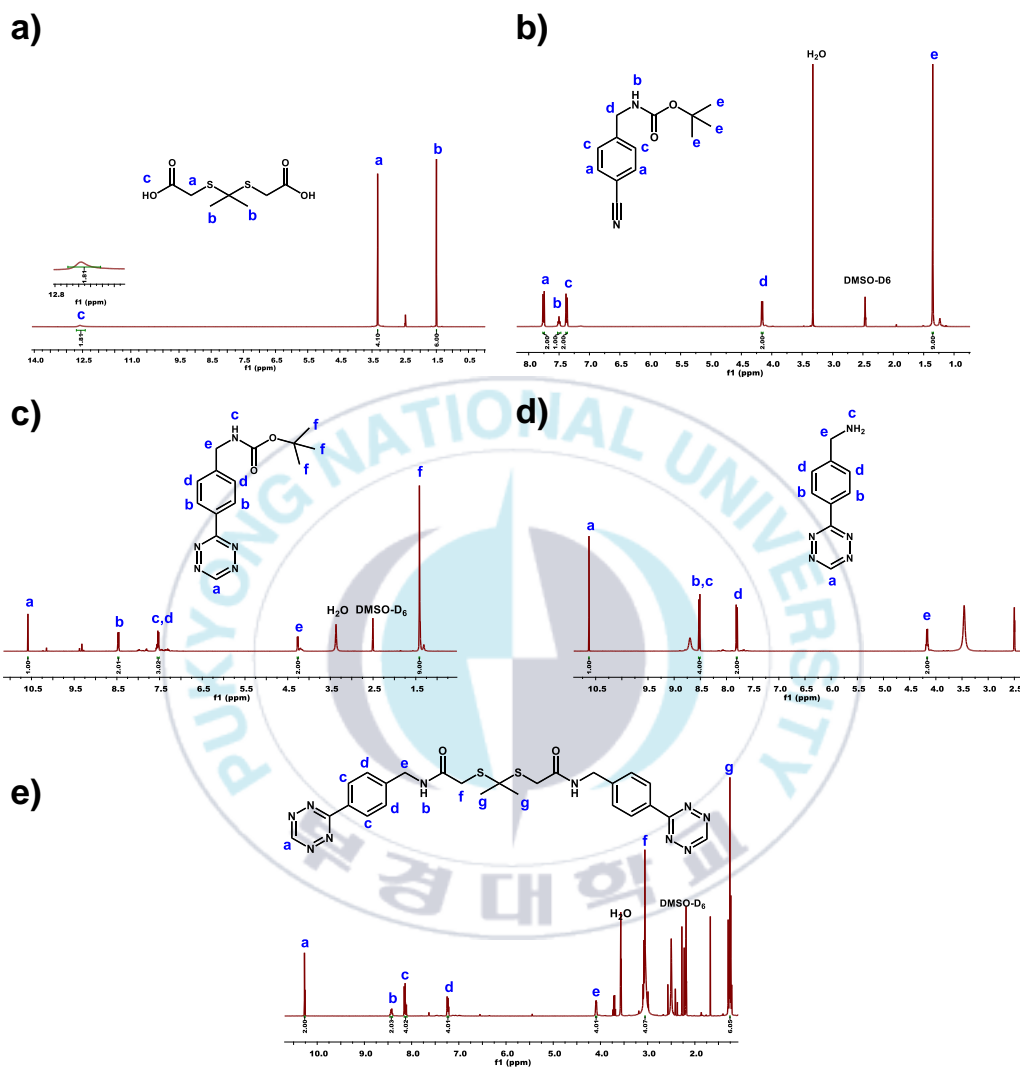


Figure 14. $^1\text{H-NMR}$ spectrum of TKDA (a), TBC (b) Tz-NH-BOC (c) Tz-NH₂ (d), and TK-DTz cross-linker (e).

3.5.2 Synthesis of CMC-Nb

Chemical derivatization represented a promising tool with the possibility of easily modifying a CMC structure to enhance its physio-chemical properties such as hydrophilicity, viscosity, bio-degradation, mechanical properties, and bioactivity. The derivatives of CMC have been created and used as biomaterial scaffolds in tissue engineering, wound healing, cosmetic fillers, 3D-bioprinting, drug delivery, and cancer therapy [113]. The carboxylate and hydroxyl groups present on the backbone of CMC have been modified by several pendent functional groups e.g., methacrylate, thiol, aldehyde, and alkyne/azide groups, [114, 115] to enhance its potential use in cancer therapy. In this study, CMC was chemically modified with Nb groups to develop a precursor for IEDDA click reaction. The modification reaction was carried out between COOH groups of CMC and NH₂ groups of Nb-NH₂ by using EDC and NHS to prepare CMC-Nb. The modified CMC-Nb was assessed by the ¹H NMR spectrum (Figure 15a). The peaks of alkene protons in the range of 5.9-6.2 ppm were attributed to Nb groups while the chemical shift appeared approximately at 4.9 could be assigned to the proton connected with the β-(1→4) glycosidic linkages of the CMC-backbone [116]. The DS of Nb was determined through the integration ratio of corresponding protons of the Nb groups and protons

of the glycosidic bonds, and found to be about 15%. CMC-Nb was further characterized by FTIR (Figure 15b). A strong absorption peak appeared at 3400 cm^{-1} could be attributed to the hydroxyl groups ($-\text{OH}$) of CMC. The presence of absorption peaks at 1600 cm^{-1} and 1409 cm^{-1} corresponded to the $\text{C}=\text{O}$ stretching and $\text{N}-\text{H}$ bending vibrations, respectively. The weak absorption peak of the alkene bond was noted at 675 cm^{-1} which confirmed the formation of CMC-Nb.



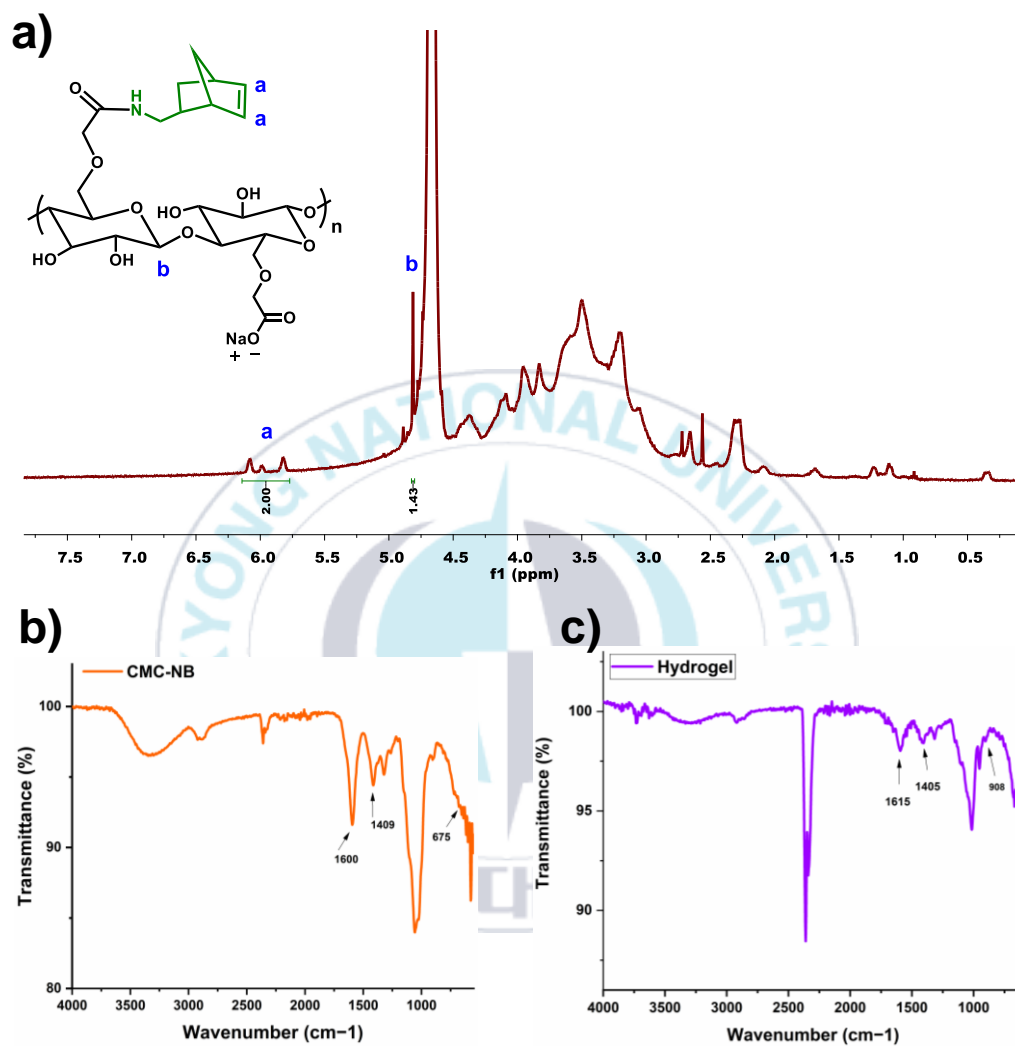


Figure 15. (a) $^1\text{H-NMR}$ spectrum of CMC-Nb, (b-c) FTIR spectra of CMC-Nb and formulated hydrogel.

3.5.3 Fabrication and characterization of the hydrogels

The utilization of Nb/Tz click reaction to form hydrogels offers some key advantages including quick gelation, precise control over stoichiometry, and potential for easy scale-up. Three kinds of hydrogels were fabricated labeled as TKHG-A, TKHG-B, and TKHG-C by varying the feed ratio of precursors CMC-Nb and TK-DTz (10:2.5, 10: 5, and 10:10, Nb/Tz, mol.ratio, respectively). During the preparation of hydrogels, the free-polymer chains of CMC underwent spontaneous cross-linking with TK-DTz cross-linkers through Nb/Tz click reaction, leading to the rapid transformation of the sol state into gel state. The cross-linked hydrogel was validated by FTIR analysis (Figure 15c), representing all the characteristics peaks of CMC and TK-DTz, which confirmed the successful chemical bonding occurred *via* Nb/Tz click reaction.

3.5.4 Gelation times and viscoelastic properties of CMC hydrogels

The sol-gel transition of hydrogels was visually confirmed *via* the invert vial test, as shown in photographs (Figure 16a). Based on the tube inversion test, hydrogels exhibited rapid gelation times between 170 and 495 s (Table 2) owing to the robust Nb/Tz reaction. The gelation times and viscoelastic properties of the CMC

hydrogels were further examined by step time and frequency dependent rheological experiments through measurement of the storage (G') modulus and loss modulus (G'') by using a rheometer. Notably, the hydrogel TKHG-A with minimum TK-DTz contents (10:2.5) exhibited the sol-gel transition time of about 450 s, as evaluated by the crossover point of G' and G'' (Figure 16b). The hydrogels TKHG-B (Fig. 3c) and TKHG-C (Figure 16d) presented shorter gelation times 325, and 220 s, respectively, resulting from higher mol. ratios of cross-linker. These sol-gel transformation time ranges indicate that the gelation time can be tuned easily by varying the stoichiometric ratios of click functionalities (Nb and Tz groups). Similarly, in a frequency sweep test at a constant strain of 1 % with ascending angular frequencies from 0 to 100 rad/s, hydrogels TKHG-A (Figure 16e), TKHG-B (Figure 16f), and TKHG-C (Figure 16g) showed the storage modulus 1220 dynes/cm², 2330 dynes/cm², and 2770 dynes/cm², respectively. These viscoelastic results exhibited that the hydrogel modulus could be controlled by different concentration of cross-linker. These results are consistent with the previous studies which reported that a higher concentration of cross-linker increased the cross-linking density in the network of hydrogels, which in turn led to increase the mechanical properties of hydrogels [117].

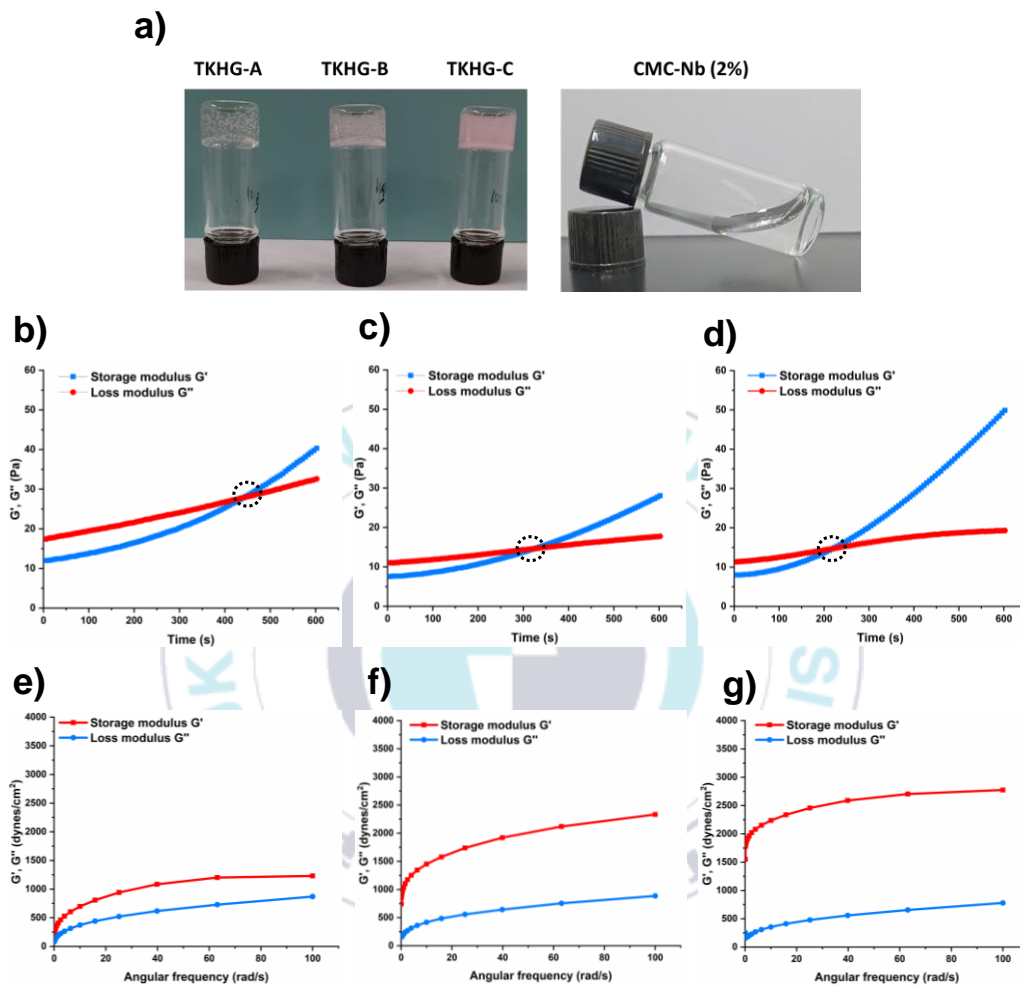


Figure 16. Mechanical properties of TKHG-C, TKHG-B, TKHG-A hydrogels. (a) Photograph pictures of hydrogels formation, (b-d) Storage and loss modulus as a function of respective step time, (e-g) Storage and loss modulus as a function of angular frequency.

3.5.5 Swelling and water retention properties

Swelling property of hydrogels is a peculiar characteristic related to their design and implications in biomedical and pharmaceutical applications [3]. In this study, the water retention capacity of the hydrogels was determined by carrying out the gravimetric measurements. The lyophilized hydrogels were submerged in PBS (pH, 7.4) at RT. After pre-determined time point, the weight of hydrated hydrogels was noted to determine the swelling ratios of hydrogels (Figure 17). All hydrogel samples exhibited high swelling in the initial 4 h. The degree of swelling increased gradually with increasing the immersing time and an equilibrium swelling was achieved after 48 h. Notably, the hydrogels TKHG-A, TKHG-B, and TKHG-C showed high degree of swelling of 5900, 3400, and 2300%, respectively. These results can be attributed to the concentration of cross-linker which showed that degree of swelling of the hydrogels decreased by increasing the concentration of cross-linker. These findings are consistent with the previous reports which indicated that higher amount of cross-linker created higher cross-linking densities and formed a more compact structure within the hydrogel networks that restrained the swelling of hydrogels by less water uptake.

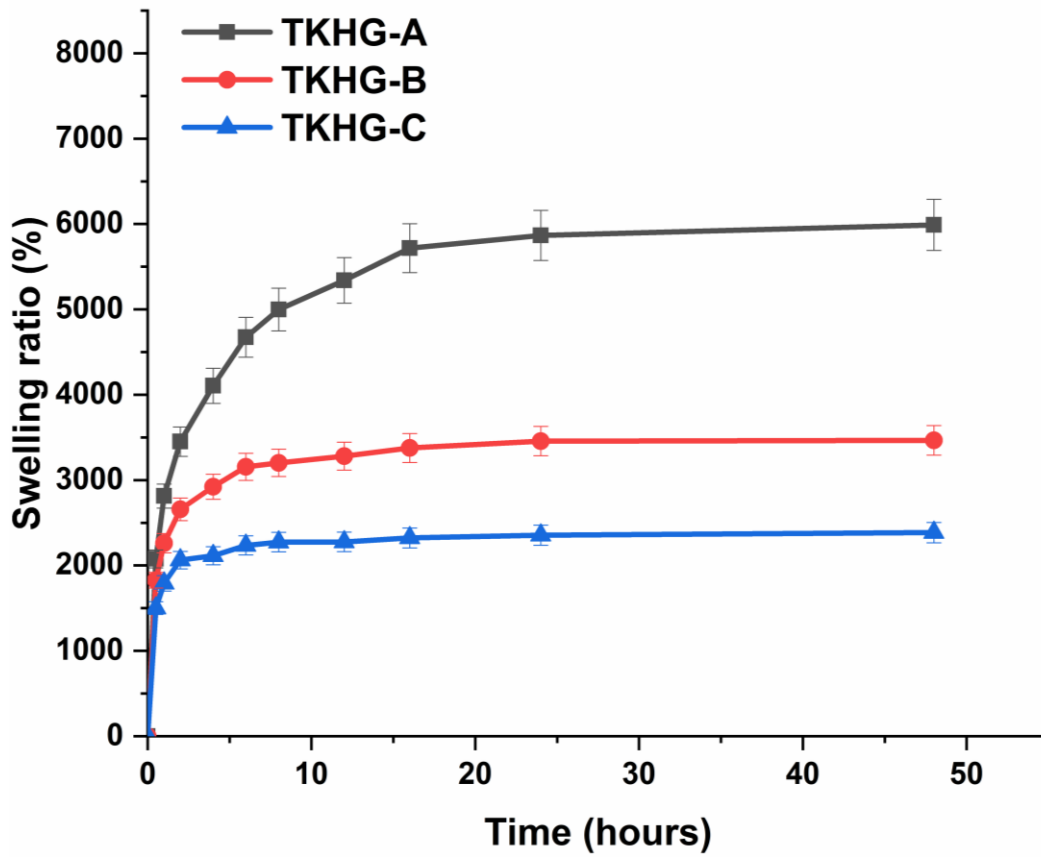


Figure 17. Swelling behavior of hydrogels in physiological condition.

3.5.6 Morphological analysis

The formulated hydrogels showed porous architectures which could be attributed to *in situ* formation of micro-bubbles within the networks caused by N₂ gas released during the IEDDA click reaction. The *in situ* porous internal structures of wet hydrogels induced by nitrogen bubbles were visually observed by an optical microscopy using a fluorescent compound (Rhodamine-G6). All formulated hydrogels exhibited apparently internal microporous structures, confirmed by red bubbles, as depicted in Figure 18a. Interestingly, the amount of bubbles increased significantly by increasing the mol ratio of cross-linker, which released more N₂ gas in the network structure and consequently generated higher porosity. Furthermore, each sample of hydrogels was probed by FE-SEM (Figure 18b) to investigate the porous network of hydrogels after lyophilized, where entrapped N₂ gas and water droplets were leached out. It was observed that the microstructure of the hydrogels varied with different concentrations of the cross-linker. Specifically, all hydrogels with different concentrations exhibited highly porous morphology, however the porosity reduced when the concentration of the cross-linker increased. This result implied that the dense network structure of hydrogels occurred owing to its high cross-linking degree at the maximum concentration of the cross-linker. It is

well known that porosity directly effects on several properties of hydrogels, including drug loading, drug release, and degradation. As a result, high porosity observed in CMC hydrogels could significantly impact on drug release and interaction between cells to matrix, as previously documented in literature [118].

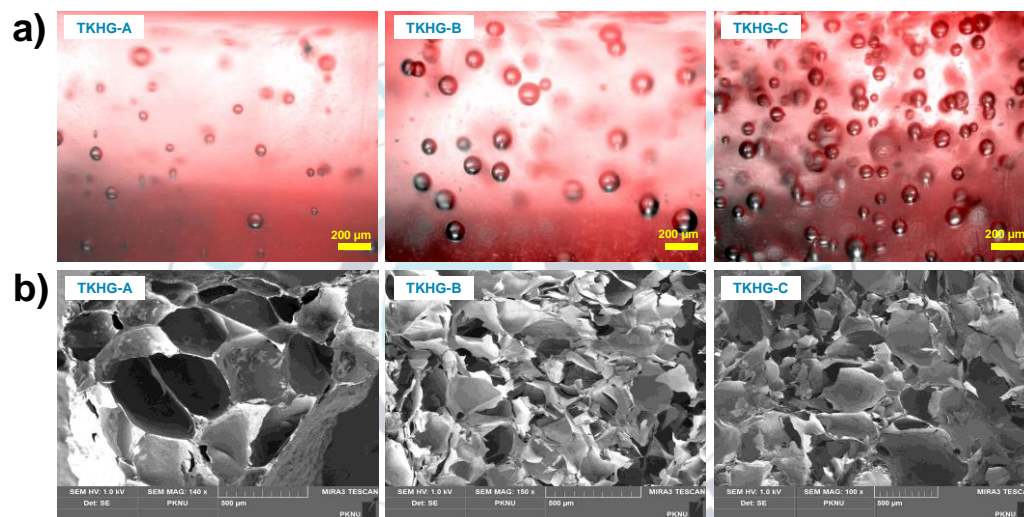


Figure 18. Morphology of hydrogels (a) optical microscopic images to find porosity by entrapment of N₂ bubbles inside hydrogels generated by IEDDA click reaction (b) SEM images of cross-sections of hydrogels.

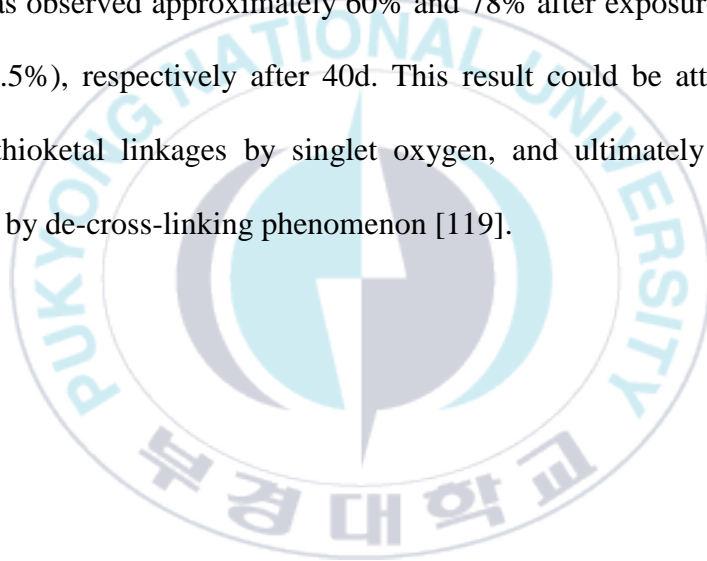
3.5.7 Drug loading and release studies

The most significant application of hydrogels in biomedical fields is drug loading and sustained release. However, it is important that a drug carrier should release drugs completely with a limited initial burst release. Promising ROS-sensitive TKHGs hydrogels could be utilized in possible applications in the encapsulation, localization, sustained, and temporal release of drugs. In this work, DOX as a model anticancer drug was used to investigate the drug loading efficiency and release profiles of TKHG-C hydrogels. The DOX-encapsulated hydrogels were freeze dried and rinse with PBS to remove the unbound and surface-adsorbed DOX. The DLE (%) and DC (%) were measured by using UV-visible spectrophotometer. Interestingly, TKHG-C hydrogel showed high drug loading efficiency and drug content of 95% and 4.54%, respectively. The high drug loading efficiency could correspond to the compact network structure of hydrogels with interlocked linkages resulting from higher cross-linking densities, which effectively restrained the drug molecules to escape from hydrogels.

In order to investigate whether the DOX release could be controlled upon NIR light or/and H₂O₂, the ROS-sensitive release behavior of the TKHG-C hydrogels was

studied with or without NIR irradiation. For this purpose, ICG, as a ROS generating molecule, was encapsulated into hydrogels along with DOX. Notably, no apparent burst release of encapsulated-DOX was observed in PBS (pH 7.4) without any stimulation, only a small fraction of DOX release of approximately 25% was detected after 168 h, as representing in Figure 19a., indicating the evidence that DOX could be stably preserved in the interlocked cross-linked networks of hydrogels. In contrast, the DOX release was markedly accelerated upon a stimulation of NIR light (Figure 19b) or/and H₂O₂ (Figure 19c). Specifically, a rapid DOX release was observed about 67% and 72% upon NIR irradiation and H₂O₂ after 24 h, respectively. The burst DOX release was further followed by a sustained and temporal DOX release, around 96% and 99% DOX release was noted after 168 h upon NIR irradiation and H₂O₂, respectively. The initial burst DOX release could be attributed to the rapid generation of ROS upon exposure of NIR or/and H₂O₂-enrich environment. The rapid interaction of NIR with ICG or/and H₂O₂-enrich environment, generated ROS which likely cleaved the thioketal bond. Consequently, the hydrogel networks breakdown by de-cross-linking and disentangled the 3D network of hydrogels which turned into the sustained release behavior of the entrapped DOX [98]. The biodegradation of hydrogel was further

studied to better understand the de-cross-linking of TKHG-C hydrogels upon exposure of NIR light or/and oxidizing environment H_2O_2 (0.5%) as represented in Figure 20. It is apparent that the hydrogel maintained the structural integrity and remained stable in PBS (pH, 7.4), showed no significant mass loss (<19%) after 40d in the absence of NIR light. However, the temporal degradation rate of hydrogels was observed approximately 60% and 78% after exposure of NIR light and H_2O_2 (0.5%), respectively after 40d. This result could be attributed to the scission of thioketal linkages by singlet oxygen, and ultimately the hydrogel disintegrated by de-cross-linking phenomenon [119].



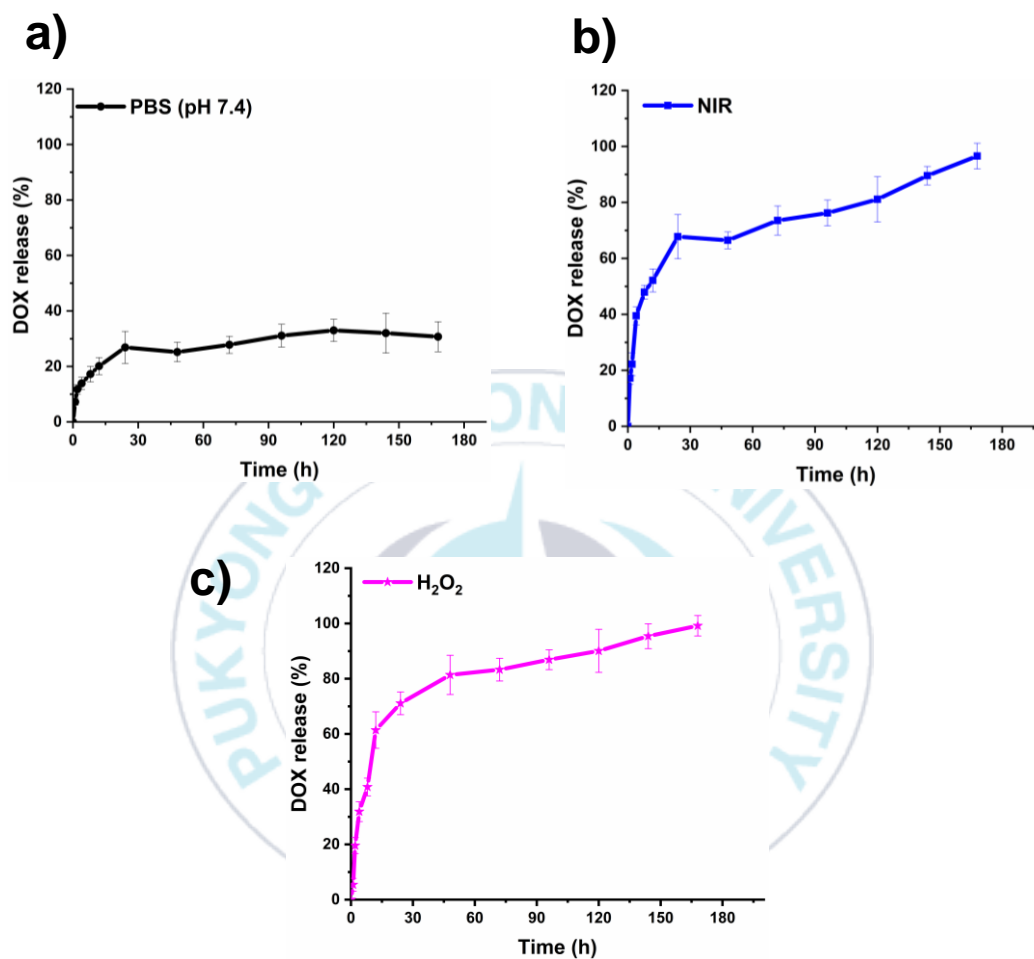


Figure 19. Cumulative DOX release profiles of the hydrogels TKHG-C. (a) Drug release profile of hydrogels in physiological condition, (b) drug release profile of DOX + ICG-encapsulated hydrogels when irradiated with NIR-light (808 nm, 4-W/cm-2, 20 min), (c) drug release profile of hydrogels in H₂O₂ (0.5%).

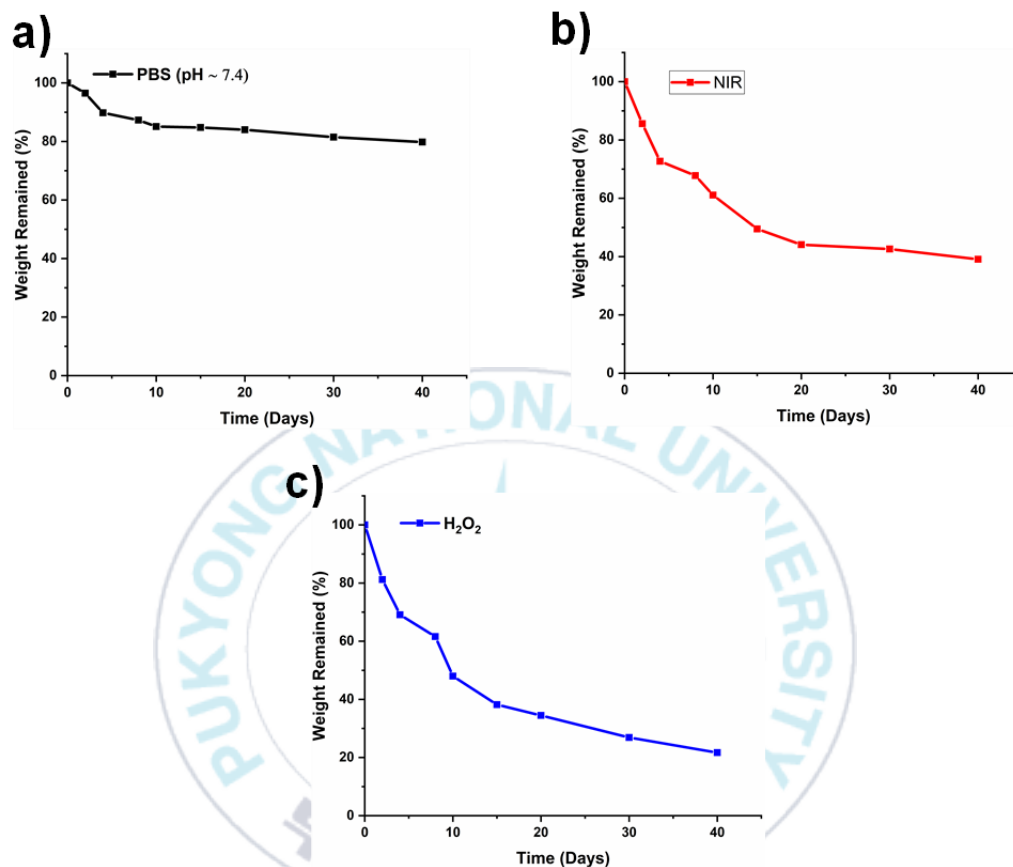
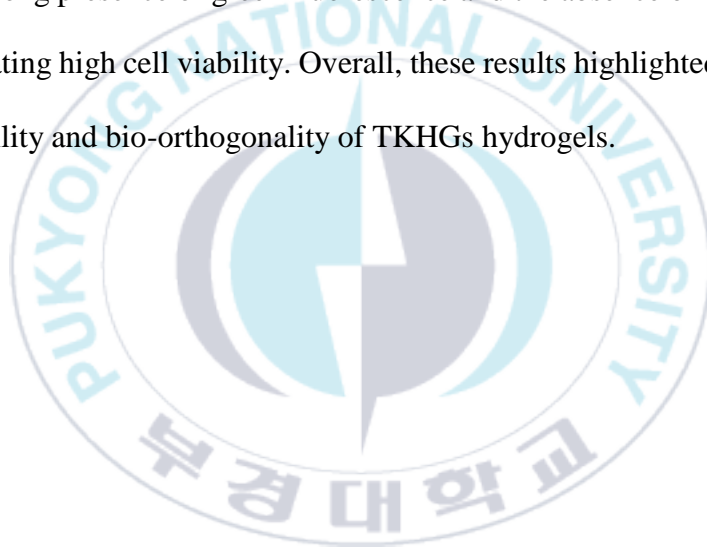


Figure 20. Biodegradation of formulated hydrogels (TKHG-C). (a) in PBS (pH, 7.4) without NIR irradiation, (b) irradiated with NIR light (808 nm, 4-watt), and (c) in H₂O₂ (0.5% in PBS).

3.5.8 *In vitro* cytocompatibility of precursors, blank hydrogels and DOX/ICG-encapsulated hydrogels

The evaluation of cytocompatibility is an important pre-requisite for hydrogels which may induce some harmful effects on biological functions. The *in vitro* cytotoxicity of CMC-Nb, TK-DTz and resulting hydrogels was assessed in normal cells (HEK-293) by using both WST assays and live/dead staining. For cytotoxicity assessment, HEK-293 cells were treated with various concentrations of CMC-Nb, TK-DTz, or blank hydrogels (TKHG-C) for 24 h, and cell viability was evaluated in the dark. From cytotoxicity results, it is apparent that the growth of HEK-293 cells was not significantly influenced by the presence of CMC-Nb, TK-DTz, or blank hydrogels. The precursor CMC-Nb exhibited biocompatibility and safety at the highest concentration of 2000 $\mu\text{g}/\text{mL}$, with 99% cell viability, as depicted in Figure 21a. This biocompatibility studies indicated that incorporating of Nb moieties into CMC did not detrimentally impact on its biocompatibility, which is important for its use in the development of bio-orthogonal hydrogels. Similarly, TK-DTz displayed cell viability around 97% after treatment with HEK-293 cells at maximum concentration of 100 $\mu\text{g}/\text{mL}$, as presented in Figure 21b. Additionally, the viability of HEK-293 cells treated with hydrogels (TKHG-C) remained 100%

after 48 h (Figure 21c). Overall, these findings indicated that the developed hydrogels were biocompatible which allowed the treated cells to proliferate effectively and also showed comparable cell viability to the control groups. The biocompatibility of CMC-Nb, TK-DTz, and TKHG-C hydrogels was further validated by live/dead assays, as illustrated in Figure 21d. The micrographs of cells revealed a strong presence of green fluorescence and the absence of dead cells (red color), indicating high cell viability. Overall, these results highlighted the excellent biocompatibility and bio-orthogonality of TKHGs hydrogels.



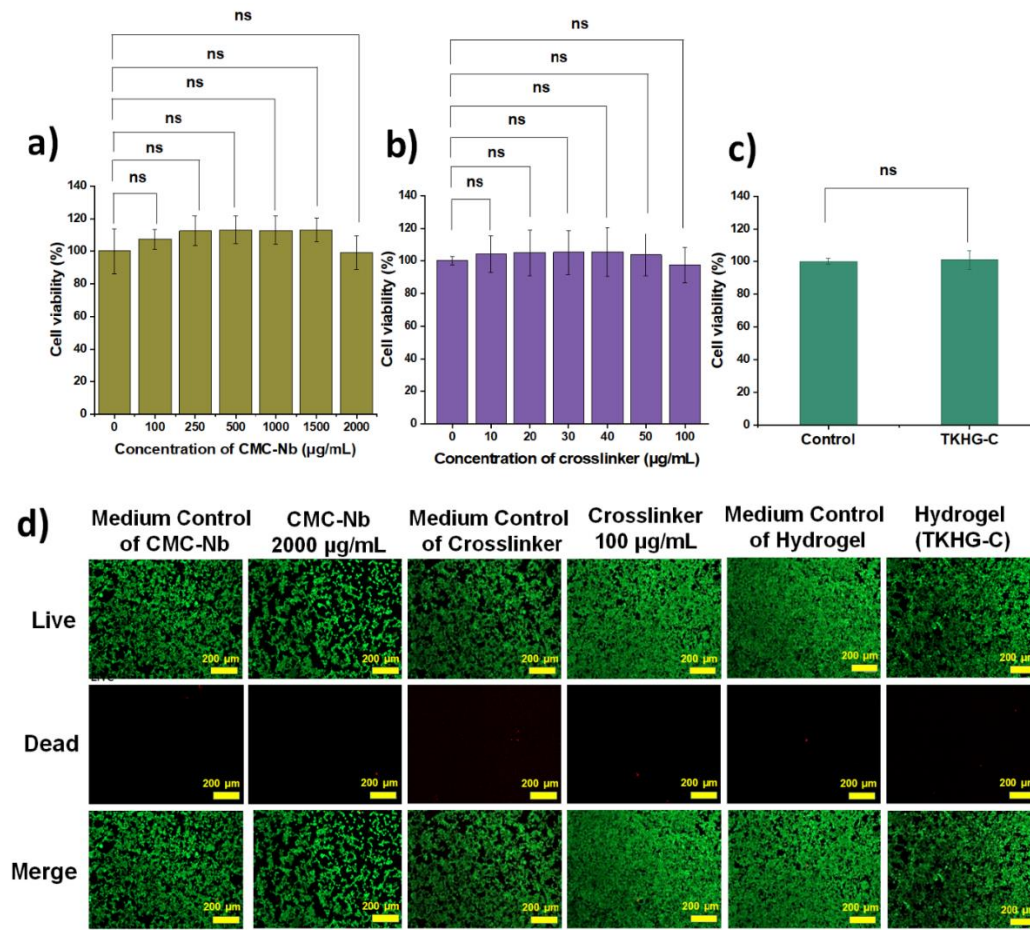


Figure 21. Cytotoxicity assessment of precursors and TKHG-C hydrogel (a) cytotoxicity of CMC-Nb (b) Cytotoxicity of TK-DTz (c) hydrogel (d) Cell viabilities were assessed by Live/dead assays to validate the cytocompatibility of CMC-Nb, TK-DTz, and TKHG-C hydrogel, respectively.

3.5.9 Hemolytic activity of hydrogels

Hemolysis test was carried out to assess the safety and hemocompatibility of the hydrogels in red blood cells. As depicted in Fig. 8a, the experimental results showed no considerable hemolysis ratio in the negative control (saline solution) and the hydrogel samples. In contrast, positive control (distilled water) exhibited the hemolytic ratio. Specifically, the hemolysis value for the positive control was set at 100%, while the extract of the hydrogels and negative control (saline solution) displayed 1.98, 1.92% hemolytic ratios, respectively, as shown in Fig. 8b. The tested hydrogels showed the hemolysis value <5.0 % and in agreement with the national standard level (ISO 10993–51,992) for medical biomaterials. The above results demonstrated that the hydrogels were safe and possessed good hemocompatibility.

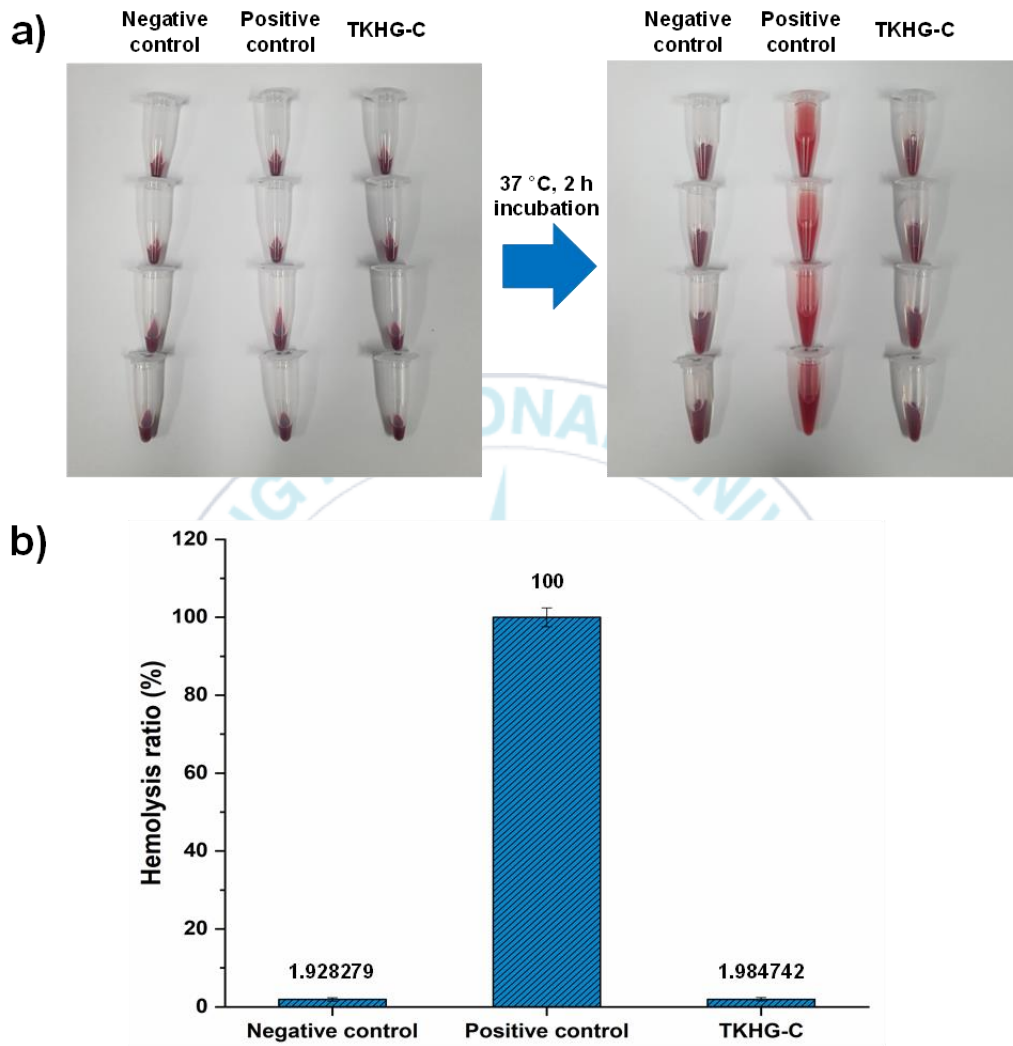


Figure 22. Hemocompatibility of hydrogels. (a) Photographs of hemolysis test performed using saline (negative control), deionized water (positive control), and TKHG-C hydrogels, and (b) hemolysis ratio of TKHG-C hydrogels.

3.5.10 The anti-cancer activity of formulated hydrogels

The HeLa cancer cell lines were used to evaluate in vitro synergistic anti-cancer efficacy of DOX + ICG-encapsulated hydrogels when exposed to NIR light. To evaluate the NIR-responsive DOX release and anticancer effect, DOX + ICG-encapsulated hydrogels (containing 5, 10, 15, 20 $\mu\text{g mL}^{-1}$) (positioned in the upper chamber of a trans-well) were subjected to NIR irradiation and incubated with HeLa cancer cells (cultivated in the lower chamber of the trans-well) for a period of 48 h. All DOX-encapsulated hydrogels and free DOX exhibited in vitro antiproliferation of tumor cells, as depicted in Fig. 23a. The cell viability rate after treatment with free-DOX (20 μg) was around 6.5%. While, upon exposure NIR irradiation to DOX + ICG-encapsulated hydrogels (containing equivalent amount of DOX) demonstrated 6.7% cell viability. The cytotoxic effect of ICG + DOX-encapsulated hydrogels was further validated by Live/dead assay. The cultured cells were exposed to respective formulations and then stained with live/dead staining agents (calcein AM and ethidium bromide). As shown in Fig. 23b, control cells exhibited green fluorescence whereas free-DOX and DOX + ICG-encapsulated hydrogels treated cells showed remarkable red fluorescence denoting the dead cells. These findings indicated the anticancer potential of the hydrogels. The enhanced

antitumor effect of DOX +ICG-encapsulated hydrogels could be attributed to the burst DOX release from the hydrogels along with photothermal effect triggered by NIR irradiation interacting with ICG molecule. Contrarily, DOX-encapsulated hydrogels (containing equivalent amount of DOX) demonstrated less antitumor activity without NIR irradiations (13% cell viability). This lower anti-cancer effect of DOX + ICG-encapsulated hydrogels in the absence of NIR-light can be attributed to the restricted DOX release from the hydrogels due to the dense hydrogel matrix. However, upon NIR irradiation, the thioketal bond was cleaved by ROS, produced by the ICG molecule that leading to de-cross-linking and loosening the network of hydrogels. This phenomenon facilitated the burst release of DOX and increased the antitumor activity [120].

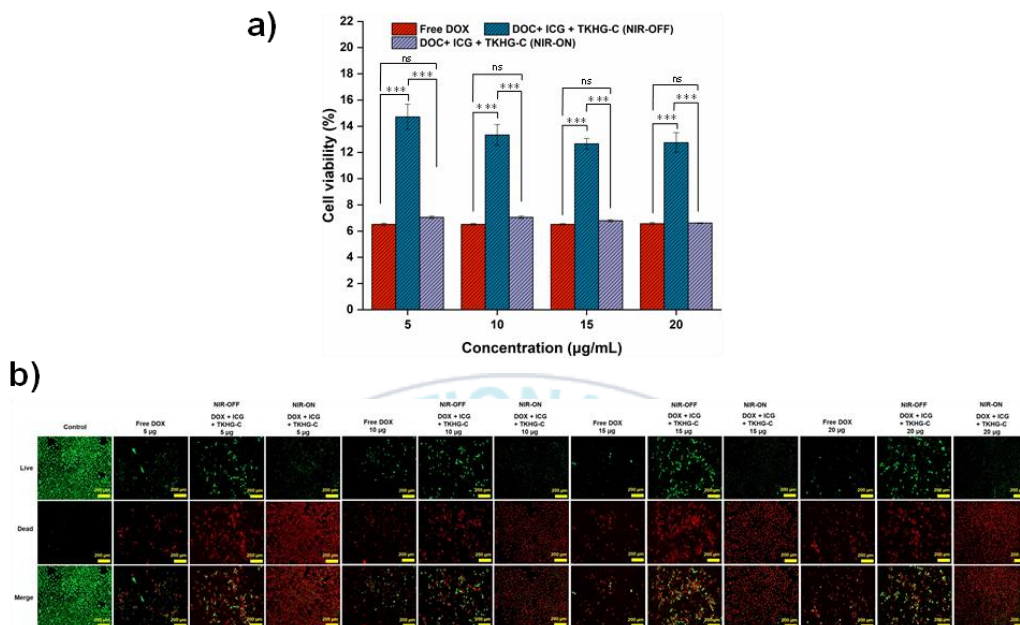


Figure 23. (a) Anti-cancer efficacy against HeLa cancer cells treated with free-DOX and DOX + TKHG-C, and DOX + ICG-encapsulated hydrogels under NIR irradiation. (b) Cell viabilities were assessed by Live/dead assays to validate the anti-tumor effect of DOX + ICG-loaded TKHG-C hydrogels.

The photothermal therapeutic effect of the ICG-encapsulated hydrogels at different concentrations of 5, 10, 15, 20 $\mu\text{g mL}^{-1}$ were tested using HeLa cancer cells. Interestingly, all ICG-encapsulated hydrogels showed 78% cell viability without NIR irradiation, as depicted in Figure 24a. However, ICG-encapsulated hydrogels

exposed to NIR light reduced the cell viability around <0.5%, confirming the photothermal effect as a result of the interaction between NIR-light and ICG. The results were further validated by Live/dead assay as depicted in Figure 24b. The experiment of *in vitro* photothermal conversion was carried out to support the above evidence and the findings are shown in Figure 24c. The temperature of PBS was not affected by NIR-light exposure. While, the temperature of the solutions of free ICG, ICG + DOX, and the ICG-encapsulated hydrogels increased under NIR-light. The solution of free ICG and ICG-encapsulated hydrogels showed maximum temperature around 56 and 57 °C, respectively under 20 min of NIR irradiation. However, the ICG + DOX solution exhibited a lower temperature of approximately 41 °C after exposing NIR light. The decrease in temperature of ICG/DOX solution as compared to ICG solution is due to electrostatic interaction between ICG and DOX and form a complex aggregation as reported in the literature [110, 121].

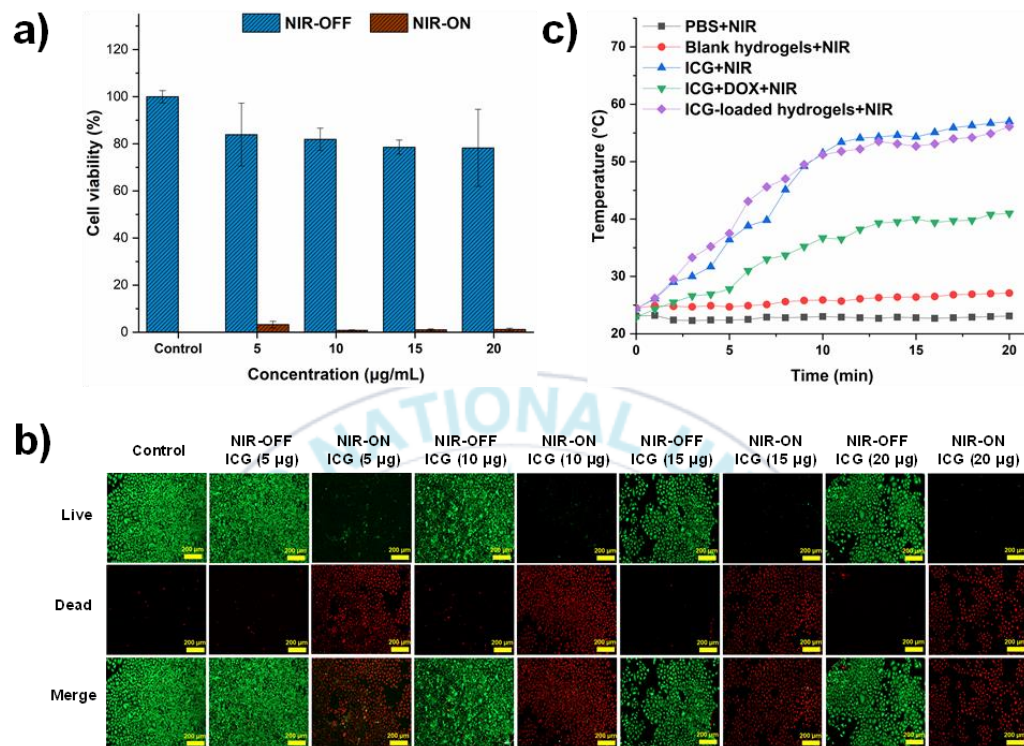


Figure 24. (a) HeLa cancer cells viability of the ICG-encapsulated TKHG-C hydrogels with or without NIR-light. (b) Cell viabilities were assessed by Live/dead assays to validate the photothermal thermal effect of ICG-loaded TKHG-C hydrogels. (c) Photothermal conversion of ICG and ICG-encapsulated/ICG + DOX hydrogels after NIR irradiation.

3.5.11 In vitro ROS production

To assess the production of ROS triggered by the interaction between NIR-light and ICG molecules, 1, 3-diphenylisobenzofuran (DPBF) was employed as a specific ROS sensor. The DPBF is a fluorescent compound known for its high reactivity with ROS oxidants, including singlet oxygen ($^1\text{O}_2$), hydroxy ($\cdot\text{OH}$), alkyloxy ($\text{RO}\cdot$), or alkylperoxy ($\text{ROO}\cdot$) radicals. When exposed to ROS, DPBF undergoes rapid oxidation and decomposed into irreversible product (1,2-dibenzoylbenzene or O-benzoylbenzophenone), resulting in a reduction in its optical densities [86]. Notably, a similar pattern of optical densities of the samples were observed without NIR irradiation or ICG, as demonstrated in Figure 22d. However, a significant decrease in the optical densities was observed in the samples that contained either ICG or ICG-encapsulated hydrogels when exposing to NIR light, affirming the production of ROS. These findings indicate that ICG/DOX + ICG-loaded hydrogels consisting thioketal-bonds have the potential to serve as a robust candidate for delivering DOX and conducting photothermal therapy for effective tumor eradication.

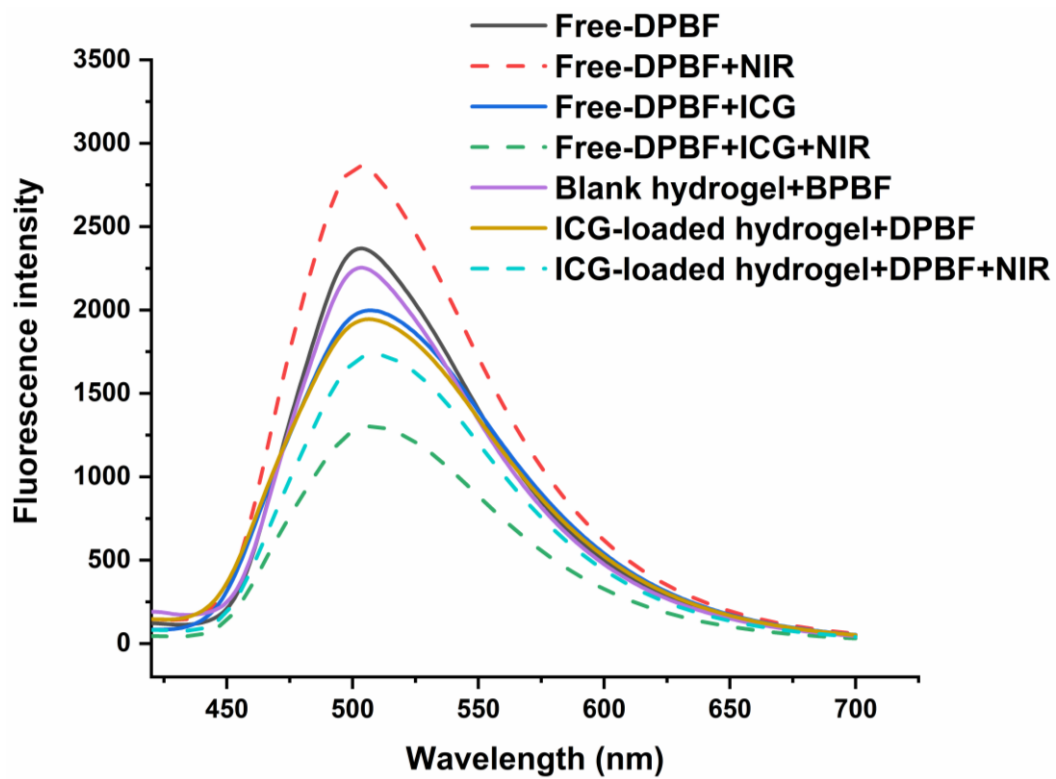
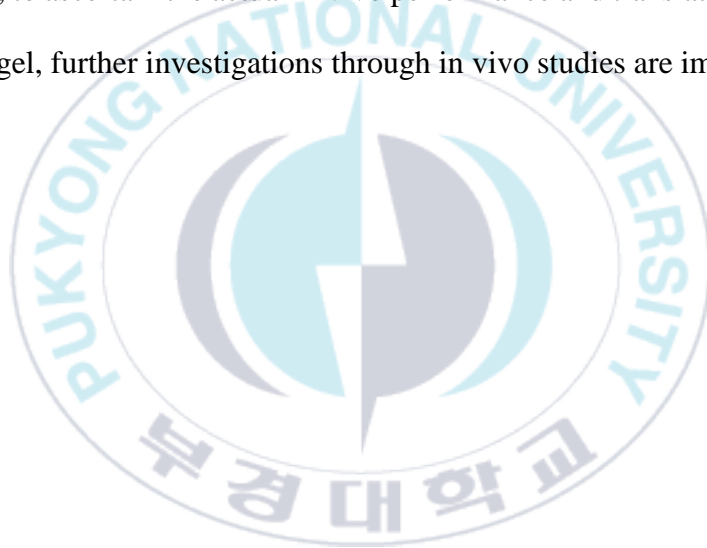


Figure 25. Graph of change in the optical densities of DPBF as a function of ROS production under NIR irradiation to ICG/ICG-encapsulated TKHG-C hydrogel.

3.6 Conclusions

NIR-responsive CMC hydrogels were fabricated using the ROS-degradable cross-linker comprising of thioketal bonds via a bio-orthogonal IEDDA “click” pathway for on-demand DOX release along with synergistic chemo-photothermal therapy. Initially, the Nb moieties were substituted on the backbone of CMC and then reacted with the TK-DTz cross-linker to develop porous hydrogels in a simulated physiological condition. The gelation times, swelling behavior, porosities and mechanical performance of the resulting hydrogels were modulated by altering the mol. ratios of the Tz group of the cross-linker. The fabricated hydrogels showed fast gelation time (220 s), high swelling ratio (>5900%) and remarkable drug loading efficiency (about 95%). Moreover, the DOX release studies showed that the ROS-stimulus generated by NIR irradiation cleaved the thioketal bond in the cross-linkage and consequently de-cross-linked the network of hydrogels. The burst DOX release was observed in initial hours, followed by the sustained and spatiotemporal release pattern. The cytotoxicity results revealed that the CMC hydrogels were highly biocompatible and did not induce any toxic effect on the HEK-293 cells. Contrarily, DOX+ICG-encapsulated hydrogels inhibited the proliferation of Hela cancer cells and effectively enhanced the anti-tumor efficacy

when exposed to NIR light compared with non-irradiated DOX-encapsulated hydrogels, which showed a combined anti-cancer and photothermal therapy. The preliminary in vitro assessment of the developed NIR-responsive hydrogel utilizing a biocompatible click chemistry approach demonstrated its promise for in situ applications within physiological conditions, allowing on-demand drug release. Nevertheless, to ascertain the actual in vivo performance and translational potential of this hydrogel, further investigations through in vivo studies are imperative.



Chapter 4 : Dissertation Summary and future perspectives

Over the last few years, the effective DDS possessing key features such as on-demand release, triggered by non-invasive methods, and spatiotemporal control release, and so on, is of paramount importance in medical treatments regardless of how potent an active therapeutic ingredient. Premature drug release or failure to achieve targeted drug delivery is one of the major issues in the development of DDS which could not only reduce the therapeutic efficacy but also led to various adverse effects to the normal tissues. Regulating the drug release behavior is therefore essential, ideally with the use of safe and non-invasive stimuli to trigger drug release. Thus, the fabrication of such DDS based on stimuli-responsive hydrogels is crucial to address these limitations. Biopolymers are known to have the potential to offer excellent biocompatibility, good swelling properties, fast degradation profiles, and rapid clearance from the body after releasing the drug molecules. In this framework, two subjects were presented in this dissertation to design, synthesis and characterization of stimuli-responsive DDS-based on carboxymethyl cellulose (CMC) hydrogels to evaluate their potential use in cancer therapy application.

Chapter 2 presents the synthesis of injectable hydrogels, investigates the influence of crosslinkers on their rheological properties, and the development of a reduction-responsive DDS. Highly porous and soft CMC-based hydrogels were successfully fabricated by the incorporation of reduction-responsive di-selenide-based cross-linker (DSe-DPEG-DTz). CMC was conjugated with Nb molecules to chemically cross-linked with DSe-DPEG-DTz via the IEDDA click reaction between Nb and Tz groups. Thus, N₂ microbubbles liberated as a by-product during the IEDDA reaction which generated in-situ pores in hydrogel networks. Porosity, gelation times, and rheological properties of the hydrogels could be tuned by adjusting the complementary click functionalities (the ratio of Nb to Tz groups). The hydrogels exhibited stimuli-responsive and fast release of drug in the presence of 10 mmol of glutathione (GSH) as compared to the normal PBS solution. This study revealed that drug release kinetics could be controlled in a tumor intracellular mimicking environment (GSH, 10 mmol). The in vitro cytotoxicity results demonstrated that the synthesized cross-linker and the hydrogels were biocompatible with normal cell lines (HEK 293), whereas, drug-loaded hydrogels induced antitumor activity in a model cancer cell line (BT-20 cancer cells). This chapter indicated the ability of hydrogels to control drug release by carefully crafting the structure of crosslinkers.

Chapter 3 deals with the preparation of novel CMC hydrogels for NIR-light responsive DDS and investigates the in vitro application. NIR-responsive hydrogels were successfully developed from reactive oxygen species (ROS)-cleavable thioketal cross-linkers which possessed terminal tetrazine groups to undergo a bio-orthogonal IEDDA reaction with Nb modified CMC. The hydrogels were rapidly formed under physiological conditions and generated N₂ gas as a by-product, which led to the formation of porous structures within the hydrogel networks. By encapsulating a NIR dye, indocyanine green (ICG) and DOX into the porous network of the hydrogels, the drug release was triggered by NIR-irradiation. Upon NIR irradiation, the hydrogels showed sustained and spatiotemporal release of encapsulated DOX owing to the cleavage of thioketal bonds by interacting with ROS generated from ICG. This study could be a remarkable for an effective and controlled drug release. Further, in vitro cytotoxicity results revealed that the hydrogels were highly cytocompatible and did not induce any toxic effects to the normal cells. On the other hand, the DOX + ICG-encapsulated hydrogels showed the chemotherapeutic effect and effectively inhibited the proliferation of cancer cells when irradiated with NIR-light. These findings indicate that the drug release could be controlled by strategically designing the crosslinker employed in hydrogel

synthesis. This confirm that stimuli-responsive CMC hydrogels are promising candidate for controlled and on-demand DDS and could be potentially utilized in different biomedical applications.

We have developed stimuli-responsive hydrogel system with finely tuned physical and chemical properties, capable of delivering the drugs controlled on-demand non-invasively. While we have demonstrated the feasibility of the system but further research is needed to enhance its efficiency and address challenges related to long-term biocompatibility and in vivo administration. We investigated the in vitro injectability of hydrogels but animal studies are required to explore the real time biodistribution and chemical stability. Further, system is required to optimize for bioimaging, study the release profiles and biodegradation behavior of hydrogels in-vivo.

Bibliography

- [1] T.-C. Ho, C.-C. Chang, H.-P. Chan, T.-W. Chung, C.-W. Shu, K.-P. Chuang, T.-H. Duh, M.-H. Yang, Y.-C. Tyan, Hydrogels: Properties and applications in biomedicine, *Molecules* 27(9) (2022) 2902.
- [2] F. Ullah, M.B.H. Othman, F. Javed, Z. Ahmad, H.M. Akil, Classification, processing and application of hydrogels: A review, *Materials Science and Engineering: C* 57 (2015) 414-433.
- [3] A.H. Karoyo, L.D. Wilson, A Review on the Design and Hydration Properties of Natural Polymer-Based Hydrogels, *Materials* 14(5) (2021) 1095.
- [4] F. Khan, M. Atif, M. Haseen, S. Kamal, M.S. Khan, S. Shahid, S.A. Nami, Synthesis, classification and properties of hydrogels: Their applications in drug delivery and agriculture, *Journal of Materials Chemistry B* 10(2) (2022) 170-203.
- [5] A. Roy, K. Manna, S. Pal, Recent advances in various stimuli-responsive hydrogels: From synthetic designs to emerging healthcare applications, *Materials Chemistry Frontiers* (2022).

- [6] S. Bhatia, S. Bhatia, Natural polymers vs synthetic polymer, Natural polymer drug delivery systems: nanoparticles, plants, and algae (2016) 95-118.
- [7] M.S.B. Reddy, D. Ponnamma, R. Choudhary, K.K. Sadasivuni, A Comparative Review of Natural and Synthetic Biopolymer Composite Scaffolds, Polymers 13(7) (2021) 1105.
- [8] X. Tong, W. Pan, T. Su, M. Zhang, W. Dong, X. Qi, Recent advances in natural polymer-based drug delivery systems, React. Funct. Polym. 148 (2020) 104501.
- [9] G. Tiwari, R. Tiwari, B. Sriwastawa, L. Bhati, S. Pandey, P. Pandey, S.K. Bannerjee, Drug delivery systems: An updated review, International journal of pharmaceutical investigation 2(1) (2012) 2.
- [10] M. Puertas-Bartolomé, A. Mora-Boza, L. García-Fernández, Emerging biofabrication techniques: A review on natural polymers for biomedical applications, Polymers 13(8) (2021) 1209.
- [11] C. Mukherjee, D. Varghese, J. Krishna, T. Boominathan, R. Rakeshkumar, S. Dineshkumar, C.B. Rao, A. Sivaramakrishna, Recent Advances in Biodegradable

Polymers–Properties, Applications and Future Prospects, European Polymer Journal (2023) 112068.

[12] Y. Yu, M. Shen, Q. Song, J. Xie, Biological activities and pharmaceutical applications of polysaccharide from natural resources: A review, Carbohydrate polymers 183 (2018) 91-101.

[13] A. Kumar, A. Sood, G. Agrawal, S. Thakur, V.K. Thakur, M. Tanaka, Y.K. Mishra, G. Christie, E. Mostafavi, R. Boukherroub, D.W. Hutmacher, S.S. Han, Polysaccharides, proteins, and synthetic polymers based multimodal hydrogels for various biomedical applications: A review, International Journal of Biological Macromolecules 247 (2023) 125606.

[14] H. Liu, Y. Hu, Y. Liu, R. Hu, X. Wu, B. Li, A review of recent advances in biomedical applications of smart cellulose-based hydrogels, International Journal of Biological Macromolecules 253 (2023) 127149.

[15] J.A. Burdick, G.D. Prestwich, Hyaluronic acid hydrogels for biomedical applications, Advanced materials 23(12) (2011) H41-H56.

- [16] H. Tan, J.P. Rubin, K.G. Marra, Injectable in situ forming biodegradable chitosan-hyaluronic acid based hydrogels for adipose tissue regeneration, *Organogenesis* 6(3) (2010) 173-180.
- [17] A. Sergeeva, N. Feoktistova, V. Prokopovic, D. Gorin, D. Volodkin, Design of porous alginate hydrogels by sacrificial CaCO₃ templates: Pore formation mechanism, *Advanced Materials Interfaces* 2(18) (2015) 1500386.
- [18] E.C. Emenike, K.O. Iwuzor, O.D. Saliu, J. Ramontja, A.G. Adeniyi, Advances in the Extraction, Classification, Modification, Emerging and Advanced Applications of Crystalline Cellulose: A Review, *Carbohydrate Polymer Technologies and Applications* (2023) 100337.
- [19] M.M.H. Rocky, I.M. Rahman, F.B. Biswas, S. Rahman, M. Endo, K.H. Wong, A.S. Mashio, H. Hasegawa, Cellulose-based materials for scavenging toxic and precious metals from water and wastewater: A review, *Chemical Engineering Journal* 472 (2023) 144677.

[20] D.M. Correia, E. Lizundia, R.M. Meira, M. Rincón-Iglesias, S. Lanceros-Méndez, Cellulose nanocrystal and water-soluble cellulose derivative based electromechanical bending actuators, *Materials* 13(10) (2020) 2294.

[21] M. Rincón-Iglesias, E. Lizundia, S. Lanceros-Méndez, Water-soluble cellulose derivatives as suitable matrices for multifunctional materials, *Biomacromolecules* 20(7) (2019) 2786-2795.

[22] L. Song, F. Liu, C. Zhu, A. Li, Facile one-step fabrication of carboxymethyl cellulose based hydrogel for highly efficient removal of Cr (VI) under mild acidic condition, *Chemical Engineering Journal* 369 (2019) 641-651.

[23] W. Zhang, Y. Liu, Y. Xuan, S. Zhang, Synthesis and applications of carboxymethyl cellulose hydrogels, *Gels* 8(9) (2022) 529.

[24] M. Onofrei, A. Filimon, Cellulose-based hydrogels: designing concepts, properties, and perspectives for biomedical and environmental applications, *Polymer science: research advances, practical applications and educational aspects* (2016) 108-20.

- [25] A. Sannino, C. Demitri, M. Madaghiele, Biodegradable Cellulose-based Hydrogels: Design and Applications, *Materials* 2(2) (2009) 353-373.
- [26] A. Thakur, H. Kaur, Synthetic chemistry of cellulose hydrogels-A review, *Materials Today: Proceedings* 48 (2022) 1431-1438.
- [27] R. Kundu, P. Mahada, B. Chhirang, B. Das, Cellulose hydrogels: Green and sustainable soft biomaterials, *Current Research in Green and Sustainable Chemistry* 5 (2022) 100252.
- [28] L.-H. Fu, C. Qi, M.-G. Ma, P. Wan, Multifunctional cellulose-based hydrogels for biomedical applications, *Journal of materials chemistry B* 7(10) (2019) 1541-1562.
- [29] F. Zhan, J. Zhu, S. Xie, J. Xu, S. Xu, Advances of bioorthogonal coupling reactions in drug development, *European Journal of Medicinal Chemistry* 253 (2023) 115338.
- [30] S. Van Vlierberghe, P. Dubruel, E. Schacht, Biopolymer-based hydrogels as scaffolds for tissue engineering applications: a review, *Biomacromolecules*, 12(5) (2011) 1387-1408.

[31] Q. Chai, Y. Jiao, X. Yu, Hydrogels for biomedical applications: their characteristics and the mechanisms behind them, *Gels*, 3(1) (2017) 6.

[32] Z. Chen, H. Wu, H. Wang, D. Zaldivar-Silva, L. Agüero, Y. Liu, Z. Zhang, Y. Yin, B. Qiu, J. Zhao, An injectable anti-microbial and adhesive hydrogel for the effective noncompressible visceral hemostasis and wound repair, *Mater. Sci. Eng. C.*, 129 (2021) 112422.

[33] S. Talebian, J. Foroughi, S.J. Wade, K.L. Vine, A. Dolatshahi-Pirouz, M. Mehrali, J. Conde, G.G. Wallace, Biopolymers for antitumor implantable drug delivery systems: recent advances and future outlook, *Adv. Mater.*, 30(31) (2018) 1706665.

[34] T.-S. Fu, Y.-H. Wei, P.-Y. Cheng, I. Chu, W.-C. Chen, A Novel Biodegradable and Thermosensitive Poly (Ester-Amide) Hydrogel for Cartilage Tissue Engineering, *Biomed Res. Int.*, 2018 (2018).

[35] Z. Sun, C. Song, C. Wang, Y. Hu, J. Wu, Hydrogel-based controlled drug delivery for cancer treatment: a review, *Mol. Pharm.*, 17(2) (2019) 373-391.

[36] S.H. Zainal, N.H. Mohd, N. Suhaili, F.H. Anuar, A.M. Lazim, R. Othaman, Preparation of cellulose-based hydrogel: A review, *J. Mater. Res. Technol.*, 10 (2021) 935-952.

[37] S.M. Carvalho, A.A. Mansur, N.S. Capanema, I.C. Carvalho, P. Chagas, L.C.A. de Oliveira, H.S. Mansur, Synthesis and in vitro assessment of anticancer hydrogels composed by carboxymethylcellulose-doxorubicin as potential transdermal delivery systems for treatment of skin cancer, *J. Mol. Liq.*, 266 (2018) 425-440.

[38] L. Song, F. Liu, C. Zhu, A. Li, Facile one-step fabrication of carboxymethyl cellulose based hydrogel for highly efficient removal of Cr (VI) under mild acidic condition, *Chem. Eng. J.*, 369 (2019) 641-651.

[39] T.V. McOscar, W.M. Gramlich, Hydrogels from norbornene-functionalized carboxymethyl cellulose using a UV-initiated thiol-ene click reaction, *Cellulose*, 25(11) (2018) 6531-6545.

[40] N.K. Devaraj, R. Weissleder, Biomedical applications of tetrazine cycloadditions, *Acc. Chem. Res.*, 44(9) (2011) 816-827.

- [41] Y.-J. Jo, M. Gulfam, S.-H. Jo, Y.-S. Gal, C.-W. Oh, S.-H. Park, K.T. Lim, Multi-stimuli responsive hydrogels derived from hyaluronic acid for cancer therapy application, *Carbohydr. Polym.*, 286 (2022) 119303.
- [42] T.T. Vu, M. Gulfam, S.-H. Jo, S.-H. Park, K.T. Lim, Injectable and biocompatible alginate-derived porous hydrogels cross-linked by IEDDA click chemistry for reduction-responsive drug release application, *Carbohydr. Polym.*, 278 (2022) 118964.
- [43] M.A.C. Stuart, W.T. Huck, J. Genzer, M. Müller, C. Ober, M. Stamm, G.B. Sukhorukov, I. Szleifer, V.V. Tsukruk, M. Urban, Emerging applications of stimuli-responsive polymer materials, *Nat. Mater.*, 9(2) (2010) 101-113.
- [44] X. Yan, F. Wang, B. Zheng, F. Huang, Stimuli-responsive supramolecular polymeric materials, *Chem. Soc. Rev.*, 41(18) (2012) 6042-6065.
- [45] P. Lavrador, M.R. Esteves, V.M. Gaspar, J.F. Mano, Stimuli-Responsive Nanocomposite Hydrogels for Biomedical Applications, *Adv. Funct. Mater.*, 31(8) (2021) 2005941.

- [46] A.C. Marques, P.J. Costa, S. Velho, M.H. Amaral, Stimuli-responsive hydrogels for intratumoral drug delivery, *Drug Discov.*, 26(10) (2021) 2397-2405.
- [47] A. Pourjavadi, R. Heydarpour, Z.M. Tehrani, Multi-stimuli-responsive hydrogels and their medical applications, *New J. Chem.*, 45(35) (2021) 15705-15717.
- [48] I. Tokarev, S. Minko, Stimuli-responsive hydrogel thin films, *Soft Matter*, 5(3) (2009) 511-524.
- [49] Y. Zhang, C. Zhu, Z. Zhang, J. Zhao, Y. Yuan, S. Wang, Oxidation triggered formation of polydopamine-modified carboxymethyl cellulose hydrogel for anti-recurrence of tumor, *Colloids Surf. B.*, 207 (2021) 112025.
- [50] L. Zhou, J. Zhao, Y. Chen, Y. Zheng, J. Li, J. Zhao, J. Zhang, Y. Liu, X. Liu, S. Wang, MoS₂-ALG-Fe/GOx hydrogel with Fenton catalytic activity for combined cancer photothermal, starvation, and chemodynamic therapy, *Colloids Surf. B.*, 195 (2020) 111243.
- [51] I. Gholamali, Stimuli-responsive polysaccharide hydrogels for biomedical applications: A review, *Regen. Eng. Transl. Med.*, 7(1) (2021) 91-114.

[52] M. Ding, L. Jing, H. Yang, C. Machnicki, X. Fu, K. Li, I. Wong, P.-Y. Chen, Multifunctional soft machines based on stimuli-responsive hydrogels: from freestanding hydrogels to smart integrated systems, *Mater. Today Adv.*, 8 (2020) 100088.

[53] Y. Zhang, C. Zhu, Z. Zhang, J. Zhao, Y. Yuan, S. Wang, Oxidation triggered formation of polydopamine-modified carboxymethyl cellulose hydrogel for anti-recurrence of tumor, *Colloids Surf B.*, 207 (2021) 112025.

[54] Y. Zhang, Y. Xu, C. Wei, Y. Zhang, L. Yang, Z. Song, M. Lang, Diselenide-containing poly (ϵ -caprolactone)-based thermo-responsive hydrogels with oxidation and reduction-triggered degradation, *Colloids Surf. B.*, 4 (2017) 172-179.

[55] L. Yan, W. Wu, W. Zhao, R. Qi, D. Cui, Z. Xie, Y. Huang, T. Tong, X. Jing, Reduction-sensitive core-cross-linked mPEG-poly (ester-carbonate) micelles for glutathione-triggered intracellular drug release, *Polym. Chem.*, 3(9) (2012) 2403-2412.

- [56] Q. Zhao, C. Wang, Y. Liu, J. Wang, Y. Gao, X. Zhang, T. Jiang, S. Wang, PEGylated mesoporous silica as a redox-responsive drug delivery system for loading thiol-containing drugs, *Int. J. Pharm.*, 477(1-2) (2014) 613-622.
- [57] Y.S. Choi, K.M. Huh, M.S. Shim, I.S. Park, Y.Y. Cho, J.Y. Lee, H.S. Lee, H.C. Kang, Disrupting the Redox Balance with a Diselenide Drug Delivery System: Synergistic or Antagonistic?, *Adv. Funct. Mater.*, 31(6) (2021) 2007275.
- [58] G. Ma, J. Liu, J. He, M. Zhang, P. Ni, Dual-responsive polyphosphoester-doxorubicin prodrug containing a diselenide bond: synthesis, characterization, and drug delivery, *ACS Biomater. Sci. Eng.*, 4(7) (2018) 2443-2452.
- [59] D.S.B. Anugrah, K. Ramesh, M. Kim, K. Hyun, K.T. Lim, Near-infrared light-responsive alginate hydrogels based on diselenide-containing cross-linkage for on demand degradation and drug release, *Carbohydr. Polym.*, 223 (2019) 115070.
- [60] M. Gulfam, S.-H. Jo, S.-W. Jo, T.T. Vu, S.-H. Park, K.T. Lim, Highly porous and injectable hydrogels derived from cartilage acellularized matrix exhibit reduction and NIR light dual-responsive drug release properties for application in antitumor therapy, *NPG Asia Mater.*, 14(1) (2022) 1-17.

[61] N. Dadoo, S.B. Landry, J.D. Bomar, W.M. Gramlich, Synthesis and spatiotemporal modification of biocompatible and Stimuli-Responsive carboxymethyl cellulose hydrogels using Thiol-Norbornene chemistry, *Macromol. Biosci.*, 17(9) (2017) 1700107.

[62] S.S. Bisht, K. Pandey, G. Joshi, S. Naithani, New route for carboxymethylation of cellulose: synthesis, structural analysis and properties, *Cellul. Chem. Technol.*, 51 (2017) 609-619.

[63] M.K. Nguyen, E. Alsberg, Bioactive factor delivery strategies from engineered polymer hydrogels for therapeutic medicine, *Prog. Polym. Sci.*, 39(7) (2014) 1235-1265.

[64] Y. Deng, A. Shavandi, O.V. Okoro, L. Nie, Alginate modification via click chemistry for biomedical applications, *Carbohydr. Polym.*, (2021) 118360.

[65] N. Latifi, M. Asgari, H. Vali, L. Mongeau, A tissue-mimetic nano-fibrillar hybrid injectable hydrogel for potential soft tissue engineering applications, *Sci. Rep.*, 8(1) (2018) 1-18.

[66] J. Li, F. Chen, X. Lin, T. Ding, Hydrogen-Bonding-Assisted Toughening of Hierarchical Carboxymethyl Cellulose Hydrogels for Biomechanical Sensing, *Carbohydr. Polym.*, (2021) 118252.

[67] G. Reshma, C. Reshmi, S.V. Nair, D. Menon, Superabsorbent sodium carboxymethyl cellulose membranes based on a new cross-linker combination for female sanitary napkin applications, *Carbohydr. Polym.*, 248 (2020) 116763.

[68] C.A. Grattoni, H.H. Al-Sharji, C. Yang, A.H. Muggeridge, R.W. Zimmerman, Rheology and permeability of crosslinked polyacrylamide gel, *J. Colloid Interface Sci.*, 240(2) (2001) 601-607.

[69] J. Han, T. Lei, Q. Wu, High-water-content mouldable polyvinyl alcohol-borax hydrogels reinforced by well-dispersed cellulose nanoparticles: Dynamic rheological properties and hydrogel formation mechanism, *Carbohydr. Polym.*, 102 (2014) 306-316.

[70] S. Gao, J. Guo, K. Nishinari, Thermoreversible konjac glucomannan gel crosslinked by borax, *Carbohydr. Polym.*, 72(2) (2008) 315-325.

[71] C. Yan, D.J. Pochan, Rheological properties of peptide-based hydrogels for biomedical and other applications, *Chem. Soc. Rev.*, 39(9) (2010) 3528-3540.

[72] N. Gull, S.M. Khan, O.M. Butt, A. Islam, A. Shah, S. Jabeen, S.U. Khan, A. Khan, R.U. Khan, M.T.Z. Butt, Inflammation targeted chitosan-based hydrogel for controlled release of diclofenac sodium, *Int. J. Biol. Macromol.*, 162 (2020) 175-187.

[73] N.S. Capanema, A.A. Mansur, S.M. Carvalho, I.C. Carvalho, P. Chagas, L.C.A. de Oliveira, H.S. Mansur, Bioengineered carboxymethyl cellulose-doxorubicin prodrug hydrogels for topical chemotherapy of melanoma skin cancer, *Carbohydr. Polym.*, 195 (2018) 401-412.

[74] D. Jeong, S.-W. Joo, Y. Hu, V.V. Shinde, E. Cho, S. Jung, Carboxymethyl cellulose-based superabsorbent hydrogels containing carboxymehtyl β -cyclodextrin for enhanced mechanical strength and effective drug delivery, *Eur. Polym. J.*, 105 (2018) 17-25.

[75] S.A. Siboro, D.S. Anugrah, K. Ramesh, S.-H. Park, H.-R. Kim, K.T. Lim, Tunable porosity of covalently crosslinked alginate-based hydrogels and its significance in drug release behavior, *Carbohydr. Polym.*, 260 (2021) 117779.

[76] L. Martin, C.G. Wilson, F. Koosha, L. Tetley, A.I. Gray, S. Senel, I.F. Uchegbu, The release of model macromolecules may be controlled by the hydrophobicity of palmitoyl glycol chitosan hydrogels, *J. Control. Release*, 80(1-3) (2002) 87-100.

[77] C. Wei, Y. Zhang, H. Xu, Y. Xu, Y. Xu, M. Lang, Well-defined labile diselenide-centered poly (ϵ -caprolactone)-based micelles for activated intracellular drug release, *J. Mater. Chem. B.*, 4(29) (2016) 5059-5067.

[78] C.W. Song, R. Griffin, H. Park, *Cancer drug resistance*, Humana press, 2006.

[79] M. Stubbs, P.M. McSheehy, J.R. Griffiths, C.L. Bashford, Causes and consequences of tumour acidity and implications for treatment, *Mol. Med. Today*, 6(1) (2000) 15-19.

[80] B. Manocha, A. Margaritis, Controlled release of doxorubicin from doxorubicin/-polyglutamic acid ionic complex, *J. Nanomater.*, 2010 (2010).

[81] Y. Yuan, J. Zhang, M. Wang, B. Mei, Y. Guan, G. Liang, Detection of glutathione in vitro and in cells by the controlled self-assembly of nanorings, *Anal. Chem.*, 85(3) (2013) 1280-1284.

[82] L. Zhang, Y. Liu, K. Zhang, Y. Chen, X. Luo, Redox-responsive comparison of diselenide micelles with disulfide micelles, *Colloid Polym. Sci.*, 297(2) (2019) 225-238.

[83] L. Wang, B. Li, F. Xu, Z. Xu, D. Wei, Y. Feng, Y. Wang, D. Jia, Y. Zhou, UV-crosslinkable and thermo-responsive chitosan hybrid hydrogel for NIR-triggered localized on-demand drug delivery, *Carbohydr. Polym.* 174 (2017) 904-914.

[84] T. Sun, C. Jiang, Stimuli-responsive drug delivery systems triggered by intracellular or subcellular microenvironments, *Adv. Drug Deliv. Rev.* 196 (2023) 114773.

[85] X. Shi, C.Y. Zhang, J. Gao, Z. Wang, Recent advances in photodynamic therapy for cancer and infectious diseases, *Wiley Interdiscip. Rev. Nanomed. Nanobiotechnol.* 11(5) (2019) e1560.

- [86] D.S.B. Anugrah, K. Ramesh, M. Kim, K. Hyun, K.T. Lim, Near-infrared light-responsive alginate hydrogels based on diselenide-containing cross-linkage for on demand degradation and drug release, *Carbohydrate polymers* 223 (2019) 115070.
- [87] M. Geven, R. d'Arcy, Z.Y. Turhan, F. El-Mohtadi, A. Alshamsan, N. Tirelli, Sulfur-based oxidation-responsive polymers. Chemistry,(chemically selective) responsiveness and biomedical applications, *Eur. Polym. J.* 149 (2021) 110387.
- [88] F. Yu, P. Li, B. Wang, K. Han, Reversible near-infrared fluorescent probe introducing tellurium to mimetic glutathione peroxidase for monitoring the redox cycles between peroxynitrite and glutathione in vivo, *Journal of the American Chemical Society* 135(20) (2013) 7674-7680.
- [89] M. Gulfam, S.-H. Jo, S.-W. Jo, T.T. Vu, S.-H. Park, K.T. Lim, Highly porous and injectable hydrogels derived from cartilage acellularized matrix exhibit reduction and NIR light dual-responsive drug release properties for application in antitumor therapy, *NPG Asia Mater.* 14(1) (2022) 8.
- [90] J. Wang, Y. Zhang, E. Archibong, F.S. Ligler, Z. Gu, Leveraging H₂O₂ levels for biomedical applications, *Adv. Biosyst.* 1(9) (2017) 1700084.

[91] P. Hu, N. Tirelli, Scavenging ROS: superoxide dismutase/catalase mimetics by the use of an oxidation-sensitive nanocarrier/enzyme conjugate, *Bioconjugate Chem.* 23(3) (2012) 438-449.

[92] P. Pei, C. Sun, W. Tao, J. Li, X. Yang, J. Wang, ROS-sensitive thioketal-linked polyphosphoester-doxorubicin conjugate for precise phototriggered locoregional chemotherapy, *Biomaterials* 188 (2019) 74-82.

[93] C.G. Dariva, J.F. Coelho, A.C. Serra, Near infrared light-triggered nanoparticles using singlet oxygen photocleavage for drug delivery systems, *J. Controlled Release* 294 (2019) 337-354.

[94] A. Rinaldi, R. Caraffi, M.V. Grazioli, N. Oddone, L. Giardino, G. Tosi, M.A. Vandelli, L. Calzà, B. Ruozi, J.T. Duskey, Applications of the ROS-responsive thioketal linker for the production of smart nanomedicines, *Polymers* 14(4) (2022) 687.

[95] L. Lin, X. Song, X. Dong, B. Li, Nano-photosensitizers for enhanced photodynamic therapy, *Photodiagnosis Photodyn. Ther.* 36 (2021) 102597.

[96] S.M. Mahalingam, J.D. Ordaz, P.S. Low, Targeting of a photosensitizer to the mitochondrion enhances the potency of photodynamic therapy, *ACS omega* 3(6) (2018) 6066-6074.

[97] S. Wang, G. Yu, Z. Wang, O. Jacobson, L.S. Lin, W. Yang, H. Deng, Z. He, Y. Liu, Z.Y. Chen, Enhanced antitumor efficacy by a cascade of reactive oxygen species generation and drug release, *Angew. Chem.* 131(41) (2019) 14900-14905.

[98] L. Yang, X. Hou, Y. Zhang, D. Wang, J. Liu, F. Huang, J. Liu, NIR-activated self-sensitized polymeric micelles for enhanced cancer chemo-photothermal therapy, *J. Controlled Release* 339 (2021) 114-129.

[99] W. Zuo, D. Chen, Z. Fan, L. Chen, Z. Zhu, Q. Zhu, X. Zhu, Design of light/ROS cascade-responsive tumor-recognizing nanotheranostics for spatiotemporally controlled drug release in locoregional photo-chemotherapy, *Acta Biomater.* 111 (2020) 327-340.

[100] M.S. Rahman, M.S. Hasan, A.S. Nitai, S. Nam, A.K. Karmakar, M.S. Ahsan, M.J.A. Shiddiky, M.B. Ahmed, Recent Developments of Carboxymethyl Cellulose, *Polymers* 13(8) (2021) 1345.

- [101] S. Javanbakht, M. Nabi, M. Shadi, M.M. Amini, A. Shaabani, Carboxymethyl cellulose/tetracycline@ UiO-66 nanocomposite hydrogel films as a potential antibacterial wound dressing, *Int. J. Biol. Macromol.* 188 (2021) 811-819.
- [102] J. Namkaew, P. Laowpanitchakorn, N. Sawaddee, S. Jirajessada, S. Honsawek, S. Yodmuang, Carboxymethyl cellulose entrapped in a poly (vinyl) alcohol network: Plant-based scaffolds for cartilage tissue engineering, *Molecules* 26(3) (2021) 578.
- [103] I. Gomez, Y. Alesanco, J.A. Blázquez, A. Viñuales, L.C. Colmenares, Room-temperature self-standing cellulose-based hydrogel electrolytes for electrochemical devices, *Polymers* 12(11) (2020) 2686.
- [104] J. Li, L. Fang, W.R. Tait, L. Sun, L. Zhao, L. Qian, Preparation of conductive composite hydrogels from carboxymethyl cellulose and polyaniline with a nontoxic crosslinking agent, *RSC Adv.* 7(86) (2017) 54823-54828.
- [105] X. Li, Y. Xiong, Application of “Click” Chemistry in Biomedical Hydrogels, *ACS omega* 7(42) (2022) 36918-36928.

- [106] J. Zhang, X.-D. Xu, D.-Q. Wu, X.-Z. Zhang, R.-X. Zhuo, Synthesis of thermosensitive P(NIPAAm-co-HEMA)/cellulose hydrogels via “click” chemistry, *Carbohydr. Polym.* 77(3) (2009) 583-589.
- [107] M. Zanon, L. Montalvillo-Jiménez, P. Bosch, R. Cue-López, E. Martínez-Campos, M. Sangermano, A. Chiappone, Photocurable Thiol–yne Alginate Hydrogels for Regenerative Medicine Purposes, *Polymers* 14(21) (2022) 4709.
- [108] B. Oliveira, Z. Guo, G. Bernardes, Inverse electron demand Diels–Alder reactions in chemical biology, *Chem. Soc. Rev.* 46(16) (2017) 4895-4950.
- [109] J. Shi, Z. Chen, B. Wang, L. Wang, T. Lu, Z. Zhang, Reactive oxygen species-manipulated drug release from a smart envelope-type mesoporous titanium nanovehicle for tumor sonodynamic-chemotherapy, *ACS Appl. Mater. Interfaces* 7(51) (2015) 28554-28565.
- [110] Y.-J. Jo, M. Gulfam, S.-H. Jo, Y.-S. Gal, C.-W. Oh, S.-H. Park, K.T. Lim, Multi-stimuli responsive hydrogels derived from hyaluronic acid for cancer therapy application, *Carbohydr. Polym.* 286 (2022) 119303.

[111] I. Ali, M. Gulfam, S.-H. Jo, J.-W. Seo, A. Rizwan, S.-H. Park, K.T. Lim, Reduction-responsive and bioorthogonal carboxymethyl cellulose based soft hydrogels cross-linked via IEDDA click chemistry for cancer therapy application, *Int. J. Biol. Macromol.* 219 (2022) 109-120.

[112] J. Yang, M.R. Karver, W. Li, S. Sahu, N.K. Devaraj, Metal-catalyzed one-pot synthesis of tetrazines directly from aliphatic nitriles and hydrazine, *Angew. Chem.* 124(21) (2012) 5312-5315.

[113] S. Javanbakht, A. Shaabani, Carboxymethyl cellulose-based oral delivery systems, *Int. J. Biol. Macromol.* 133 (2019) 21-29.

[114] A.L. Mohamed, A.A. Soliman, E.A. Ali, N.Y. Abou-Zeid, A.A. Nada, Hydrogel bioink based on clickable cellulose derivatives: Synthesis, characterization and in vitro assessment, *Int. J. Biol. Macromol.* 163 (2020) 888-897.

[115] A. Pettignano, A. Charlot, E. Fleury, Carboxyl-functionalized derivatives of carboxymethyl cellulose: Towards advanced biomedical applications, *Polym Rev* 59(3) (2019) 510-560.

[116] H. Kono, ¹H and ¹³C chemical shift assignment of the monomers that comprise carboxymethyl cellulose, *Carbohydr. Polym.* 97(2) (2013) 384-390.

[117] O. Jeon, K.H. Bouhadir, J.M. Mansour, E. Alsberg, Photocrosslinked alginate hydrogels with tunable biodegradation rates and mechanical properties, *Biomaterials* 30(14) (2009) 2724-2734.

[118] H. Li, C.-w. Wu, S. Wang, W. Zhang, Mechanically strong poly (vinyl alcohol) hydrogel with macropores and high porosity, *Mater. Lett.* 266 (2020) 127504.

[119] X. Xu, Z. Zeng, Z. Huang, Y. Sun, Y. Huang, J. Chen, J. Ye, H. Yang, C. Yang, C. Zhao, Near-infrared light-triggered degradable hyaluronic acid hydrogel for on-demand drug release and combined chemo-photodynamic therapy, *Carbohydr. Polym.* 229 (2020) 115394.

[120] Q. Pan, X. Deng, W. Gao, J. Chang, Y. Pu, B. He, ROS triggered cleavage of thioketal moiety to dissociate prodrug nanoparticles for chemotherapy, *Colloids Surf. B* 194 (2020) 111223.

[121] S. Jaiswal, S.B. Dutta, D. Nayak, S. Gupta, Effect of doxorubicin on the near-infrared optical properties of indocyanine green, ACS omega 6(50) (2021) 34842-34849.

